Afonso Pereira Correia de Sousa

Investigation of detection limits of ZnSe and Cu2SnSe3 secondary phases in Cu2ZnSnSe4

Master's degree thesis in Physics Engineering,
under the supervision of Professor Doctor Susan Schorr, Helmholtz-Zentrum Berlin, and Doctor Professor Manuela Ramos Silva,
presented to Faculty of Sciences and Technology of University of Coimbra.

June 2016

· U C ·

UNIVERSIDADE DE COIMBRA

Investigation of detection limits of $ZnSe$ and Cu_2SnSe_3 secondary phases in $Cu_2ZnSnSe_4$

Afonso Pereira Correia de Sousa

Departamento de Física

Universidade de Coimbra

A thesis submitted for the degree of

Mestrado em Engenharia Física

Junho de 2016

Abstract

Quaternary $Cu_2ZnSnSe_4$ (CZTSe) is a promising semiconductor material for absorber layer in thin film solar cells due to direct band gap around $1eV$ and high absorption coefficient ($> 10^4 cm^{-1}$) (7). The highest conversion efficiency of CZTSe solar cells is above 11% (8). Nevertheless, a low open circuit voltage with respect to the band gap is a common phenomenon in CZTSe photovoltaic devices. A plausible reason for this is a reduction in the effective band gap due to inhomogeneities in structure, phase, or composition. To gain a detailed knowledge of the influence of phase inhomogeneities on the performance of solar cells, the understanding of detection limits of conventionally used characterization methods is essential. The aim of this work is to study the sensitivity limits of X-ray diffraction and Raman spectroscopy to the presence of two very common secondary phases for $Cu_2ZnSnSe_4$–$ZnSe$ and Cu_2SnSe_3.

Polycrystalline powder of two CZTSe samples (slightly Zn-rich) and one Cu_2SnSe_3 sample have been grown using the solid state reaction method in evacuated silica tubes. Additionally, an industrially produced powder of $ZnSe$ has been used to produce a number of mixtures of corresponding CZTSe with 1%, 2%, 3%, 5%, 10% and 20% of $ZnSe$ or Cu_2SnSe_3 respectively.

The structural characterization of the starting materials as well as of mixtures was carried out by powder X-ray diffraction (PXRD) and subsequent Rietveld analysis of the diffraction data using the FullProf suite (11). Rietveld refinement of diffraction data of the mixtures was performed, paying a special attention to the influence of amounts of $ZnSe$ and Cu_2SnSe_3 on the diffraction patterns of the mixtures. The amounts of secondary phases determined by Rietveld refinement have been compared with the initial data,

determining in this way the detection limits of PXRD for these secondary phases.

To study the crystal structure of the synthesized mixtures at the micrometer scale Raman spectroscopy has been employed. In these measurements a $632.8nm$ laser line was employed and it was found to be efficient for both $ZnSe$ and Cu_2SnSe_3 phase detection. By performing Raman line scan measurements we evaluated characteristic Raman mode intensities corresponding to the different phases and thus are able to estimate the mixture composition.

Abstract

O quaternário $Cu_2ZnSnSe_4$ (CZTSe) é um material semiconductor promissor para a camada de absorção em células solares de filme fino devido ao facto de a banda de gap ser de cerca de 1eV e ter um coeficiente de absorção elevado ($> 10^4 cm^{-1}$) (7). A eficiência de conversão mais elevada de células solares de CZTSe é superior a 11% (8). No entanto, a baixa tensão em malha aberta com respeito à banda de gap é um fenómeno comum nos dispositivos fotovoltáicos CZTSe. Uma razão plausível para tal é a redução na banda de gap efectiva por heterogeneidades na estrutura, fase ou composição. Para obter um conhecimento detalhado da influência das heterogeneidades de fase na performance das células solares, é essencial a compreensão dos limites de deteção dos metodos de caracterização convencionais. O objectivo deste trabalho é o estudo dos limites de sensibilidade das difração de Raio-X e Espectroscopia de Raman na presença de duas fases secundárias muito comuns para $Cu_2ZnSnSe_4$–$ZnSe$ e Cu_2SnSe_3.

Duas amostras de pó policristalino de CZTSe (ligeiramente rico em Zn) e uma amostra de Cu_2SnSe_3 foram sintetizadas usando o método de reação de estado sólido em tubos de silica evacuados. Adicionalmente, $ZnSe$ em pó produzido industrailmente foi usado para produzir um número de misturas de CZTSe correspondente com 1%, 2%, 3%, 5%, 10% e 20% de $ZnSe$ ou Cu_2SnSe_3 respectivamente.

A caracterização estructural dos materiais iniciais e das misturas foi reazliado por difração de Raio-X (PXRD) e subsequente análise Rietveld dos dados de difração usando o pacote de software FullProf (11). Foi efectuado o refinamento de Rietveld dos dados das difrações, dando especial atenção à influência das quantidades de $ZnSe$ e Cu_2SnSe_3 nos diferentes padrões

das misturas. A quantidade de fases secundárias determinada pelo refinamento de Rietveld foi comparada com os dados iniciais, determinando assim os limites de deteção de PXRD para estas fases secundárias.

Para o estudo à escala micrométrica da estrutura do cristal das misturas sintetizadas, foi usado a Espectroscopia de Raman. Nessas medidas um laser de $632.8nm$ foi usado e aparentou ser efeciente para a deteção de ambas as fases de $ZnSe$ e Cu_2SnSe_3. Ao usar medidas de linhas de scan Raman, avaliámos modos de intensidades Raman característicos correspondendo às diferentes fases, permitindo-nos estimar a composição da mistura.

Acknowledgements

Firstly, I would like to thank the institutions Universidade de Coimbra and Helmholtz-Zentrum Berlin for this unique opportunity to do my Master Thesis in Berlin.

To all my colleagues at the Department *Structure and Dynamics of Energy Materials*, my gratitude for all those good office moments and companionship. A special thanks to Professor Doctor Susan Schorr for accepting me as a master student allowing me to have a glimpse into the academical world, to Doctor Galina Gurieva for all the support, patience and advices that made it possible to conclude my thesis, and to Doctor Sergej Levcenco for all the late night measurements and creativity. To all my Berlin friends, thank you for being there shaping what the city felt like during these months.

To all my Portuguese friends and family:

Um obrigado aos meus amigos de Coimbra que me acompanharam durante o meu percurso irregular, com especial atenção ao Luís Antunes, Johnny Araujo e Sérgio Pereira. Aos meus amigos de Bologna/Lisboa, por me alargarem os horizontes e mostrarem novos lares, em especial ao João Serodio, à Nina Glória, ao Tiago Duarte e à Ana Piçarra. Aos amigos do Sátão, porque uma pessoa nunca esquece de onde vem, Vasco Amaral e Nelson Gomes.

Um agradecimento muito especial à minha família, por nunca ter duvidado de mim, em especial aos meus pais, por sempre me apoiarem nas minhas aventuras e loucuras.

E por último, um obrigado à Rita, por ser como família, por me mostrar como se fazem planos de estudo e sem saber me ajudar a tornar uma pessoa mais decidida.

Contents

List of Figures

List of Tables

1

Introduction

1.1 Motivation

Mankind currently lives some of its most challenging times, with a population more than seven billion and growing at an yearly rate of 1,132%, (1), increase in the energy consumption is unavoidable and a problem that need to be tackled and solved. The fact that, not only fossil fuels are a finite energy source but is also one of the main causes of global warming that endangers our planet ecosystems and consequently humans source of sustenance makes it fundamental to find an alternative.

Renewable energies are one of the answers, namely hydro-electrical energy, wind energy and solar energy. In Germany, over 90% of the energy needed by the country was momentarily supplied by renewable sources in May, (2), while in Portugal, a record of 107 consecutive hours running only on renewable energy was attained between May, 7th and May, (3). The crossing of the barriers of production is the result of many years of effort and ecological policies, and most importantly of technological and scientific research.

Earth receives an average of 174 000 terawatts of solar radiation, and even though part of it is reflected in the upper layers of the atmosphere, in an utopian world the sun alone would be sufficient to power the entire civilization. Two main problems prohibit us from achieving that, the efficiency of the power conversion, and the costs of producing the energy conversion cells.

Currently, the solar energy market is dominate by silicon based photovoltaic cells, accounting for around 90% of the total production, with a maximum laboratory efficiency

of 25%, but due to the high cost of purification of the material (needed to produce the cell) and the high demand for silicon for other technology industries, alternatives using low cost materials alloys are being investigated. The compound semiconductor with bigger market share is Cadmium Telluride ($CdTe$), but as we can see in figure 1.1, Te is an expensive and rare element, and as Cd is an heavy metal some environmental issues are raised. $Cu(In, Ga)Se_2$ (CIGS) has also proven to be an reliable alternative for silicon in terms of efficiency, exceeding the 20% in laboratory, but again, the problem of abundance and cost remains.

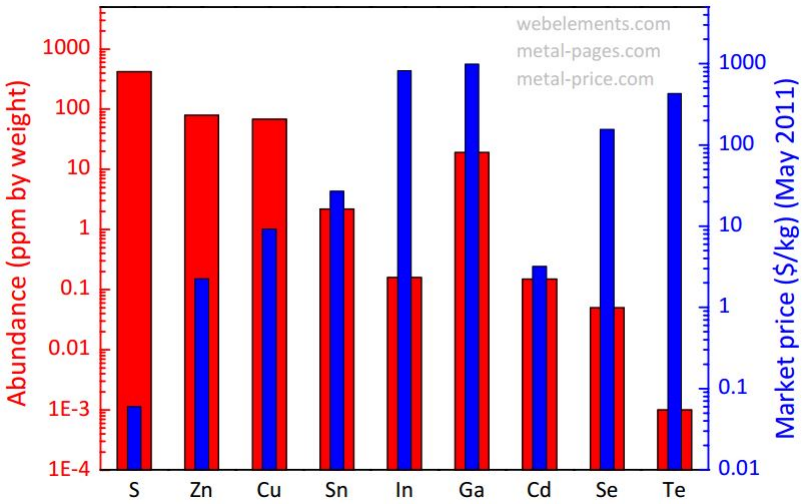

Figure 1.1: Abundance in the Earth's crust and market price (2011) of the elements used to produce CZTS, CZTSe, CIGS and CdTe.

A promising materials are the $Cu_2ZnSn(S, Se)_4$, already recognized as a potential compound for photovoltaic applications in 1988 (7) due to its characteristics, absorption coefficient of $\alpha > 10^4 cm^{-1}$ and a band gap of around $1eV$ for CZTSe and $1,5eV$ for CZTS. In this work, we will focus on CZTSe.

Currently, the efficiency of CZTSe solar cells is above 12% (8), but the open circuit voltage is low compared to the band gap. This might be caused by a reduction of the effective band gap due to inhomogeneities in structure, phase or composition.

This inhomogeneities are possibly caused by the presence of secondary phases. It is extremely difficult to grow single phase CZTSe (10), and to understand the influence of those secondary phases, we first need to know the amount of it in the sample.

1.2 Objectives of this work

The research described in this work was realized from September 2015 to April 2016 in the Helmholtz-Zentrum Berlin, where I was part of the Department of Structure and Dynamics of Energy Materials. The research was oriented by Professor Doctor Susan Schorr, and the laboratory work and data analysis was done under the supervision and with support of Doctor Galina Gurieva. The Raman measurements were performed in collaboration with Doctor Sergej Levcenco.

This work has the purpose to determine the detection limit of powder X-ray diffraction technique, and if whether or not it is possible to use Raman Spectroscopy to perform a quantitative analysis to our powder samples. With this in mind, 16 different samples were prepared, 4 of the *pure* compounds $ZnSe$, Cu_2SnSe_3 and two samples of $Cu_2ZnSnSe_4$. The remaining 12 samples were mixtures of the pure samples, CZTSe-$ZnSe$ and CZTSe-CTSe, at known proportions of 1%, 2%, 3%, 5%, 10% and 20%.

A similar work was done with thin films (9), but using powder samples we can know exactly the initial quantities of each phase before analysing, and verify not only the detection limit but also if the detection is correct or not.

1.3 Structure of the thesis

This thesis, besides the chapter Introduction, is divided in five different chapters that provide an overview of all the steps of this work.

In chapter 2 a short introduction to the equipment and techniques used throughout the experiment. The emphasis is to explain theoretically all the techniques used to analyse the samples.

In chapter 3 the synthesis of the secondary phases, $ZnSe$ and CTSe, are described in detail.

Chapter 4 serves to exhibit the final results obtained from all the measurements performed to our samples. The chapter is divided by technique and organized chronologically, meaning that the techniques that were executed first are shown first.

Chapter 5 is the discussion chapter, where we relate the results obtained with the expected values, compare the results for the different samples and with the different techniques and derive a conclusion.

In chapter 6 we write a short resume of what we concluded with this work.

2

Procedures and Equipment used

This chapter briefly introduces the techniques and equipment used throughout the work. It's organised in a chronological way, from the first equipments used in the first steps of the project and so forth.

2.1 Solid State Reaction

The CTSe and $ZnSe$ samples, as well as CZTSe were synthesized using the Solid State Reaction method, consisting of two steps - synthesis using the pure elements and annealing, of the pressed pellets, result of the synthesis, at temperatures below the melting point of the final compound.

2.1.1 Weighing the starting elements

The first step when preparing is deciding the amount of sample we want to synthesise. The quantities are stoichiometric, and with the following example, one can understand how to obtain the quantities.

For our first sample, we wanted to obtain $5g$ of Zinc Selenide ($ZnSe$). Knowing the atomic weight values for the elements presented in the table 2.1, by its definition we can easily extrapolate the percentage each element in the sample. If we have one mole of Zn and one mole of Se, we have a sample of:

$$65,38_{g/mol} + 78,971_{g/mol} = 144,351_{g/mol}$$

This means that the sample is made of $45,29\% Zn$ and $54,71\% Se$. So, for a $5g$ sample we need $2,2648g$ of Zn and $2,7352g$ of Se.

Coumpound	Atomic Weight
Zn	65,38(2)
Se	78.971(8)

Table 2.1: Atomic weight of Zn and Se

For this measurements was used an Analytical balance from the company Kern, model ABT 100-5m . The samples were measured with a precision of $\pm 0,0001g$.

2.1.2 Homogenization

After having all the elements weighed and prepared, they are placed in a pyrolitic graphite boat, which in turn is loaded to a quartz ampoule. The boat is made of carbon and the ampoule of quartz to withstand high temperatures. Subsequently the ampoule must be evacuated, so the reaction occurs uniquely between the elements we had chosen and not with any residual gas present in the ampoule. To obtain this we use the vacuum system PM Z01 300 from Pfeiffer (21) . A plug made from a quartz rod is placed at the end of the ampoule to close it.

When the ampoule is evacuated to $10^{-5}mbar$, it is sealed using a Hydrogen-Oxygen flame, which is hot enough to melt down quartz, so applying the flame where the ampoule and the plug meet, the quartz melts and the plug is soldered to the ampoule, isolating its interior from the outside.

Afterwards, the sealed ampoules are placed in an one-zone tube furnace and annealed according to a plan previously defined. The furnace was made by the company Gero that has a range from $30°C$ to $3000°C$. (22) These furnaces allow us not only to control the temperature and time at which we leave a certain sample, but also the "speed" at which that temperature is reached.

It is important to be careful while choosing the maximum temperature the furnace will reach. This temperature should be at minimum $50°C$ lower than the melting temperature of the compound we are trying to synthesise.

2.2 X-ray diffraction

To determine the structure of a crystal, the most widely used technique is the X-ray diffraction. Contrary to the medical use of X-rays, in our case we are interested in the

diffracted beams, as the name suggests, and not in those that manage to travel through the crystal.

In 1895, Wilhelm Röntgen produced and detected the first X-rays, coincidently at around the same period as when the first studies about the the crystals symmetry were being conducted by the physicist Auguste Bravais and geologist William Barlow among others. Several crystal structures were proposed, but only later when the X-ray diffraction technique was more developed were they confirmed.

The electrons in the crystal will cause the X-rays to scatter in all directions, and hence will interfere constructive and destructively. Since a crystal is an arrangement of atoms in a particular pattern, it is possible to derive a law that describes the condition for constructive interaction to happen. This law is called Bragg's law. (4)

Having a look to a representation of a crystal structure, one can understand the geometry behind this law, by assuming the crystal structure as made out of parallel planes of ions spaced a distance d.

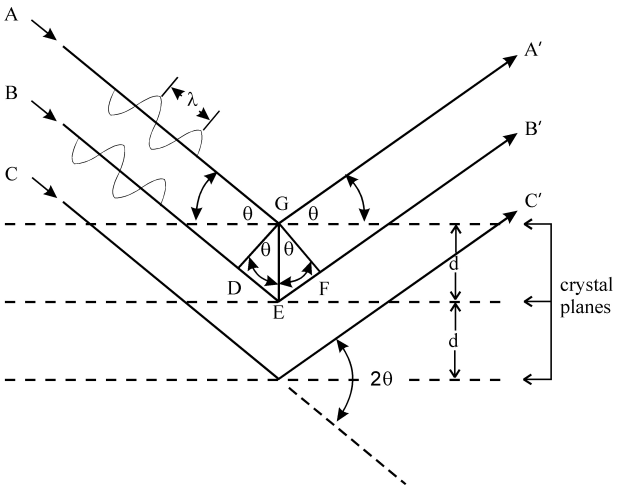

Figure 2.1: Schematic of Bragg's law

If the wavelength is constant, as in our case, the constructive interference will only happen at certain angles, depending on the atom forming the crystal. The path difference between the incident ray and the scattered ray is given by the Bragg equation (5)

$$n\lambda = 2d\sin(\theta) \tag{2.1}$$

The first X-ray diffractions were performed by Max von Laue together with Walter Friedrich and Paul Knipping, by irradiating a copper sulphate crystal with X-rays and using a photographic plate as a detector. The developed photographic plate showed a pattern of well-defined spots, making it possible to prove the scattering laws.

Our X-ray diffraction machine (XRD) is a X'Pert, built by the company Pananalytical. This XRD is composed of three main parts: the X-ray source, the sample holder and the sensor (18).

The same sample holder and schematics were used throughout the entire work, in an attempt to try to reduce any random error. The source was used with a 5mm mask, a divergence slit of $\frac{1}{4}^{\circ}$ and a $0,04RAD$ collimator. The sample holder was a sample spinner with a zero background base made of silicon. The sensor used was a PIXcel with a P8 slit, a $0,04RAD$ collimator and a Nickel filter.

The measuring program chosen was a three hours full scan with a step of $0,013132^{\circ}$

2.3 Rietveld Analysis

After having all the data collected, there's the need to analyse it in order to understand and characterize the structure of our sample. This is done using the Rietveld Refinement. This is a method developed by the Dutch scientist Hugo Rietveld (19) that consists on minimizing a function M that describes the difference between the observed data and the calculated data. M is defined as:

$$M = \sum_i W_i \left\{ y_{i,obs} - \frac{1}{c_s} y_{i,cal} \right\}^2 \tag{2.2}$$

Where $y_{i,obs}$ and $y_{i,cal}$ are respectively the observed data and the calculated data, W_i describes the statistical weight and c_s the overall scale factor. It is also defined for this method the Bragg factor, that is one of the parameters used to measure how good the refinement is:

$$R_B = 100 \frac{\sum_i \left| y_{i,obs} - y_{i,cal} \right|}{\sum_i \left| y_{i,obs} \right|} \tag{2.3}$$

The second parameter is the χ^2 factor. This factor is defined as:

$$\chi^2 = \left[\frac{R_{wp}}{R_{exp}}\right]^2 = \frac{100\left[\frac{\sum\limits_{i=1,n} w_i\left|y_i - y_{c,i}\right|^2}{\sum\limits_{i=1,n} w_i y_i^2}\right]^{\frac{1}{2}}}{100\left[\frac{n-p}{\sum\limits_{i}}\right]^{\frac{1}{2}}} \tag{2.4}$$

Where R_{wp} is the weighted profile factor, and R_{exp} is the expected weighted profile factor. All this calculations are done by computer, using a software suit called FullProf, developed by Juan Rodríguez-Carvajal of the Institut Laue-Langevin, Grenoble, France, that consists on a set of crystallographic programs. For the purpose of this work, we were interested in Winplotr, which allow us to analyse powder diffraction patterns

In our case, the refinements were made using a Thompson-Cox-Hastings pseudo-Voigt convoluted with axial divergence asymmetry function (16) , function number 5, that has the same half widths H_L and H_G, depending on:

$$pV(x) = \eta L'(x)+)(1-\eta)G'(x) \tag{2.5}$$

After choosing the best starting model for our samples and defining the background, we start by refining the scale factor and the Zero shift factor and the background. The next steps are the lattice parameters (a,b and c), the U, V, W and X values, the shape1 factor, the asymmetry parameters and the B_{iso}. If needed, also the preferred orientation factor would be refined, pref1. This factor describes the texturing, and if $pref1 > 1$ implies a needle like habit, $pref1 < 1$ a platy habit and $pref1 = 1$ implies no preferred orientation.

This is not an automatic method and the refinement is not trivial for every different type of sample, but this process was used as a base for all the refinements. The refinements of each sample will be discussed in detail in further chapters.

2.4 Scanning Electron Microscopy

To overcome the limits of typical optical instruments, some techniques use an electron beam to "illuminate" the sample. The interaction of the electrons with the sample allows a deeper understanding of the morphology and the bulk of the sample.

The interaction of electrons with matter produces different kinds of radiation: *Auger* and secondary electrons are created more on the surface, while back-scattered electrons

and characteristic X-rays are originated in the bulk. If we are more interested on the morphological information, the Scanning electron microscopy (SEM) is focused in the detection of *Auger* and secondary electrons, while if we want to know elemental differences we need to detect the back-scattered electrons.

Back-scattered electrons are also detected with the same technology as secondary electrons, so, to obtain more information about the surface than about the bulk, we need to make sure that mostly just the secondary electrons are detected. This is easy to obtain by choosing a specific geometry for the detector, since the back-scattered electrons follow a specific trajectory while the secondary electrons are emitted randomly.

We know that heavier atoms have a larger scattering cross section than lighter atoms, so by analysing the back-scattered electrons we can get the elemental differences in certain areas of the sample, even if morphologically they look the same.

2.5 Electron Microprobe Analysis - WDX

Another technique using an electron beam is the Electron Microprobe (EMPA). In this case, our radiation of interest is the characteristic X-rays emitted by the bulk, and with it, not only we can have the elemental composition of the sample, but also its relative composition. This means that with this technique, it is possible to determine how much, in %, of an element is present in a sample.

Characteristic X-rays are produced when an atom is bombarded with high-energy particles, may them be photons, electrons or ions. The collision between this particles and the atom will, in some cases, eject an electron from the electron cloud, the higher the energy of the beam, the deeper in the shell the ejected electron is located. This leaves a vacant energy level in the atom, which consequently will be fill by the electrons in the outer shells, emitting photons during this transition. The energy of the photons is quantized and equals the difference of energy between the shell of the vacant electron with the shell of the transiting electron. This transition is usually to the K-shell from an outer shell, and the energy of the emitted photon, X-ray, is unique for every element.

There are several techniques to analyse these characteristic X-rays, but we will focus on the one we used, the wavelength-dispersive X-ray spectroscopy (WDX). This method only detects X-rays with a specific wavelength per detector, which means that before starting a measurement we need to choose which elements we will be looking for. The

1% was performed together as for this samples we need ≈ 200 points per sample in order to have a result with some statistical meaning. During the transition between samples, some of the points registered belong to the glass. The spectra of the glass resembles noise and it is quickly distinguished from the spectra of the samples. As the data for the four samples collected in one file, the glass spectra is used as the separation between samples in the data analysis.

Having the graphics for all the mixtures presented as in figure 4.23b, each line represents one different point in the sample. With MATLAB, we can do a quick analysis of each line and distinguish if each line represents a CTSe grain or a secondary phase grain.

Analysing first the $ZnSe$ mixtures, we know by analysing the spectra of the pure samples that the main peak is located in different positions for the different compounds. One way to distinguish if either one line is $ZnSe$ or not, we can determine the maximum of that line in the cm^{-1} interval where the main $ZnSe$ peak is located. If the maximum is higher than a certain value, statistically we consider it a $ZnSe$ grain. If we count the number of points that can be considered $ZnSe$ and divide it by the total number of points measured, we obtain a good approximation of the percentage of secondary phase in the sample. The code shown in figure 4.25 does exactly that.

```
283 -    Z=0;
284 -  for q=1:m(2)
285 -       o=num(450:520,q);
286 -       M=max(o);
287 -      if M>30
288 -          Z=Z+1;
289 -      end
290 -  end
```

Figure 4.25: Example of the MATLAB code used to determine the presence of $ZnSe$.

We define the integer $Z = 0$ to count the number of times we detect a $ZnSe$ grain. The for loop from 1 to *m(2)* allows us to run the program through all the points measured for that sample. For each point, we create a new matrix containing the values just between the position of the $ZnSe$ peak, called *o*. With the MATLAB function *max()* we determine the maximum in that interval, if the maximum is higher than a value imposed by us, we increment 1 to the integer Z, if not, the loop continues. The results obtained with this technique are shown in table 4.12.

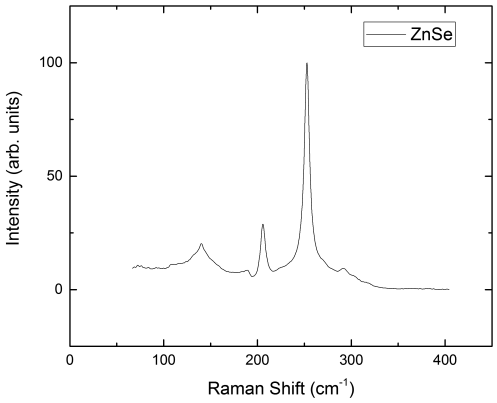

Figure 2.2: Raman scattering spectrum for $ZnSe$

The peaks belong to the eigenfrequencies Ω_j of the excitations, and analysing its properties like position and widths, we can obtain information about the crystalline quality and chemical composition of the sample. It is possible to derive semi-classically an equation for the intensity of the scattered light:

$$I_s = I_i \frac{\omega_s^4 V_{vol}}{(4\pi\epsilon\epsilon_0)^2 c^4} \left| e_s \tilde{\chi}(\omega_i, \omega_s) e_i \right|^2 \tag{2.7}$$

Where V_{vol} represents the scattering volume, $I_{s,i}$ and $e_{s,i}$ the intensity and polarization unit vector of the scattered and incident light, and $\tilde{\chi}(\omega_i, \omega_s)$, defined as:

$$\tilde{\chi}_{\alpha,\beta}(\omega_i, \omega_s) \propto \sum_{e,e'} \frac{\langle 0|p_\alpha|e'\rangle \langle e'|\hat{\mathcal{H}}_{E-L}|e\rangle \langle e|p_\beta|0\rangle}{(E_{e'} - \hbar\omega_s)(E_e - \hbar\omega_i)} \tag{2.8}$$

Where α and β are the directions of the scattered and incident light, $p_{\alpha\beta}$ the respective vector components of the dipole operator, $\hat{\mathcal{H}}_{E-L}$ the Hamiltonian of the interaction between the electron and the phonon, and $E_{e,e'}$ the energy of the electron and the phonon respectively.

Technically, to detect the Raman scattering, first we need to filter the Rayleigh scattering, which is typically much stronger, using notch filters and monochromators. The laser used was a red laser with an wavelength of $632,8nm$, a neutral density filter ND03 used to vary the laser intensity (measuring we got $1,2mW$) and a central wavelength of $251cm^{-1}$. The detector was cooled down until $-60°C$.

3

Synthesis of the powder samples

3.1 $ZnSe$

The first sample we prepared was the $ZnSe$. The synthesis seemed to be a simple process at first, but we encountered some difficulties in the first trials. The melting points for Zn, Se and $ZnSe$ can be seen in the table 3.1. On a first trial we programmed a fast reaction, table 3.2, but not only not all the material had reacted, as the Zinc shot seemed to not have melted.

Compound	Melting point (°C)
Zn	419,58
Se	221
$ZnSe$	1525

Table 3.1: Melting points of Zn, Se, and $ZnSe$

On a second trial, we increased the temperature and the heating time, table 3.3, but the result was the same. Taking the opportunity to analyse the sample before grinding it, we realise that the Zinc shots are covered by a thin layer of black and yellow powder, where the black powder corresponds to Selenium and the yellow powder to $ZnSe$.

K/h	Temperature(°C)	Time (h)
20	460	24
10	700	172

Table 3.2: Heating process for the first attempt of synthesising $ZnSe$

K/h	Temperature(°C)	Time (h)
20	450	24
10	650	24
10	850	336

Table 3.3: Heating process for the second attempt of synthesising $ZnSe$

Recalling the table 3.1, we realise that the $ZnSe$ will not melt at the temperature reached by the furnace, hence the Zinc will be prevented from reacting with selenium and its shape is preserved. This means that having big pieces of Zinc will always prevent the complete reaction of all the sample, since as soon as the exterior of the Zinc piece starts melting, it reacts with the selenium synthesising $ZnSe$ around it and stopping the reaction.

In order not to delay the experiment, we bought industrially made $ZnSe$ and used it throughout the rest of the experiment, but as a personal milestone we decided to try one more time to obtain $ZnSe$. By our understanding of what happened, the heating process was not the problem since even during the first attempt we obtained some $ZnSe$, so we used a very similar on for this last attempt, table 3.4, only this time staying a total of 34 days in the furnace.

K/h	Temperature(°C)	Time (h)
20	450	10
20	750	792

Table 3.4: Heating process for the third attempt of synthesising $ZnSe$

What we changed in this last attempt was the preparation of the samples. Using material that have not reacted in the previous two synthesis we prepared two samples, and using new starting elements to produce two more grams of $ZnSe$ we prepared a third sample. The samples were prepared in three different ways, but always following the same idea, the Zinc should be in small pieces and mixed as homogeneously as possible with the selenium.

For the two first samples, the Zinc pieces were cut into smaller pieces with a pliers and mixed everything with the $ZnSe$ and Se powder we obtained in the previous synthesis. One of the samples, that we designated as "$ZnSe$ I" was pressed into a pallet and then

sealed, while the other, that we designated as "$ZnSe$ II" was just homogeneously mixed in the carbon boat and sealed.

The third sample, that we designated as "$ZnSe$ III", was prepared using laminated Zinc and mixed homogeneously in the carbon boat. As we can see by the results in figure 3.1, just by looking at the samples we can notice which of the samples reacted as expected, since the color of $ZnSe$ is yellow, and Selenium is black.

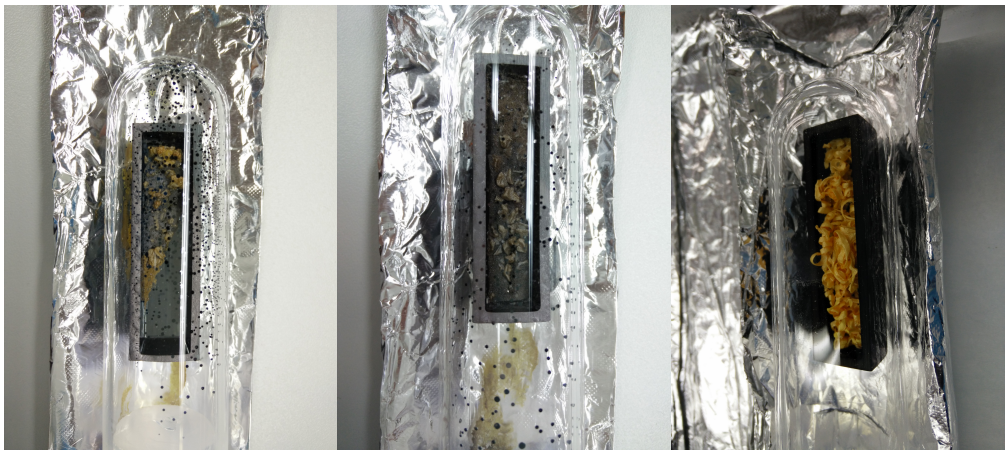

(a) $ZnSe$ I **(b)** $ZnSe$ II **(c)** $ZnSe$ III

Figure 3.1: $ZnSe$ synthesis

With this we conclude that the reaction that creates $ZnSe$ is very fast, since by looking closely at sample III in figure 3.1c we notice that the $ZnSe$ formed as the exact same shape of the laminated Zinc used.

3.2 Cu_2SnSe_3

The second sample we tried to obtain was the ternary Cu_2SnSe_3. On our first trial we programmed the furnace to heat the sample as showed in table 3.5, and not only all the material reacted, as we also obtained a few single crystals. Some of the single crystals were removed for being analysed later by single crystal X-ray diffraction, while the rest of the sample was ground and observed with powder X-ray diffraction.

K/h	Temperature(°C)	Time (h)
10	250	24
10	450	24
10	640	200

Table 3.5: Heating process for the Cu_2SnSe_3 synthesis

Giving a quick look at the diffractogram we observe some obvious secondary phases, so we proceed to do an homogenization of the sample. We pressed the sample into a pellet, placed it in a small quartz ampoule and then sealed it after evacuated.

The pressing is done using a hydraulic pressing tool. The powder to press is placed in a special holder for this procedure. After everything is ready, we place the holder in the pressing tool, as we can see in figure 3.2a.

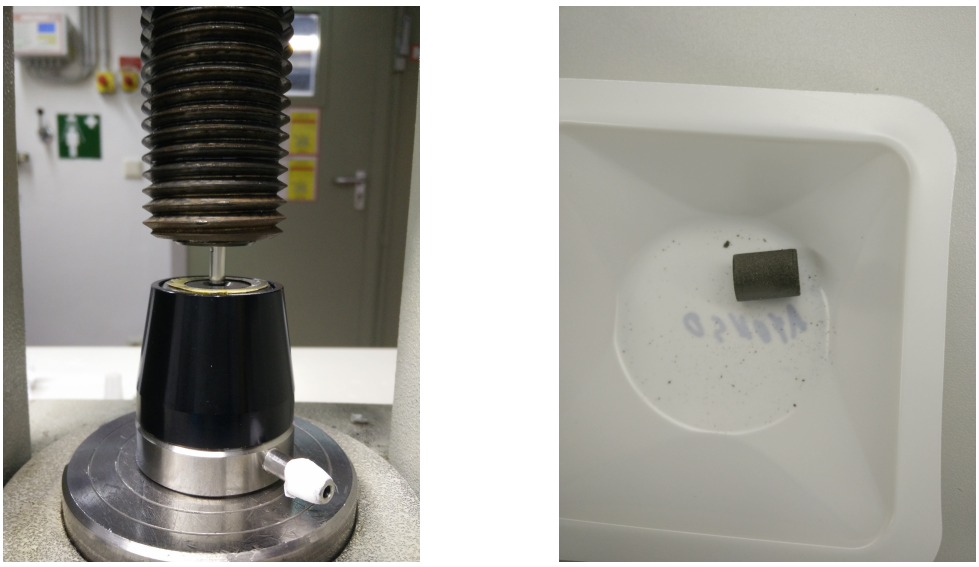

(a) The holder in the pressing tool **(b)** CTSe pellet

Figure 3.2: The pressing tool and an example of a pellet

Pulling the leaver of the pressing tool, we start to apply pressure to our sample. This is done slowly and always being careful not to surpass the limit pressure of the holder, in our case $5bar$. Then, the sample would stay for a few minutes under that pressure, removing it from the holder afterwards and obtaining the pellet that we can see in figure 3.2b.

The heating process described in table 3.6 is used. In order to avoid secondary phases, we program the cooling to be slow. As for higher temperatures the cooling rate is faster than the one chosen, and it is possible to "slow it down" with the furnace, but for lower temperatures the cooling rate is slower and the total time can not be determined so easily.

K/h	Temperature(°C)	Time (h)
50	640	312
50	20	-

Table 3.6: Annealing process for the Cu_2SnSe_3 sample

4

Results

4.1 Electron Microprobe Analysis - WDX

As explained in section 2.5, the WDX analysis allow us to determine the quantity of each element present in the sample. This is very important as a first step of the analysis, as we know the stoichiometry that we expect to obtain, and therefore, if we obtained the desired compound or not.

To prepare the samples for microprobe, it is only needed a very small amount of powder, not more than $0,1g$. The preparations were all made by Mrs Behr and the measurements done with the help of Dr. Galina Gurieva.

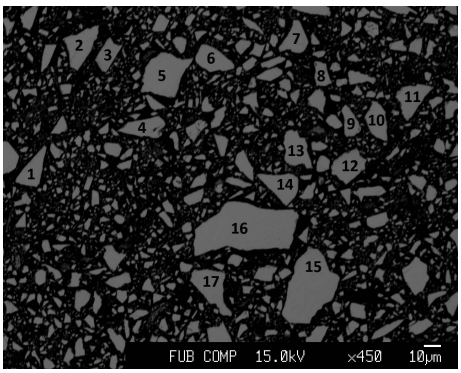

Figure 4.1: BSE micrograph of the $ZnSe$ sample (grey - $ZnSe$ grains, black - epoxy matrix)

For each sample 45 grains were chosen, and in each grain 10 points were measured in order to have good statistics and observe eventual secondary phases. In figure 4.1 we

can an example of the grains selected for the WDX analysis of the $ZnSe$ sample.

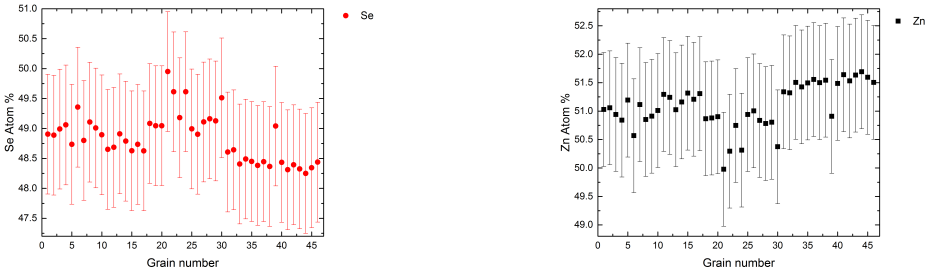

(a) Selenium **(b)** Zinc

Figure 4.2: Results of the WDX analysis for the sample $ZnSe$

The samples that were analysed were the industrial $ZnSe$, the ternary Cu_2SnSe_3, and the two samples of $Cu_2ZnSnSe_4$, Kest1 and Kest2. In figure 4.2 we can observe the results for $ZnSe$, and in 4.3 for Cu_2SnSe_3. All the graphics have the error bars of 1%.

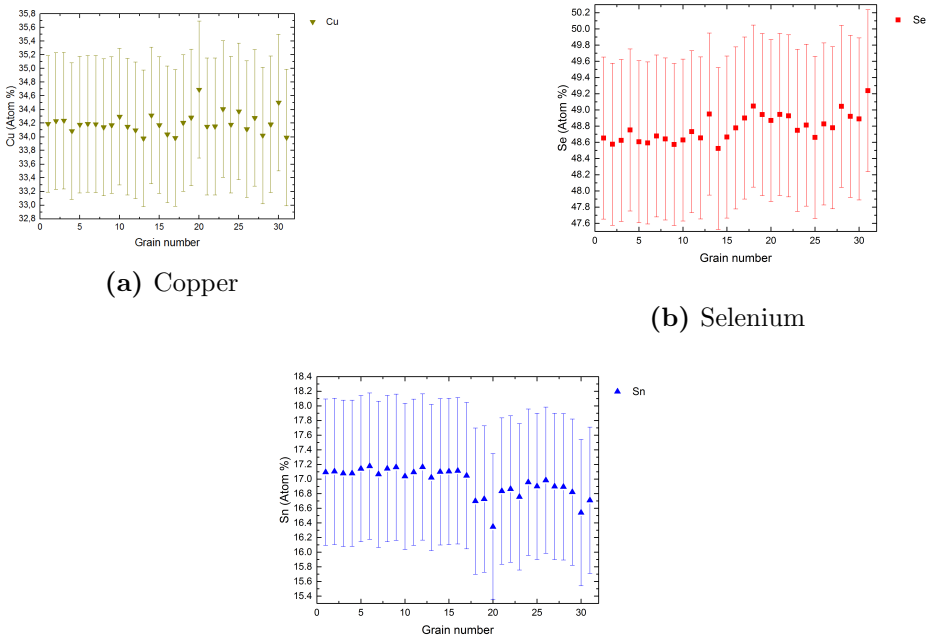

(a) Copper

(b) Selenium

(c) Zinc

Figure 4.3: Results of the WDX analysis for the sample Cu_2SnSe_3

We can observe that for $ZnSe$ the stoichiometry is very much respected. All of the points that we have chosen to analyse have Zn and Se in its composition in a ratio close to the proportion of 1:1. In table 4.1 we can see an average of the percentage of each element of all points.

Cu (%)	Se(%)
51,1	48,84

Table 4.1: Averages of the values obtained with the WDX analysis for the sample $ZnSe$

In figure 4.3 we have the results for the ternary. The stoichiometry desired seems to be obtained, since the points in the graphics seem to be within the errorbar. It was important for our project to understand that our sample had the three elements uniformly distributed throughout all the grains. As a first approach in our analysis, this would mean that our synthesis produced a ternary, and not only single elements.

Zn (%)	Sn(%)	Se (%)
34,2	16,96	48,78

Table 4.2: Averages of the values obtained with the WDX analysis for the sample Cu_2SnSe_3

In table 4.2 we see an average of the percentage of each element in all the grains of the sample, confirming the stoichiometry. In figure 4.4 we se the WDX results for the first sample of kesterite.

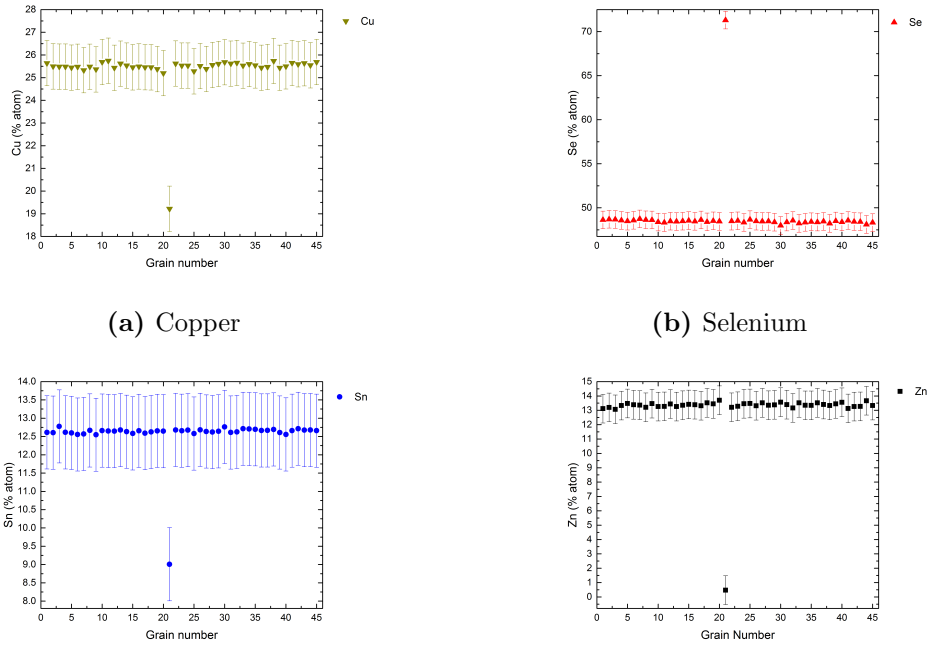

(a) Copper **(b)** Selenium

(c) Tin **(d)** Zinc

Figure 4.4: Results of the WDX analysis for the sample $Cu_{1,98}Zn_{1,04}Sn_{0,84}Se_4$

Looking closely to the four graphics, with the exception of grains number 21, the desired stoichiometry seems to be respected. Looking closely to 4.4d we see that the quantity of Zinc is approximately 0%, Copper around 19%, Selenium 71% and Tin 9%. With this quantities we can say that the secondary phase found in this grains is not $ZnSe$ nor Cu_2SnSe_3, but as it is just one grain we can dismiss it. Making the average for all grains we obtain the results shown in table 4.3.

Cu (%)	Zn (%)	Sn(%)	Se (%)
25,5	13,4	15,6	48,5

Table 4.3: Averages of the values obtained with the WDX analysis for the sample $Cu_{1,98}Zn_{1,04}Sn_{0,84}Se_4$

Using an algorithm to determine the real stoichiometry of our sample, we obtain $Cu_{1,98}Zn_{1,04}Sn_{0,84}Se_4$. The sample is 85% B-type and 15% F-type (14), meaning that it is Cu-poor and Zn-rich.

The kesterite structure has the ability to deviate from stoichiometry. (15) Taking into account the charge balance, four cation substitution reactions and related intrinsic point defect complex formations were proposed: A-type Cu-poor/Zn-rich where copper is substituted forming a copper vacancy (V_{Cu}) and zinc on copper antisite (Zn_{Cu}), B-type Cu-poor/Zn-rich where copper and tin are substituted by zinc forming zinc on copper (Zn_{Cu}) and zinc on tin (Zn_{Sn}), C-type Cu-rich/Zn-poor which zinc substitutions form copper on zinc (Cu_{Zn}) and tin on zinc (Sn_{Zn}) defects and D-type Cu-rich/Zn-poor where copper substitute zinc forming copper on zinc antisite (Cu_{Zn}) and additional copper interstitial (Cu_i)(14). An illustration of these cation substitutions can be seen in figure 4.5.

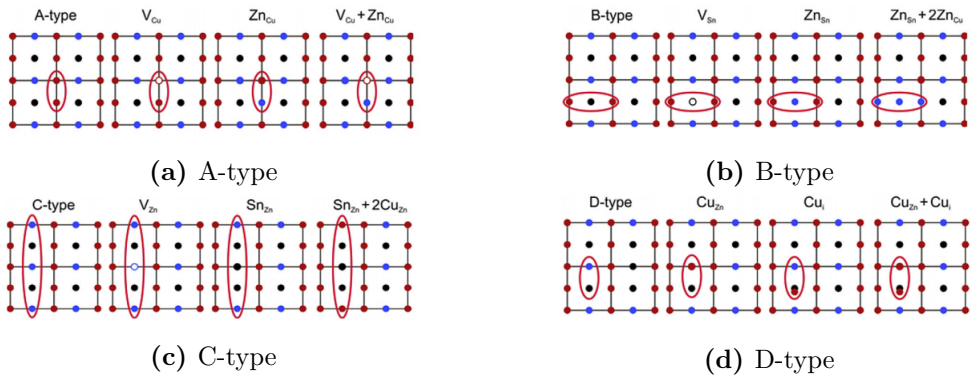

(a) A-type **(b)** B-type

(c) C-type **(d)** D-type

Figure 4.5: Illustration of the cation substitution process resulting in A-, B-, C- and D-type off-stoichiometric CZTS/Se. The circles represent: copper in red, zinc in blue and tin in black.

The same was done for the sample *Kest II*. In figure 4.6, we see two grains that are completely off of what was expected. Looking closely to its percentages, we realise that Copper and Tin are approximately 0% of the elements present in that grain, and that Zn and Se are present at a proportion of 1:1, so it is expected that the secondary phase present in this grains is $ZnSe$. This is why we chose to mix the sample *Kest II* with the ternary, and not with the $ZnSe$.

In table 4.4 we can see the averages for all the grains with the exception of grains 2 and 40. The stoichiometry obtained was $Cu_{2,01}Zn_{1,03}Sn_{0,98}Se_4$, being 48% B-type, and 52% F-type.

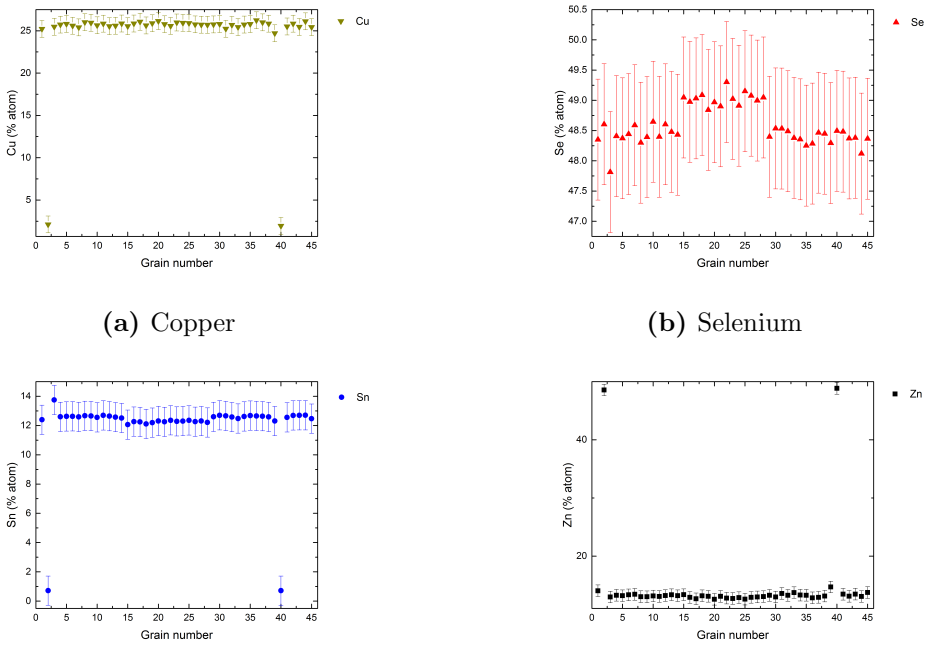

(a) Copper **(b)** Selenium

(c) Tin **(d)** Zinc

Figure 4.6: Results of the WDX analysis for the sample $Cu_{2,01}Zn_{1,03}Sn_{0,98}Se_4$

Cu (%)	Zn (%)	Sn(%)	Se (%)
25,7	13,2	12,5	48,6

Table 4.4: Averages of the values obtained with the WDX analysis for the sample $Cu_{2,01}Zn_{1,03}Sn_{0,98}Se_4$

4.2 X-ray Diffraction

In this chapter we will analyse the data obtained with the X-ray diffraction technique, at a first approach we will analyse the diffractograms in a qualitative and comparative approach, and then the refinements will be presented.

4.2.1 $ZnSe$

For the purpose of our work, it is very important to characterize the pure samples before starting the mixtures. For $ZnSe$ the interest of comparing the pure sample is

even greater as although we bought, and used, industrially made $ZnSe$, we were also able to synthesise it in the laboratory.

As said in 3.1, we were able to grow three different samples of $ZnSe$, $ZnSe$ I, $ZnSe$ II and $ZnSe$ III. By the colour of the powders obtained, it is possible to foresee that we obtained $ZnSe$ with some secondary phases for the two first, and $ZnSe$ for the latter, but only recurring to the X-ray diffraction technique can we be certain of that. Having bought industrially made $ZnSe$, we can in a first phase compare the diffractograms of the synthesised samples with the industrial one, using it as the standard measurement.

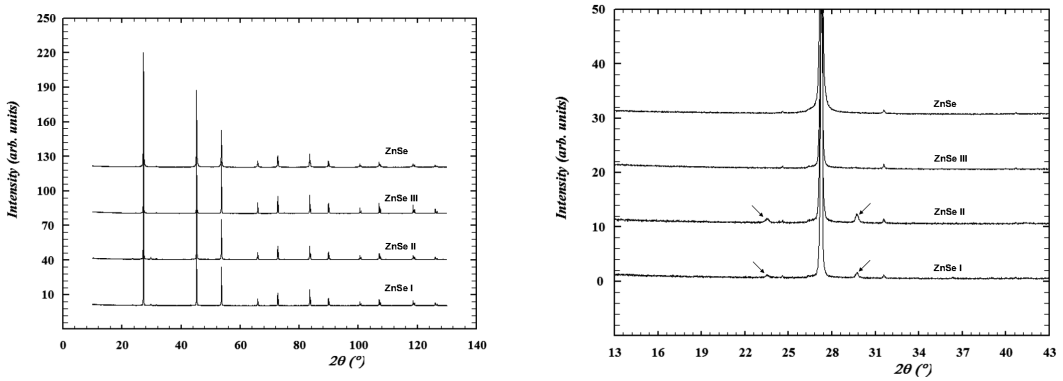

(a) Complete diffraction pattern

(b) Detail of the 111 peak.

Figure 4.7: Comparison of the diffraction patterns for the synthesised and industrially grown $ZnSe$

As we can see in figure 4.7, the four patterns are quite similar, but already by looking at the entire diffractrograms, figure 4.7a, it is possible to see some differences in the samples $ZnSe$ I and $ZnSe$ II comparing with the Industrial $ZnSe$. Looking closely to the main peak, figure 4.7b, the differences are even more obvious.

Between the values 22° to 25° and 28° to 31° of 2θ, we observe two peaks that do not occur for the industrial $ZnSe$ and the sample $ZnSe$ III. These two peaks prove the existence of secondary phases in those two samples, although we can not tell which secondary phase it is just by looking at the diffraction pattern, but we can assume it to be Selenium. We make this assumption having the knowledge of the growing process.

All the three samples were synthesised using starting materials with a purity of $99,999\%$, placed in a carbon boat and evacuated in order to assure the reaction occurs just between the elements we have chosen. Thus said, the only possible secondary

phases would have been the starting materials if the totality of them had not reacted. As described in 3.1, samples $ZnSe$ I and $ZnSe$ II did not reacted entirely. In both cases the Zinc shots were intact, and surrounded by an yellow and black powder, $ZnSe$ and Se respectively. This, and the fact that $ZnSe$ III does not show any secondary phases, leads us to believe that the secondary we detect in the diffractogram is a result of the inability of separating the powders.

4.2.2 Mixtures

Having done all the X-ray diffraction measurements, it is interesting to look at the diffractrograms and see if there is any visible difference comparing the mixtures with the CZTSe. Plotting all the data in one graph, we can compare how the difractogram evolves with different quantities of secondary phases. In figure 4.8 we can see the graphics of $Cu_2ZnSnSe_4$ and $ZnSe$, and $Cu_2ZnSnSe_4$ and Cu_2SnSe_3, before mixing the powders.

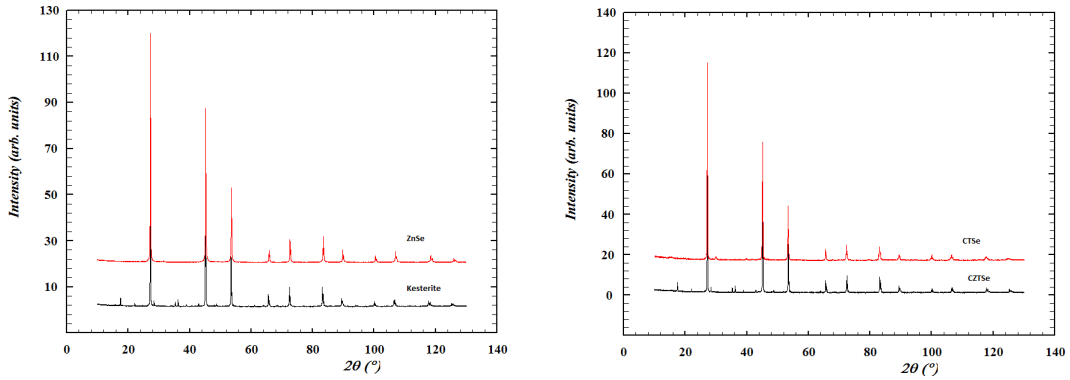

(a) Diffractogram of $Cu_2ZnSnSe_4$ and $ZnSe$

(b) Diffractogram of $Cu_2ZnSnSe_4$ and Cu_2SnSe_3

Figure 4.8: Diffractograms for the CZTSe, CTSe and $ZnSe$ samples

4.2.2.1 Mixtures of $Cu_2ZnSnSe_4$ and $ZnSe$

First we analyse the mixtures of $Cu_2ZnSnSe_4$ and $ZnSe$. In the figure 4.9 we can see the entire graph of all the mixtures, as well as the difractogram of the pure $Cu_2ZnSnSe_4$ as a comparison.

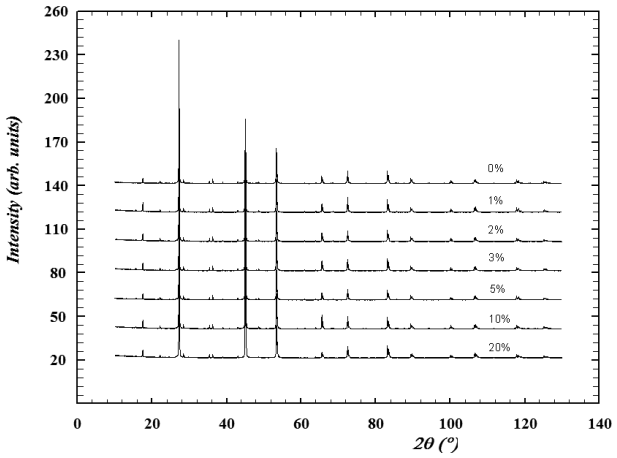

Figure 4.9: The complete diffractogram for the mixture $ZnSe$ and $Cu_2ZnSnSe_4$

It is already possible to observe some changes related with the amount of secondary phase, but it is hard to describe them. It is important to notice that, the higher the value of 2θ, the bigger the shift between $ZnSe$ and $Cu_2ZnSnSe_4$. This is due to the fact that $ZnSe$ is cubic, while $Cu_2ZnSnSe_4$ is tetragonal. Zooming in some specific peaks we are able to better understand what is happening. Figure 4.10 shows the peak 112.

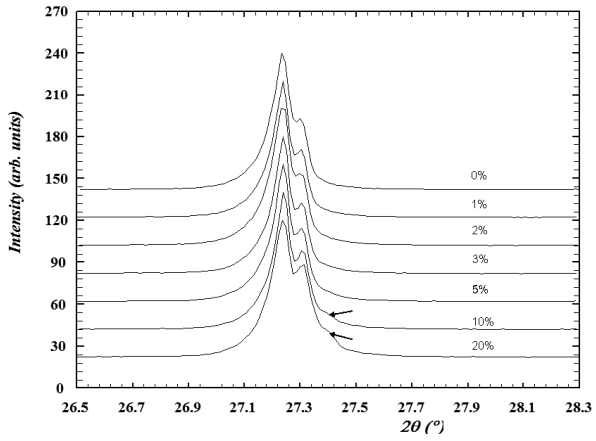

Figure 4.10: Zoom of the 112 peak for the $ZnSe$ mixtures

We were expecting to observe some changes in the peak shape for high 2θ values, due to the different structures of the two samples, but these changes can already be detected for small 2θ values. This changes are due to the difference in the lattice parameters, while for the cubic structure the lattice parameters have the same value, in the tetragonal

we have $c \approx 2a$, thus explaining the differences in the diffraction pattern. In this peak, 4.10, the mixtures with 20 and 10% of $ZnSe$ we see a small shoulder appearing on the right side of the peak. This is the 111 peak from the $ZnSe$ sample overlapping with the peak 112 from the CZTSe sample.

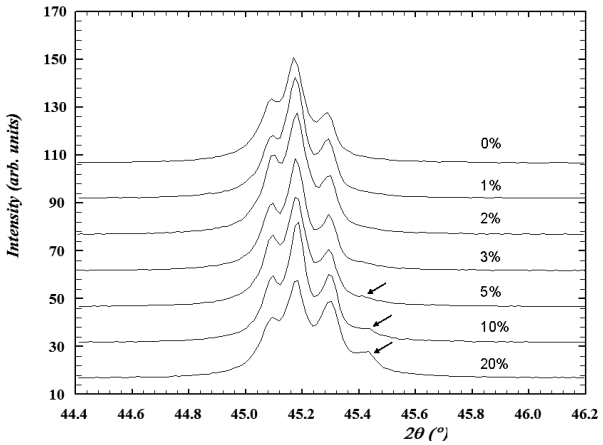

Figure 4.11: Zoom of the 220 peak for the $ZnSe$ mixtures

In figure 4.11 we see a zoom for a peak located at higher values of 2θ, the peak (2 2 0). Once again, we see a small shoulder appearing on the right side, only this time we see the influence of the $ZnSe$ peak for the 5% mixture, due to the already explained difference between the two structures.

4.2.2.2 Mixtures of $Cu_2ZnSnSe_4$ and Cu_2SnSe_3

Analysing the diffractrogram of the mixtures of $Cu_2ZnSnSe_4$ and Cu_2SnSe_3, we observe that the differences between the two patterns are harder to distinguish, but we expect for higher concentrations of the secondary phase some slight changes. In figure 4.12 we can see the complete diffractrogram.

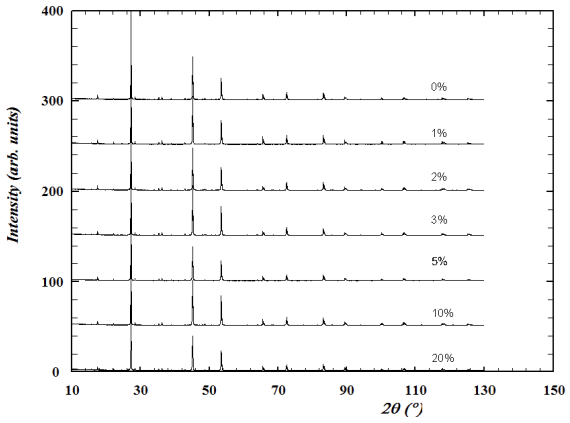

Figure 4.12: The complete diffractogram for the mixture Cu_2SnSe_3 and $Cu_2ZnSnSe_4$

In figure 4.13 we see a zoom in of the main peak, 112. This is probably due to the small protuberance visible on the left side of the pure Cu_2SnSe_3 peak.

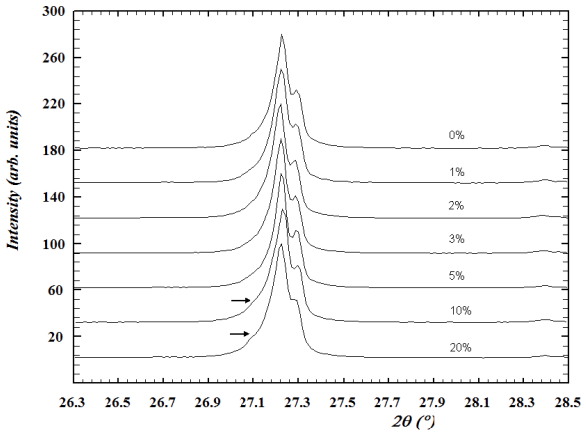

Figure 4.13: Zoom of the peak 112 for the CTSe mixture

This is due to the different peak shapes for the Kesterite and the CTSe, as we can see in figure 4.14. The right side of both peaks is quite similar, but CTSe peak has a second peak on the left side, non existing in the CZTSe pattern. The influence of this second peak is very weak, and thus just noticeable for higher concentrations.

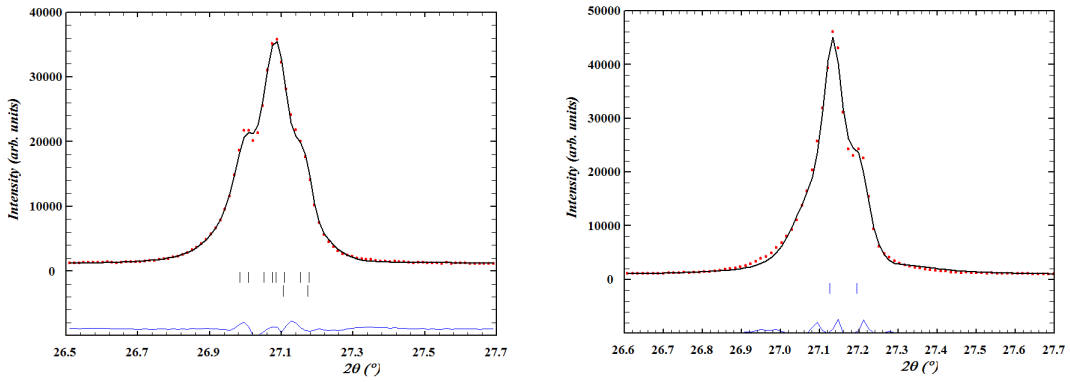

(a) 112 peak for the CTSe sample.

(b) 112 peak for the CTZSe sample.

Figure 4.14: Comparison between the main peaks for CZTSe and CTSe.

4.2.3 Simulations

As we proved in the last two sections, the presence of the secondary phases is visible just by analysing the differences between the patterns for higher concentrations with the pure CZTSe. This is specially true for the mixtures with $ZnSe$, as we can observe differences in the pattern in several peaks, while for CTSe just in the main peak we can perceive its presence.

With the program PowderCell it is possible to simulate powder patterns, and thus we can verify if the differences between the patterns are also visible in the simulations, and if so, verify if for other off-stoichiometric Kesterite samples this changes also appear. This simulations will just be done for the $ZnSe$ mixtures, as the changes were more noticeable, and for a concentration of 20% of secondary phase.

For this simulations, we load the .cel files for $ZnSe$ and for CZTSe and, for each sample, replace the values for the lattice and peak shape parameters with the ones obtained when refining the pure samples. This gives us the simulation of our samples, changing the scale factor in order to obtain the desired ratios (0.2 for $ZnSe$ and 0.8 for CZTSe), we can now use the option Sum from the PowderCell menu. This will give us the sum of the two simulated patterns, meaning, it will simulate a sample composed of 20% $ZnSe$ and 80% of CZTSe.

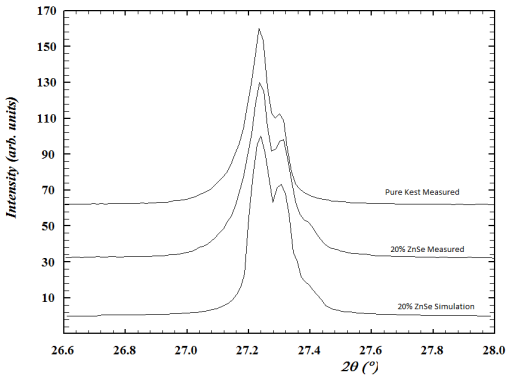

Figure 4.15: Detailed view of the simulated and measured pattern with the pattern for pure CZTSe

In figure 4.15 we observe the same broadening in the main peak in the simulated pattern as in the measured pattern. With the same procedure, we can now simulate the same mixture for different off-stoichiometric CZTSe. The sample used to be mixed with $ZnSe$ in the experimental part of this work is 85% B-type and 25% F-type, and we simulated the following:

- 3% A-type 97% B-type
- 25% A-type 75% B-type
- 37% A-type 63% B-type
- Stoichiometric

For this, we use the lattice parameters found in the article "Existence of off-stoichiometric single phase kesterite" (14) and replace them in the simulation. For this we use the same peak shape parameters and the $ZnSe$ simulation remains unaltered. In figure 4.16 we can see the detail of the 112 peak for all the simulated patterns. The broadening is visible in all of the simulations, independently of the slight shift that was expected for the different samples.

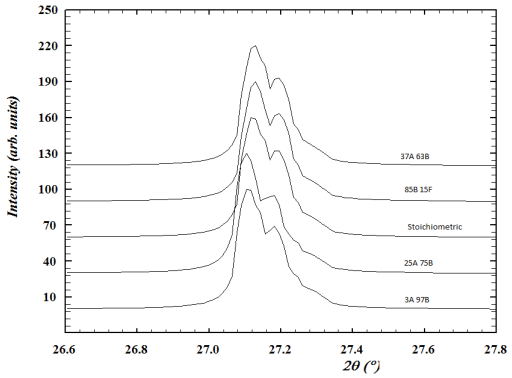

Figure 4.16: Comparison between all the simulated patterns.

By comparing the simulation of the mixtures with the simulation of the off-stoichiometric CZTSe samples, we assure ourselves that the broadening is distinguishable from the pure sample, and we can predict that the experiment could be successfully conducted with different CZTSe samples and be able to detect $ZnSe$ in the samples.

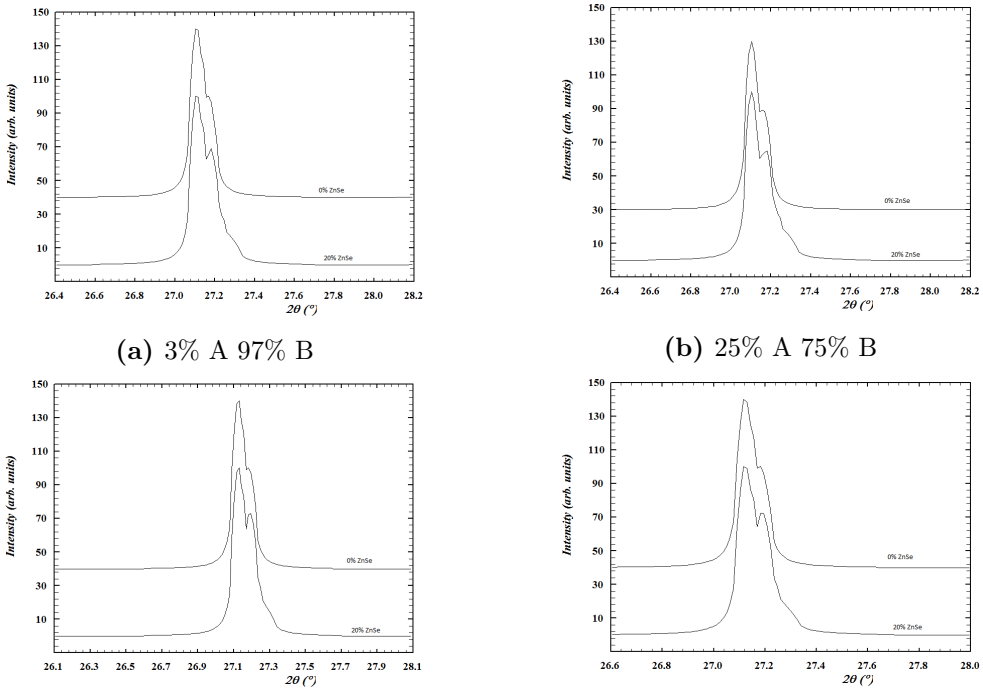

(a) 3% A 97% B

(b) 25% A 75% B

(c) 37% A 63% B

(d) Stoichiometric

Figure 4.17: Comparing the simulated mixtures and pure CZTSe

4.2.4 Rietveld Analysis

FullProf allows us to perform a quantitative analysis of our crystalline sample. For that, we first need the refined diffractrogram of the pure samples we want to determine as a reference.

The intensity of the diffracted radiation by a crystalline phase is proportional to the quantity of irradiated material. Measuring a multiphase powder like our mixtures, the scale factor for each point of the diffractrogram can be written as:

$$S_j = \frac{C'}{\mu}\Big(\frac{V}{V_c^2}\Big)_j = \frac{C'\rho'}{\mu'}\Big(\frac{V}{\rho V_c^2}\Big)_j \tag{4.1}$$

In equation 4.1 ρ and μ represent the density and the linear absorption coefficients of the solid substance, while ρ' and μ' of the powder. The terms C and C' have the experimental constants that apply to all the contributing phases of the diffraction pattern. The linear absorption of the phase j present in the sample is

$$\mu_j = (\rho' V)_j \tag{4.2}$$

Where $(\rho' V)_j$ is the mass of the same compound by unit cell. Having the mass by elementary formula M_j of the phase j and Z_j the number of elementary formulae by unit cell, we get the relation:

$$S_j \propto \frac{m_j}{(ZMV_c)_j} \tag{4.3}$$

From this we understand that, for samples with an negligible absorption, the masses of different phases of the mixture are proportional to $S_j(ZMV_c)_j$, where S_j is the scale factor obtained for the phase j in the Rietveld analysis. (12) By constraining the sum of the weight fractions present in the sample we get:

$$W_j = \frac{S_j Z_j M_j V_{cj}}{\sum_i^N S_i(Z_i M_i V_{ci})} \tag{4.4}$$

This relation allows us to determine the relative mass of any of the components. In a mixture of N different phases, the weight fraction W_j of the phase j give by FullProf is given by (13) :

$$W_j = \frac{S_j Z_j f_j^2 M_j \frac{V_j}{t_j}}{\sum_i^N \Big(S_i Z_i f_i^2 M_i \frac{V_i}{t_i}\Big)} = \frac{S_j A T Z_j V_j}{\sum_i^N (S_i A T Z_i V_i)} \tag{4.5}$$

With:

$$ATZ_j = Z_j f_j^2 \frac{M_j}{t_j} \tag{4.6}$$

Where:

- S_j is the scale factor of the phase j
- Z_j is the number of formula units per cell
- M_j is the molar mass of the unit cell
- V_j is the volume of the unit cell
- f_j is used to transform the site multiplicities to their true values. We obtain $f = 1$ for a stoichiometric phase if these multiplicities are calculated by dividing the Whyckoff multiplicity m of the site by the general multiplicity M. Otherwise $f = Occ\frac{M}{m}$, where Occ is the occupation number.
- t_j is the Brindley coefficient that accounts for micro-absorption effects, defined as

  $$t_j = \frac{1}{V_j} \int e^{-(\mu_i - \bar{\mu})x} dV_j$$

  where:

  - V_j is the volume of a particle
  - μ_j is the linear absorption coefficient of the particles
  - $\bar{\mu}$ is the average linear absorption coefficient of the solid material of the powder sample
  - x is the trajectory of the radiation through the particle of phase j, reflected by an element of volume dV_j

The parameter t_j takes into account the effects of micro-absorption that become very important when the powder coefficients of linear absorption of the present compounds are very different. (12)

Taking this into account, the first step is to refine the XRD results of the samples *Kest I* and *II*, CTSe and *ZnSe*.

4.2.4.1 Rietveld Analysis for $Cu_2ZnSnSe_4$

We start by refining the sample $Cu_{1,98}Zn_{1,04}Sn_{0,84}Se_4$, and we follow a procedure very similar to the one described in section 2.3. The background is selected manually point by point. In this case we have a single phase kesterite sample, that has a Tetragonal type of structure so we use the space group *I -4*.

The starting values for the lattice parameters were chosen according to the existent literature, while the starting values for the peak shape parameters were taken from the resolution file created for the calibration of the X-ray diffractometer. For our set of refinements no resolution file was used.

The refinement is started as explained in 2.3, and the fit runs smoothly. Lattice parameters, peak shape parameters and shape parameter are refined. At this point we see that the refinement could still be largely improved, and that it seems to have a very strong asymmetry, so we start refining the asymmetry parameters, refining *Asy1, Asy2, Asy3* and *Asy4*. After correcting the asymmetry the fit seems to describe quite well the diffractrogram without any preferred orientations. The specifications of the refinement are described in table 4.5.

a,Å	c, Å	$\frac{c}{2a}$	R_{Bragg}	χ^2
5,6964(4)	11,3506(9)	0,996	6,88	3,63

Table 4.5: Lattice parameters, Rbragg and χ^2 for $Cu_{1,98}Zn_{1,04}Sn_{0,84}Se_4$

For the sample $Cu_{2,01}Zn_{1,03}Sn_{0,98}Se_4$ the refinement process was conducted as before. The fit had a very strong asymmetry that was corrected by refining the asymmetry parameters. The specifications of the refinement are described in table 4.6.

a,Å	c, Å	$\frac{c}{2a}$	R_{Bragg}	χ^2
5,6941(9)	11,3454(4)	0,996	5,73	1,93

Table 4.6: Lattice parameters, R_{Bragg} and χ^2 for $Cu_{2,01}Zn_{1,03}Sn_{0,98}Se_4$

4.2.4.2 Rietveld Analysis for $ZnSe$ and Cu_2SnSe_3

The same process was carried for $ZnSe$. As with the previous refinements for the Kesterite samples, the asymmetry is noticeable but not so strong as in the previous

cases. To correct the asymmetry we refine the parameters *Asy1* and *Asy2*. With the asymmetry corrected, we observe that there is still a very strong preferred orientation in the 111 peak. By refining the parameters *Pref1* and *Pref2* we correct considerably the preferred orientation. The parameter *Pref1* has a value of $0,69425$ which means that the texturing has a platy habit. In table 4.7 we can see the specifications of the refinement.

a,$\mathring{A}$	R_{Bragg}	χ^2
5,671(6)	3,06	6,01

Table 4.7: Lattice parameters, R_{Bragg} and χ^2 for $ZnSe$

Although we obtained a good refinement, by looking closely to the region of 2θ values between 24 and 25, there is a peak that is unaccounted by the fit. We can see this peak in figure 4.18a. This peak can be explained by the K_β emission from the X-ray beam that also diffracts in the sample. We can simulate that using the program PowderCell as we can see in figure 4.18b, plotted together with the pattern for $ZnSe$.

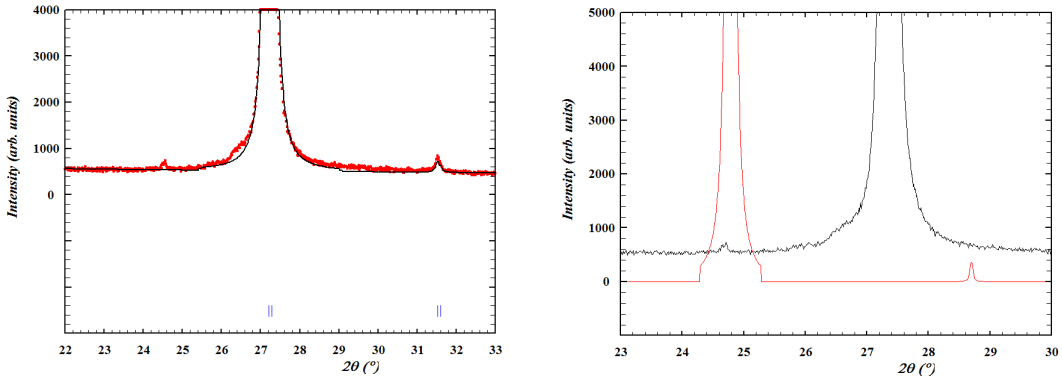

(a) Zoom of the K_β peak.

(b) Simulation of the K_β peak.

Figure 4.18: Zoom of the K_β radiation present in the $ZnSe$ pattern and respective simulation.

Judging by the position of both the simulated K_β emission and the unaccounted peak, we can assume that it is the result of the diffraction of K_β radiation.

For the CTSe, the process is the same, although we have to be careful as CTSe has two different phases. As we can see in figure 4.19, trying to refine just with one phase does not give a satisfactory fit, thus we must use both the monoclinic and cubic phase, *C 1 c 1* and *F -43m* respectively.

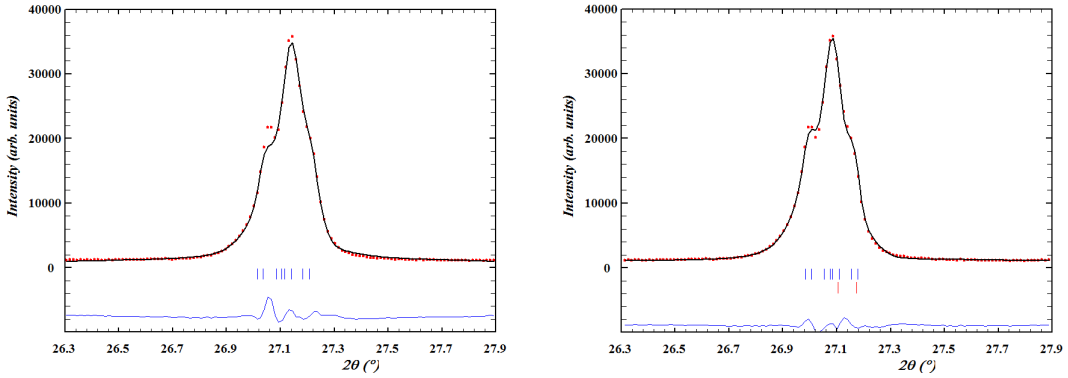

(a) Refinement using one phase. **(b)** Refinement using two phases.

Figure 4.19: Zoom of the 111 peak for the refinements of CTSe using just one phase with the space group *F -43m*, 4.19a, and using two phases with *F -43m* and *C 1 c 1* space groups, 4.19b

Refining a sample with two phases require more attention as the program, by trying to find the best fit can assign values that make no physical sense to the refined parameters more easily than when refining just one phase. Taking that into consideration, the refinement can proceed as described in section 2.3.

Once more there was the need to refine the asymmetry parameters. The parameters *Asy1* and *Asy2* were refined in both phases. The refinement could still be improved has it seemed to have some preferred orientation in one of the peaks characteristic from the *C 1 c 1* phase. The parameter *Pref1* was refined for that phase, and it reached the value 0,97549, meaning that like *ZnSe* the texturing has a platy habit.

C 1 c 1					*F -43m*		
a,Å	b,Å	c,Å	R_{Bragg}	χ^2	a,Å	R_{Bragg}	χ^2
6,992(6)	12,072(5)	6,972(3)	10,55	2,74	5,6934(1)	3,71	2,74

Table 4.8: Lattice parameters, R_{Bragg} and χ^2 for CTSe

4.2.4.3 Rietveld Analysis for the Mixtures

For the analysis of the mixtures, we follow what is described in section 4.2.4 in order to obtain the fraction of each phase present in the mixtures. For each measurement the refinement procedure is similar to the one performed in the pure samples. We first

select the background points manually and add them to the .PCR file. The .PCR file is prepared for a two phases analysis, the CZTSe phase and the secondary phase that was mixed.

The starting values for the lattice parameters and the peak shape parameters are taken from the previous refinements for the pure samples. These parameters will not be refined. The only parameters to be refined are the *Zeroshift*, the scale factor and the background. Before starting the refinement, it is necessary to make sure that the ATZ parameter is zero in both phases.

The same procedure is repeated for all the samples with different percentages of secondary phase. In a first analysis just the three factors referred before are refined, a procedure that we called Scale Technique. As we know that factors such as the asymmetry and the preferred orientation depend of the way the measurement is performed, and not only of the powder composition, so in a second analysis also the preferred orientation and asymmetry parameters are refined, a procedure that we called Asymmetry Technique. The results are shown in table 4.9.

$ZnSe$ weighed in (%)	Scale Technique (%)	Asymmetry Technique (%)
20,30	3,56	3,14
10,26	1,26	1,18
4,94	0,58	0,58
3,01	0,58	0,12
1,92	0,13	0,29
0,93	0,00	0,00

Table 4.9: Percentages of $ZnSe$ expected compared with the obtained refining just the Scale factor and Zeroshift and refining also the asymmetry and preferred orientation.

For the mixtures with CTSe, the preparation of the .PCR file is the same. Although to refine the pure CTSe measurement we used two phases, cubic and monoclinic, in the mixtures it makes no sense to include the monoclinic phase, as its contribution in the mixtures is minimal and the peaks positions overlaps the positions of CTZSe. The results showed in table 4.10 were obtained excluding the *C 1 c 1* phase from the .PCR file. It was tried to include the phase in the .PCR but for concentrations bellow 20% CTSe the results for the percentage of the *C 1 c 1* phase were always zero.

CTSe weighed in (%)	Scale Technique (%)	Asymmetry Technique (%)
19,26	12,48	14,33
9,64	10,48	15,96
4,50	5,17	5,94
2,78	1,72	2,55
1,58	2,16	4,03
1,18	0,63	4,13

Table 4.10: Percentages of CTSe expected compared with the obtained refining just the Scale factor and Zeroshift and refining also the asymmetry and preferred orientation.

The same techniques were used in a different method. While for the previous results the structural information was inserted manually, that information can also be taken from the .hkl files. If in the .new file of the *pure* samples refinements we make the parameter *Hkl* 5, the output in the .hkl file will be the Miller indices, hkl, *mult*, F_{calc}, T_{hkl}, d_{hkl} and Q_{hkl}, where F_{calc} is the module of the calculated structure factor.

Using this .hkl file can be used as an input, allowing for a quantitative analysis without recalculating the structure factors (11). This is done by making the parameters $Jbt = -3$ and $Irf = 2$ in the .new file. The results obtained with this method can be seen in table 4.11.

$ZnSe$ weighed in (%)	Scale Technique (%)	Asymmetry Technique (%)
20,30	3,56	3,14
10,26	1,31	1,15
4,94	0,60	0,64
3,01	0,16	0,19
1,92	0,16	0,18
0,93	0,00	0,00
CTSe weighed in (%)	Scale Technique (%)	Asymmetry Technique (%)
19,26	13.73	14.13
9,64	10.54	15.55
4,50	5.37	6.05
2,78	1.71	2.60
1,58	2.59	4.60
1,18	0.02	0.79

Table 4.11: Percentages of $ZnSe$ and CTSe expected compared with the obtained using the .hkl files and refining just the Scale factor and Zeroshift and refining also the asymmetry and preferred orientation.

4.3 Raman Spectroscopy

The second technique used to analyse our samples was the Raman Spectroscopy. All the measurements were performed in the Helmholtz-Zentrum Berlin with the help of Dr. Sergej Levcenco.

4.3.1 Characterization of the samples

Raman Spectroscopy is a qualitative measurement, and it was widely believed that it was not possible to detect $ZnSe$ with a red laser (wavelength of $632.8nm$). Our work not only proved that it is possible to detect it, but that it has a very strong signal. The first measurements performed had the purpose to characterize our samples and were done with an exposure time of sixty seconds, recording five points per sample, and averaging the five points in order to obtain the graphics of figure 4.20.

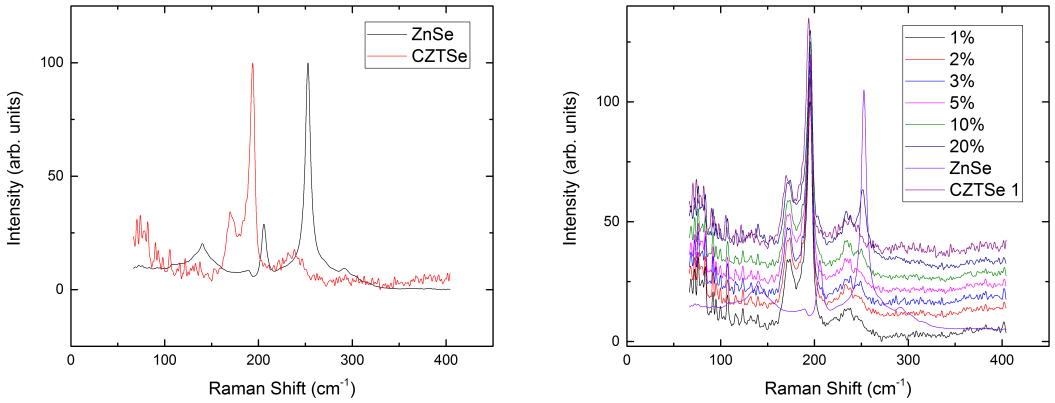

(a) $ZnSe$ and CZTSe. **(b)** All the samples with $ZnSe$

Figure 4.20: Raman Spectroscopy for the mixtures of $Cu_2ZnSnSe_4$ and $ZnSe$.

The graphics were normalized to the interval [0 - 100]. In figure 4.20a we have the spectra for the pure samples, and we observe that $ZnSe$ has a well defined spectra, easy to distinguish from CZTSe. In figure 4.20b we have the spectra for all of the samples plotted together with an offset to facilitate the viewing. Here we can compare how the presence of $ZnSe$ in CZTSe changes the shape of its Raman spectra. Analysing this graphic, we notice the appearance of a peak in the spectra of the mixtures in the position for the main peak of $ZnSe$. The intensity of this peak increases with the concentration of $ZnSe$. This fact helped us develop a quantitative technique out of the qualitative method by using some mathematical tools, that will be explained further on.

The same characterization process was done for the samples with CZSe, with the same exposure time and number of points per sample. The result can be seen in figure 4.21.

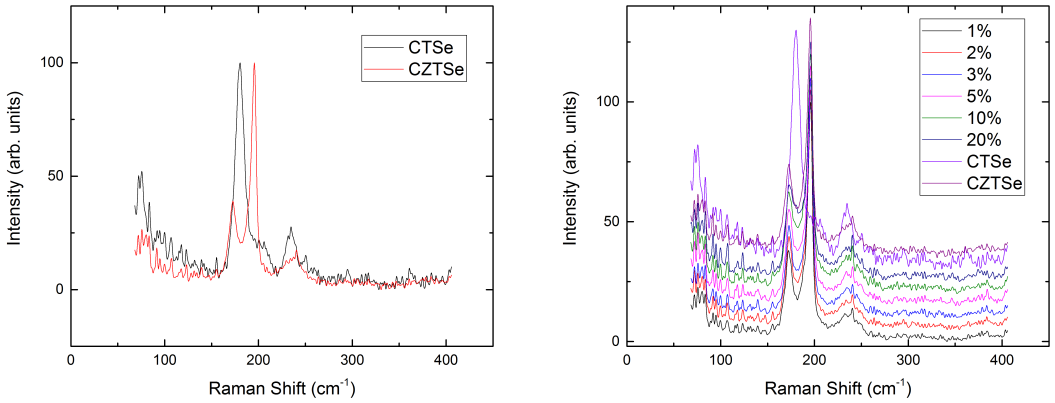

(a) Pure CZTSe and CZSe.

(b) All the samples with CZSe.

Figure 4.21: Raman Spectroscopy for the mixtures of $Cu_2ZnSnSe_4$ and Cu_2SnSe_3.

In figure 4.21a we can see the spectra for the pure samples of CZTSe and CTSe, once again normalized to the interval [0 - 100]. Here we can observe that the main peaks for both samples are very close to each other, meaning that it will be harder to detect its influence in the mixtures. Analysing figure 4.21b we realise just that, the only significant change is a slight broadening between the main peak and the smaller peak located to its left.

It is important to note that the graphics are normalized to 100, but that in reality the spectra for CTSe has a lower intensity than CZTSe, explaining why the second higher peak for CTSe located approximately at $250cm^{-1}$ does not have an effect on the mixtures.

4.3.2 Quantitative Method

As explained before, the Raman Spectroscopy is a qualitative technique, meaning that with each measurement it is possible to determine what compound is present in a certain area of our sample. The laser used has a spot-size of $3\mu m^2$, and the grains from our samples were between $6-100\mu m^2$ before grinding, so it is reasonable to assume that, measuring one of the mixtures, each point can be located in one grain, either of CZTSe or one of the secondary phases being studied, or in the edge between two grains.

Thus said, if we start looking to this experiment from a statistical point of view, the probability of detecting one grain of one of the secondary phases will correspond to its percentage in the mixture. If we register enough points, one can determine the number of points that correspond to the secondary and to CZTSe phases and speculate the quantities of each with statistical meaning.

The equipment allows us to perform line scans in order to measure several points. For instance, if we take the mixture of 20% $ZnSe$ and measure sixty points, 20% of the points should be of $ZnSe$, which means twelve of the sixty points would be of $ZnSe$ and the others of CZTSe. But if we analyse the sample with 1% $ZnSe$ registering the same number of points, statistically we would not detect any point of $ZnSe$. This means that, although sixty point gives already a good statistical result for the 20% mixtures, to analyse the less concentrated ones we need more points.

There were two main challenges to do so. One is that there is no software that could handle the data collected. The graphics shown in figure 4.20 and 4.21 were plotted using the Origin software (23) as we only had five points per sample, being possible to remove manually all the cosmic ray peaks, but for the analysis we intended, that would not be practical. The other is that we need to focus the laser on the surface of our sample, in order to obtain a good spectra.

To tackle the first challenge, we chose to use MATLAB (24). As the data collected was saved in a .txt file, using MATLAB we can easily read any .txt or .xls file an convert it to a matrix and analyse it with the several mathematical tools available in the software.

The .txt file came in a quite confusing format, each point measured was separated by a vertical spacing and the standard x-scale. Copying all the information to an Excel file and using the Text to columns tool with the option of one vertical space we obtain an .xls in which each line represents one of the measured points. By personal preference, the data would be transposed in order to have each column representing one measurement. With function xlsread we can transfer the information to a matrix in MATLAB.

Thus we have one matrix with all the intensities where each column is a different point. To obtain the x-scale, meaning the Raman shift axis, we need to calibrate the Raman spectrum with a red light near the region of the laser, between $638,299nm$ and $640,225nm$ (in cm^{-1}, $136,14$ and $183,27$). We then upload it to MATLAB in a different matrix. The calculations for the calibration were all done by Dr. Sergej Levcenco.

Having the data organized in this way, it would be rather trivial to plot all the points in the same graph using a for loop. But the detection of cosmic rays is quite frequent, and thus we need to filter them in order to obtain a clean spectra. As the detector of the Raman equipment is a charge-coupled device (CCD), it is impossible to avoid the detection of cosmic rays.

The cosmic rays detected in our measurements are typically more intense than our spectra and very steep. On a first phase, we level all the peaks above a certain intensity to the average of the baseline of our spectra. The baseline is defined as the line where our spectra begins and is supposed to be zero. The rest of the cosmic rays need to be filtered in a different way.

```
filename='20znse.xlsx';
x='xscale.xlsx';
num = xlsread(filename);
xscale=xlsread(x);
m=size(num);
num(num > 1200)=760;
for i=1:m(2)
 [pks,locs] = findpeaks(num(:,i));
 l=length(locs);
for j=1:l
     a=num(locs(j),i);
     b=num(locs(j)-1,i);
     c=num(locs(j)+1,i);
     if a-b>100 && a-c>100
        num(locs(j),i)=(c+b)/2;
     end
end
     hold on
     num(:,i)=smooth(num(:,i));
     figure(1)
plot(xscale(175:860,1),num(175:860,i))
box on
title('20 % ZnSe')
xlabel('Raman shift (cm^{-1})')
ylabel('Intensity (arb. units)')

end
```

Figure 4.22: Example of the code to filter the cosmic rays and plot the Raman spectra.

In figure 4.22 we can see an example of the code used to plot the data for the sample with 20% $ZnSe$. In order to be more efficient, the plot of the graphic is done in the same loop used to filter the cosmic rays.

Analysing the code, in the first four lines we see what was already described to create two matrices, *num* and *xscale*, containing the intensities of the Raman measurement and the x-scale, respectively. Then, we define m as the size of the matrix *num*. m is a vector and *m(1)* gives us the number of lines and *m(2)* the number of columns. Next in line six we have first phase of cosmic ray filtering, where all the points with an intensity higher than 1200 are matched to 760. This values are chosen by doing a previous single measurement to know what we are expecting, and also by analysing the plot obtained

with this code. If we are removing any peak of interest or not removing enough cosmic ray peaks, that will be visible in the plot and we can correct these values.

For the rest we use a loop inside a loop. With the first for loop, we are able to analyse each column matrix *num*, and for each column we identify all the peaks of that column using the function *findpeaks*. That function will save two vectors, *pks* that contains the information of the intensity of the peak, and *locs* that contains the information about the positions of said peaks. Knowing the length of the vector *locs* we can analyse each peak individually using another for loop.

As the cosmic rays peaks are very steep, if the intensities in the neighbouring positions of the Raman shift differ considerably we can assume that it is a cosmic ray. That is what we compare in the loop, for every peak detected previously, we make the floats *a, b* and *c* correspond to the intensity of the peak, the intensity of the position right before the peak and to the intensity of the position right after the peak. If the difference between the intensities is greater than a certain value (in our case 100, as that it approximately the difference of intensities between the main peak and the baseline), we equal that peak to the value of the average of the surrounding positions.

We can now plot all the graphics in the same figure. For that we need to use the *hold on* command so that MATLAB wont delete the graphics for each new cycle. We use a function to smooth the data to obtain a cleaner graphic.

To solve the second problem, our approach was to make a pellet with our powder samples. The pellets were done using the same procedures as for the annealing process for the CTSe sample, 3.2, but using a smaller quantity of powder, around $0.1g$.

Using pellets we came across two problems. First, the pellets are very fragile, and as they were pressed in a different laboratory from where the Raman measurements were performed, it happened quite often that the pellet would break during the transport, destroying the flat surface that we needed.

Second, as we can see in figure 4.23a, it was not possible to detect $ZnSe$ using pellets. Measuring 1534 points not even one of the points detected the secondary phase for the mixture of 10% $ZnSe$, which is statistically very unlikely. We repeated the same measurement for a powder sample, pressing the powder in a glass slide, but this time measuring only 50 points. Looking at figure 4.23b we see clearly that $ZnSe$ was detected.

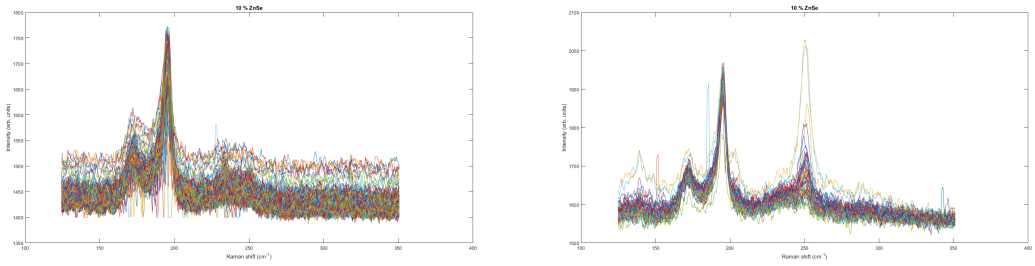

(a) Pellet sample. **(b)** Powder sample.

Figure 4.23: Comparison between the Raman measurements for the pellet and the powder sample. For the pellet were measured 1534 points, while for the powder only 50.

From this point forward, we used only powder samples, pressing them carefully to obtain a flat surface. In order to optimize the measuring time, as we needed a large number of points per sample for the mixtures with smaller percentages of secondary phase, we developed a technique to perform a line scan of several samples with just one measurement overnight. The experimental set-up can be seen in figure 4.24, the glass slides where the powder samples were pressed powder samples were placed side by side and the line scan was programmed to start in a point in the first sample, and finish in a point in the last sample.

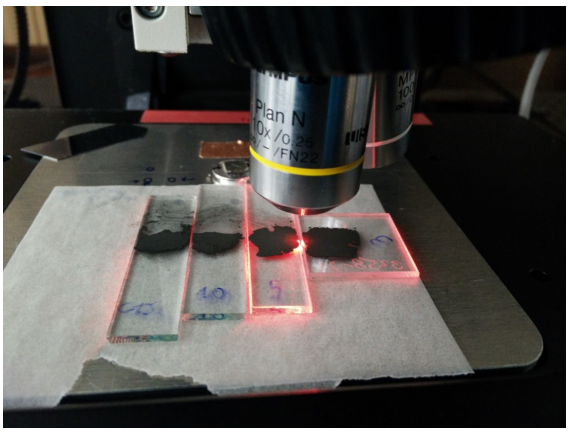

Figure 4.24: Experimental Set-up used to perform a line Raman scan of several sample with just one measurement.

The sample holder of the Raman equipment allowed us to perform the scan of four samples at the same time. The scan for the samples with quantities of 5%, 3%, 2% and

1% was performed together as for this samples we need ≈ 200 points per sample in order to have a result with some statistical meaning. During the transition between samples, some of the points registered belong to the glass. The spectra of the glass resembles noise and it is quickly distinguished from the spectra of the samples. As the data for the four samples collected in one file, the glass spectra is used as the separation between samples in the data analysis.

Having the graphics for all the mixtures presented as in figure 4.23b, each line represents one different point in the sample. With MATLAB, we can do a quick analysis of each line and distinguish if each line represents a CTSe grain or a secondary phase grain.

Analysing first the $ZnSe$ mixtures, we know by analysing the spectra of the pure samples that the main peak is located in different positions for the different compounds. One way to distinguish if either one line is $ZnSe$ or not, we can determine the maximum of that line in the cm^{-1} interval where the main $ZnSe$ peak is located. If the maximum is higher than a certain value, statistically we consider it a $ZnSe$ grain. If we count the number of points that can be considered $ZnSe$ and divide it by the total number of points measured, we obtain a good approximation of the percentage of secondary phase in the sample. The code shown in figure 4.25 does exactly that.

```
283 -    Z=0;
284 -  for q=1:m(2)
285 -       o=num(450:520,q);
286 -       M=max(o);
287 -      if M>30
288 -          Z=Z+1;
289 -      end
290 -  end
```

Figure 4.25: Example of the MATLAB code used to determine the presence of $ZnSe$.

We define the integer $Z = 0$ to count the number of times we detect a $ZnSe$ grain. The for loop from 1 to *m(2)* allows us to run the program through all the points measured for that sample. For each point, we create a new matrix containing the values just between the position of the $ZnSe$ peak, called *o*. With the MATLAB function *max()* we determine the maximum in that interval, if the maximum is higher than a value imposed by us, we increment 1 to the integer Z, if not, the loop continues. The results obtained with this technique are shown in table 4.12.

$ZnSe$ weighed in (%)	$N°$ of measured points	$ZnSe$ obtained (%)
20,30	61	21,31
10,26	54	12,96
4,94	295	4,40
3,01	311	2,89
1,92	219	1,82
0,93	286	0,35

Table 4.12: Results obtained for the mixtures of $ZnSe$ and CTSe using a quantitative method of the Raman spectroscopy.

The value chosen to compare with M to determine if either the peak belonged to the secondary phase or not could be determined by looking at each graphic independently at first, as the values for the intensities are arbitrary, depending on the exposure time and the focus of the laser. As we can see in figure 4.23 the baseline is not the same for all the points measured.

This can be solved by calculating the average of each measurement, and subtracting each value of that measurement by its average. This will give an offset that will align the baseline of all the points to zero, removing the inherent focusing problem of measuring powder samples, and also of performing line scans of multiple samples.

All the mixtures with $ZnSe$ were measured with an exposure time of 30 seconds, so all the measurements will have approximately the same maxima after we correct the baseline to zero. In this situation the value for the maximum in the *pure* CZTSe spectra is around 20 and 25 arbitrary units, so we can define the value to compare with M to be 30.

Performing a line scan for a quantitative the same exposure time is used for all the points, and for the CTSe mixtures that time was 60 seconds. Unlike $ZnSe$, CTSe has a less intense Raman spectra than CZTSe, as was said before. Looking at figure 4.26 we see the graphical representation of the average for all the measured points in the line scan for each *pure* sample, CZTSe and CTSe. The data was corrected by adding an offset, so it keeps the real amplitude and we can distinguish the differences in the intensity, while in figure 4.20 the data was normalized individually to have a better perception of its shape and peak position. We can see that the main peak for the ternary barely has the same intensity as the small peak of the quaternary.

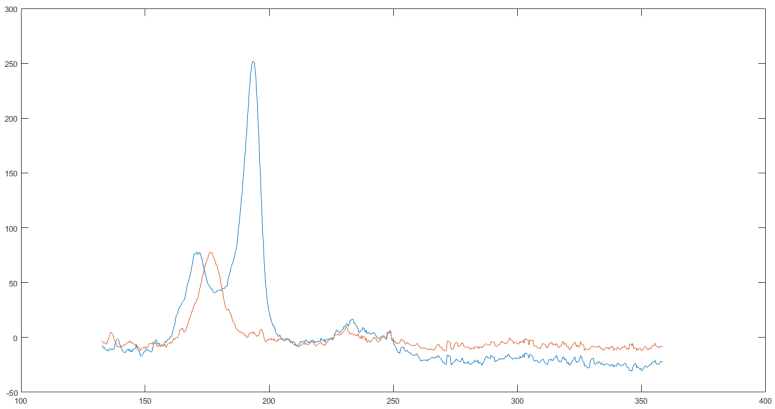

Figure 4.26: Comparison of the spectra for CZTSe and CTSe for an exposure time of 60s. The blue line represents the CZTSe sample and the orange line the CTSe sample.

This makes it virtually impossible to detect if we have detected a CTSe grain or not due to the inherent noise associated to any measurement and the incapability of perfectly filter the cosmic peaks. The opposite could be done and assume that a CTSe grain was detected if the main CZTSe peak was not present in the spectra, but such occurrence was not detected in any of the points of any of the different mixtures. This means that every time a CTSe grain was under the laser, also a grain of CZTSe was detected and their spectra would overlap.

This force us to try and find different solutions, although not having any success. The intensity of the mixtures spectra visibly reduces compared to the CZTSe, but no reliable relation that could give us a quantitative result was found.

5

Discussion

Taking into account the results shown in its respective chapter, we can start by dividing the discussion in two parts, corresponding to the two different secondary phases mixed. First we will analyse the results for the $ZnSe$ mixtures and later on the results for the CTSe mixtures.

In table 5.1, the results differ largely comparing the two different techniques used. With the XRD, the results fall short compared to the expected percentages, while using Raman the results are closer to the expected.

Although the percentages obtained using XRD differ greatly from the expected, the values are proportional. At first the possibility of loosing powder each time the sample was handled was considered. $ZnSe$ is a very adherent powder, being very hard to handle, and our sample in particular having very small grains was more susceptible to stick in the bottle where the sample was saved or in the holder for the XRD measurement.

$ZnSe$ weighed in (%)	XRD Scale (%)	XRD Asymmetry (%)	Raman (%)
20,30	3,56	3,14	11,00
10,26	1,26	1,18	8,00
4,94	0,58	0,58	5,08
3,01	0,58	0,12	2,57
1,92	0,13	0,29	1,84
0,93	0,00	0,00	0,35

Table 5.1: Comparison of the results obtained for the $ZnSe$ samples with the different techniques used throughout our work.

To verify if this was the case, we mixed two more samples with 20%$ZnSe$, one using the same industrial $ZnSe$ as before, another with the synthesised sample described in section 4.2.1. For both cases, the measurement was performed immediately after the mixture was ready in order to avoid using bottles or other kind of recipients where some powder could be lost.

New Industrial $ZnSe$		
Weighed in (%)	Scale Technique (%)	Asymmetry Technique (%)
19,95	4,14	3,80
Synthesised $ZnSe$		
Weighed in (%)	Scale Technique (%)	Asymmetry Technique (%)
20,52	1,83	1,82

Table 5.2: Results for the new $ZnSe$ samples using XRD

As we can see in table 5.2, although for the mixture with synthesised $ZnSe$ gives a smaller percentage, the mixture with industrial $ZnSe$ gives consistent results comparing with values in table 5.1. This means that the program might be underestimating the presence of the secondary phase. It is possible to estimate a value for this underestimation, by plotting all the points and performing a linear fit with a first degree function of the type $y = mx$, where m is the slope. In our case it makes no sense to add a invariable constant to the function, as for a mixture with 0% of secondary phase the program should give zero.

The slope of the function will give us an idea of how much the program is underestimating, and possibly be able to correct the results in order to obtain values closer to the expected. In figure 5.1 we can see the plot of both the results of the XRD and Raman, and respective fits. The fit was performed with the program Gnuplot, and the slope obtained were 0,16 with an asymptotic error of $7,685\%$ for the points obtained with the scale technique, and 0,15 with and error of $7,49\%$.

Defining $U = \frac{1}{a}$ as the the factor by which the measurements were underestimated by FullProf, where a is the slope of the linear fits, we get $U_{scale} = 6,17$ and $U_{asymmetry} = 6,89$, for the scale and asymmetry technique respectively. If we perform a linear fit to the points for both techniques together, we get a slope of 0,15 with an error of $5,387\%$ that gives and factor $U = 6,51$.

We can assume that FullProf underestimates the fraction of $ZnSe$ by a factor of $U \approx 6,5$, probably due to the overlap of the CZTSe peaks with the $ZnSe$ peaks.

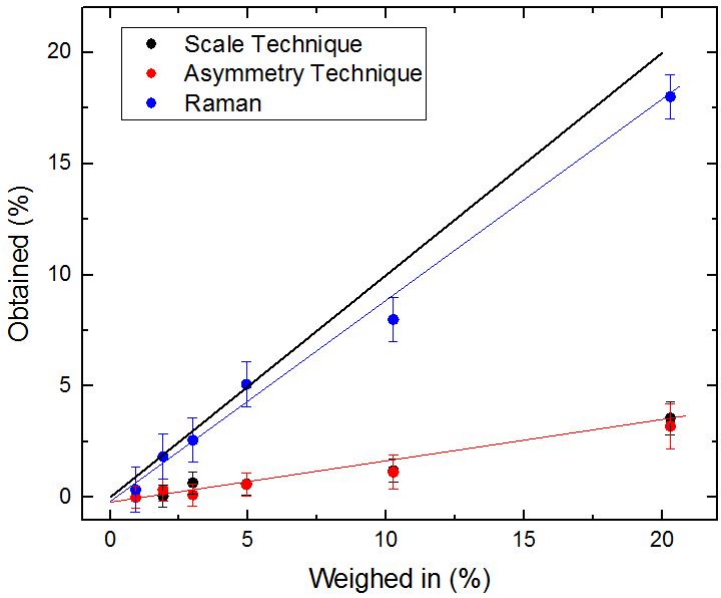

Figure 5.1: Comparison between the percentages values obtained for $ZnSe$ using different techniques.

We can also conclude from table 5.1 and figure 5.1 that for mixtures of 3% $ZnSe$ and below the results obtained with the XRD are no longer reliable. While for the mixtures of 5% the values obtained are still consistent with the linear fit, for 3 and 2% its values start making no sense, where depending of the technique we can have the same percentage for 3% as for 5%, or a higher percentage for 2% than for 3%. For 1% the value obtained is always zero, confirming that it is below the detection limit.

Regarding the Raman results, the values that differ more from the ones for higher concentrations of the secondary phase. This is due to the fact that for the mixtures with 20% and 10% were measured just 60 and 50 points respectively, while for all the remaining samples were measured $\approx$ 200 points per sample, as we see in table 4.12. It is important to note that in the points where $ZnSe$ was detected, also CZTSe was detected, meaning that in the spotlight of the laser are present grains of both samples.

Technically, and taking in account the results in table 4.12, we can say that with our samples we didn't reach the detection limit. Statistically, if we measure enough points

we ought to have a reliable result, and that seems to be the case with our measurements. But if we take a closer look the the graphics obtained for the mixtures of 2% and 1%, we realize some limitations of our technique. In figure 5.2 we can see the spectra of both mixtures.

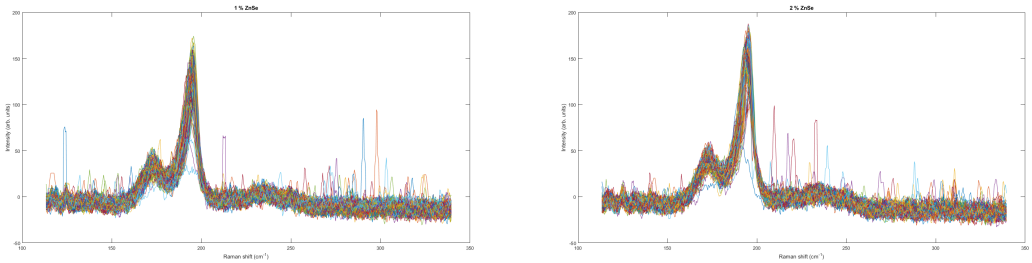

(a) Sample with 1% $ZnSe$. **(b)** Sample with 2% $ZnSe$.

Figure 5.2: Raman spectra for the $ZnSe$ mixtures with an concentration of 1% and 2%.

There are two main details that we can take from that figure. First, some of the cosmic spikes are broader than normal, and are not efficiently filtered with our algorithm. Second, graphically we do not see any $ZnSe$ influence, although our counting algorithm detected it. For the 3% sample, we can see the $ZnSe$ influence graphically, confirming the counting from the algorithm.

The problem is our counting algorithm being so closely related to the cosmic spikes filtering. As, to detect the presence of $ZnSe$ we detect the value of the maximum in a certain interval of the spectra, that maximum could correspond to an unfiltered cosmic spike.

Analysing now the results for CTSe mixtures, the results for XRD are closer to the expected values than the results for $ZnSe$. In table 5.3 we can see that once again for mixtures with concentrations of 3% or less, the results are no longer reliable. In this case, the values for the mixture corresponding to 20% of secondary phase, the results fall short from the expected values. This seems an isolated problem of that sample, as all the other mixtures seem to behave in accordance with the expected. The reason might be that some error occurred during the mixing process, and in reality we have less than $19,26\%$.

CTSe weighed in (%)	XRD Scale (%)	XRD Asymmetry (%)
19,26	12,48	14,33
9,64	10,48	15,96
4,50	5,17	5,94
2,78	1,72	2,55
1,58	2,16	4,03
1,18	0,63	4,13

Table 5.3: Comparison of the results obtained for the CTSe samples with the different techniques used throughout our work.

In figure 5.3 we can see a graphical representation for the two different Rietveld analysis techniques for the CTSe mixtures. Here we see once more that the results for the sample corresponding to the 20% mix are not in accordance with the rest of the results, as said before, and that all the other points have a linear behaviour corresponding to the expected.

Comparing the two figures, 5.3 and 5.1, we can also conclude that for the rietveld analysis both techniques are equivalent, the only improvement using the Asymmetry Technique is the diffractrogram fit, quantitatively the result is approximately the same.

As said in the previous chapter, it was not possible to derive a quantitative answer from the Raman analysis of the samples. Qualitatively, we can detect either there is CTSe present in the sample or not, but to determine the quantity a greater mathematical approach would be required, for which there was no time during this master thesis.

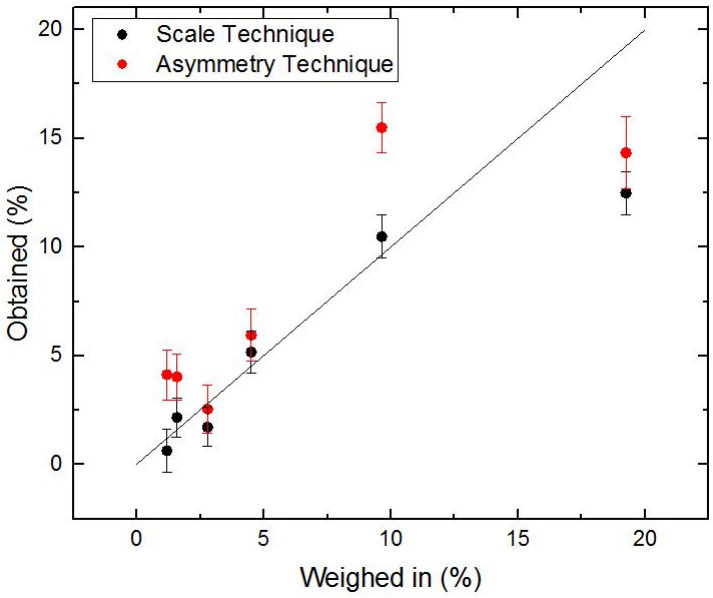

Figure 5.3: Comparison between the percentages values obtained for CTSe using different techniques.

Some improvements on the measurement process could also be developed in order to make the Raman powder analysis more practical and reliable, namely designing special holders to facilitate the pressing of the powder and its placement under the laser, so more samples could be scanned at the same time. The MATLAB analysis could also be improved, developing a more complex algorithms to remove the cosmic spikes and to perform a Lorentzian fit to better describe and distinguish the spectra.

6

Conclusion

With this work we can conclude that the detection limit for the X-ray diffraction technique is located between 3 and 5 %, as the results for concentrations bellow 5% are no longer reliable. Of the two techniques used we have seen that for a reliable quantitative result the refinement of the Zeroshift, Scale factor and background is enough, and also that for both methods, using the .hkl file or copying the structural information, we obtain equivalent results.

With the Raman Spectroscopy we were able to reach an statistical meaningful result for the mixtures of $ZnSe$, while for CTSe the results were inconclusive.

Appendices

a,$\mathring{A}$	c, $\mathring{A}$	R_{Bragg}	χ^2
5.696414	11.350698	6.88	3.628

Table 1: Lattice parameters, R_{Bragg} and χ^2 for $Cu_{1,98}Zn_{1,04}Sn_{0,84}Se_4$

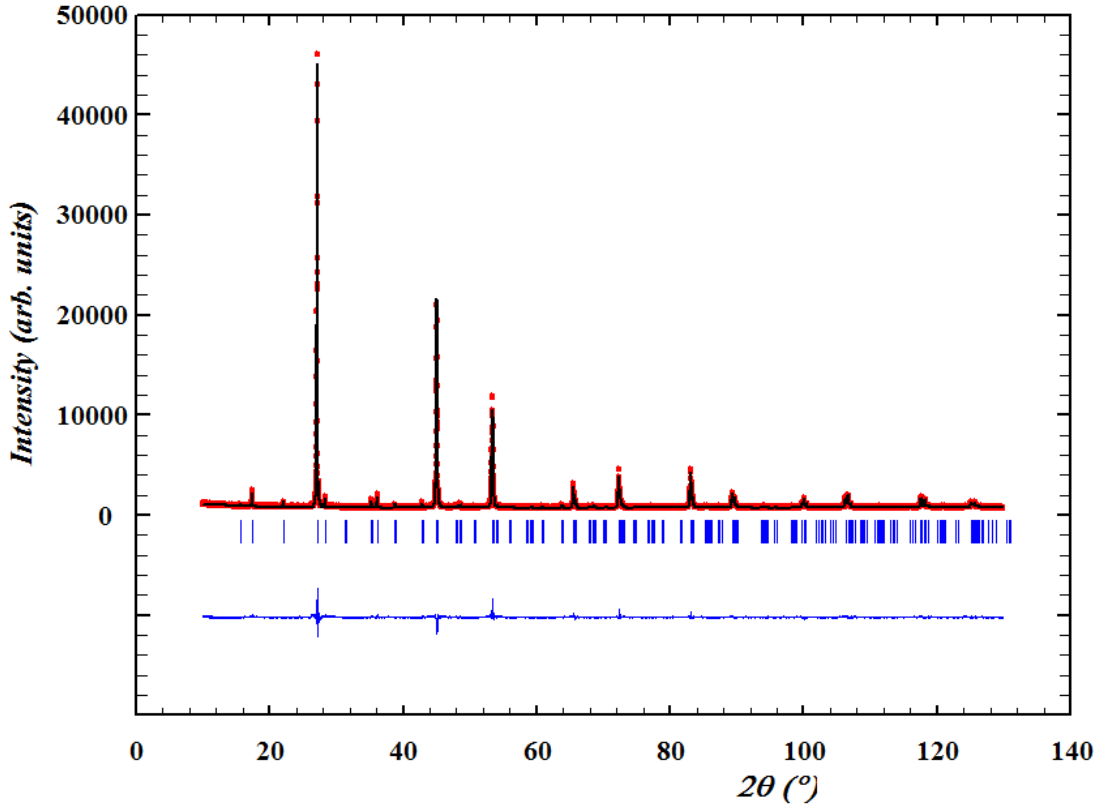

Figure 1: Diffractrogram for $Cu_{1,98}Zn_{1,04}Sn_{0,84}Se_4$

a,Å	c, Å	R_{Bragg}	χ^2
5.694095	11.345442	5.73	1.933

Table 2: Lattice parameters, R_{Bragg}br and χ^2 for $Cu_{2,01}Zn_{1,03}Sn_{0,98}Se_4$

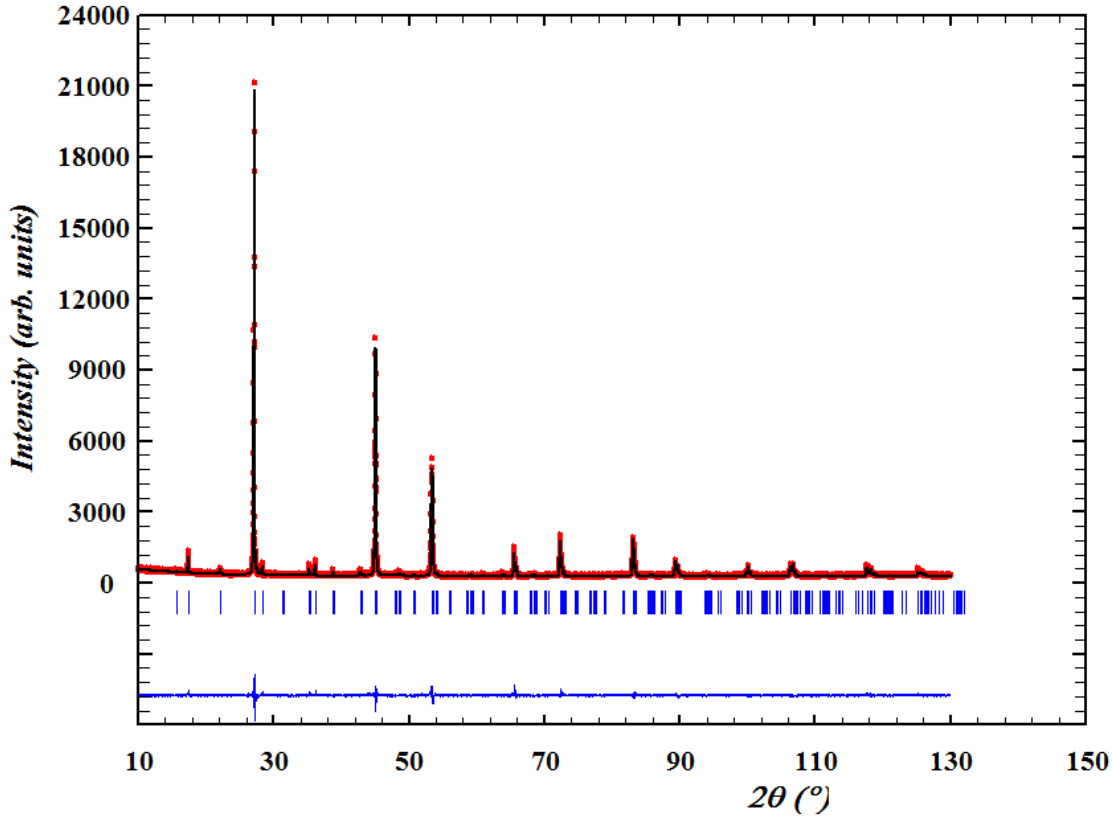

Figure 2: Diffractrogram for $Cu_{2,01}Zn_{1,03}Sn_{0,98}Se_4$

a,$\mathring{A}$	R_{Bragg}	χ^2
5.671062	3.06	6.006

Table 3: Lattice parameters, R_{Bragg} and χ^2 for $ZnSe$

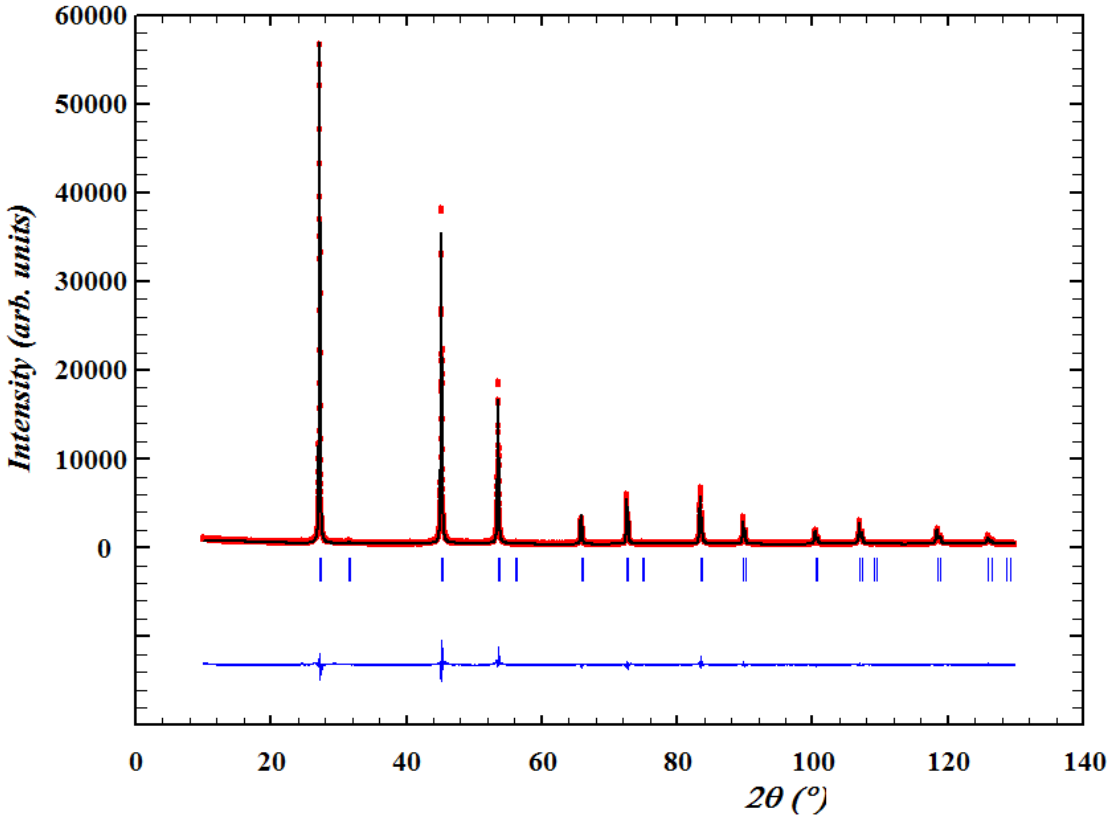

Figure 3: Diffractrogram for $ZnSe$

C 1 c 1					*F -43m*		
a,Å	b,Å	c,Å	R_{Bragg}	χ^2	a,Å	R_{Bragg}	χ^2
6,992(6)	12,072(5)	6,972(3)	10,55	2,74	5,6934(1)	3,71	2,74

Table 4: Lattice parameters, R_{Bragg} and χ^2 for CTSe

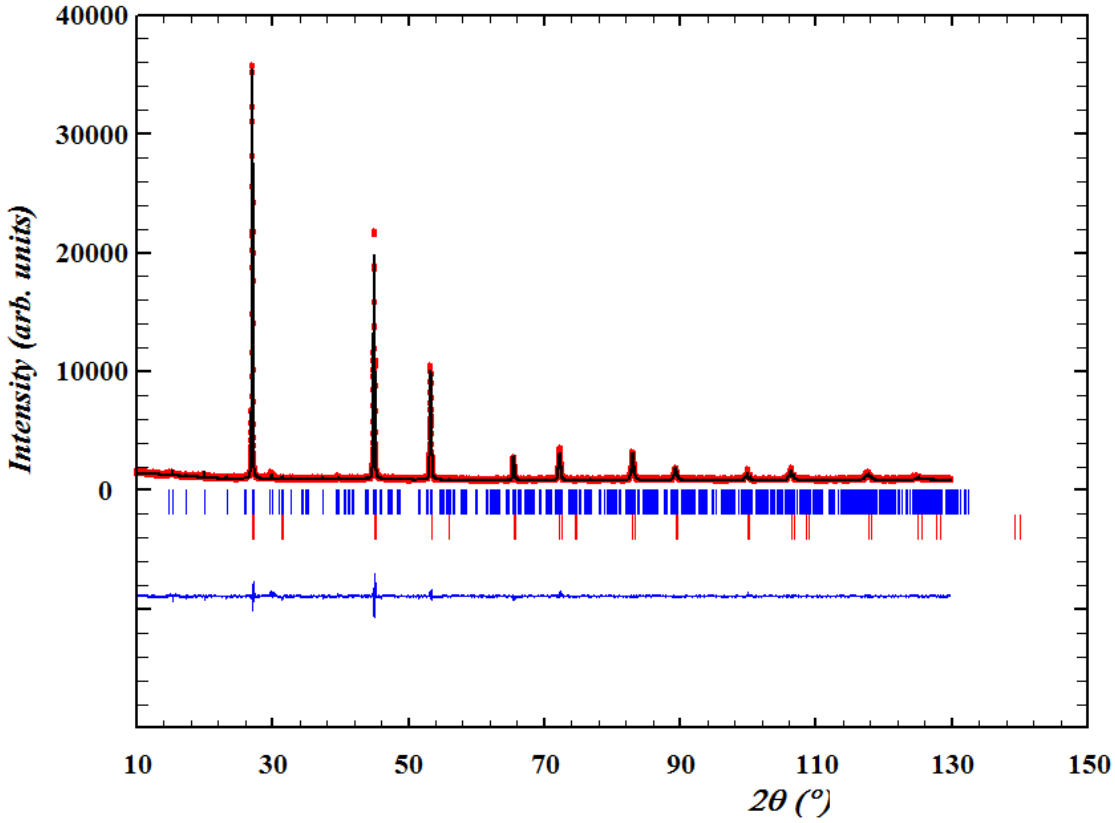

Figure 4: Diffractrogram for Cu_2SnSe_4

a,Å	R_{Bragg}	χ^2
5.668662	3.39	7.704

Table 5: Lattice parameters, R_{Bragg} and χ^2 for synthesised $ZnSe$, sample $ZnSe\ I$

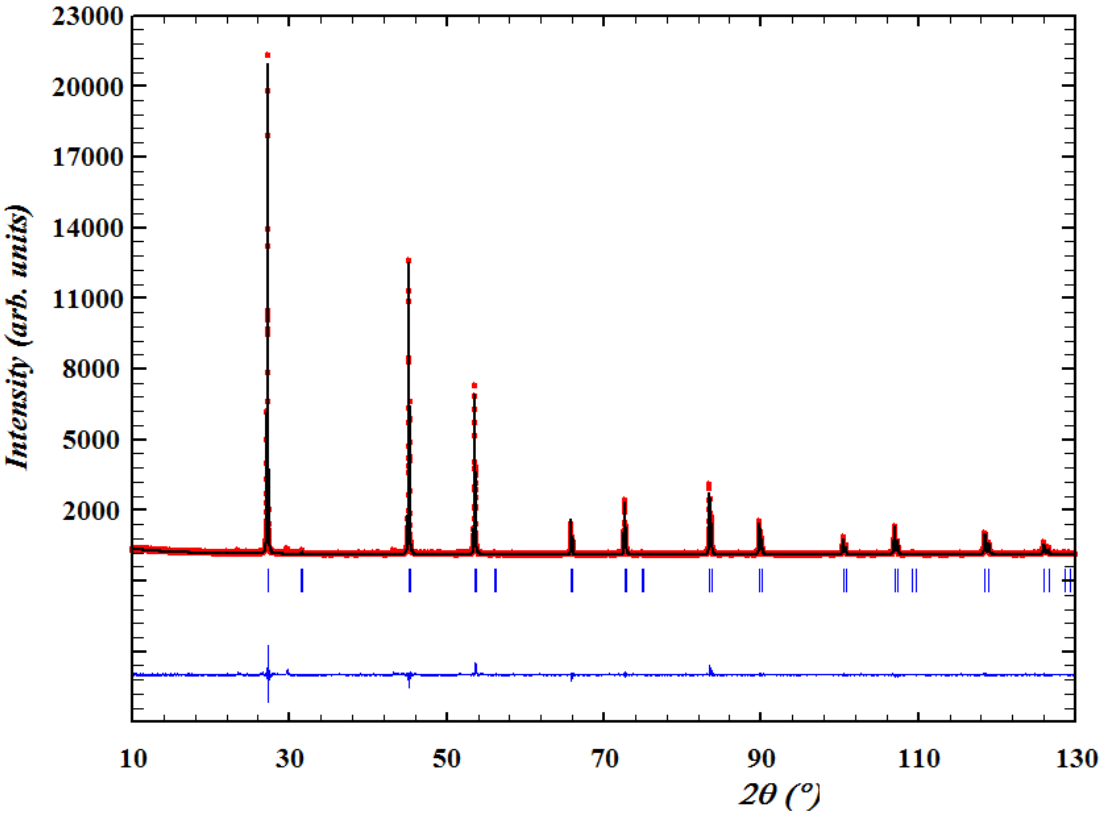

Figure 5: Diffractrogram for synthesised $ZnSe$, sample $ZnSe\ I$

a,$\mathring{A}$	R_{Bragg}	χ^2
5.668606	2.73	4.393

Table 6: Lattice parameters, R_{Bragg} and χ^2 for synthesised $ZnSe$, sample $ZnSe\ II$

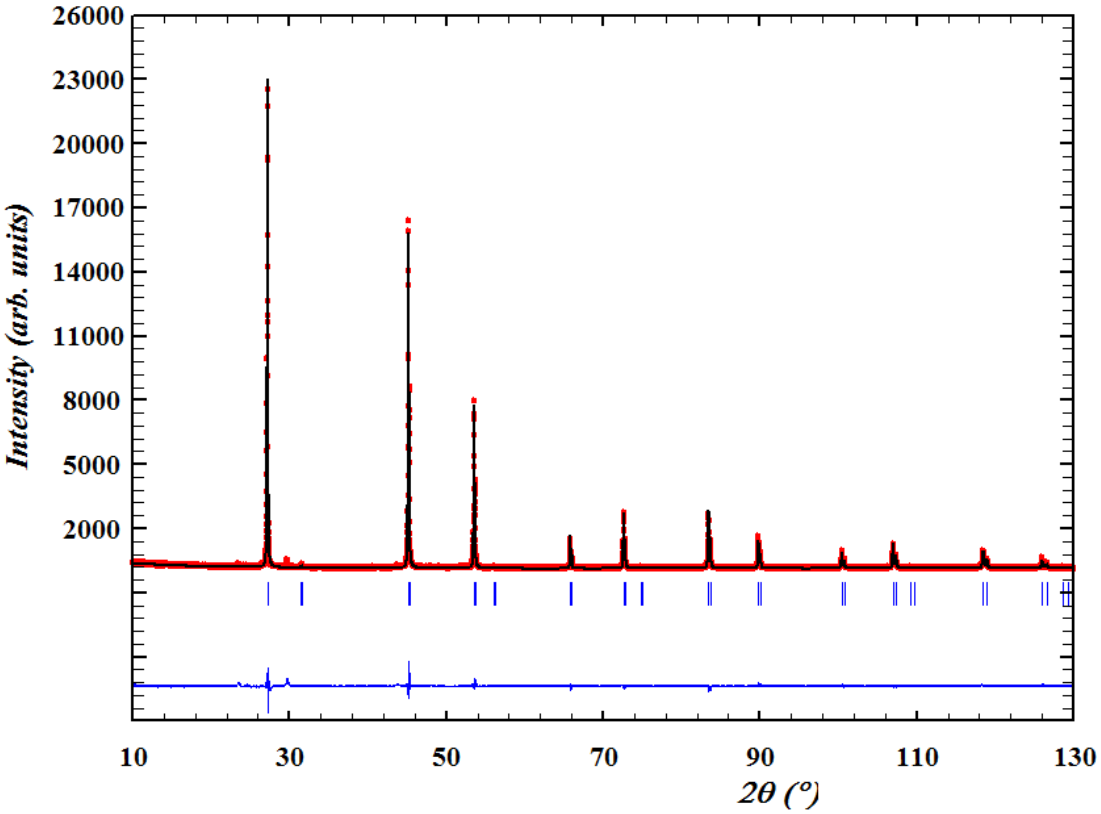

Figure 6: Diffractrogram for synthesised $ZnSe$, sample $ZnSe\ II$

a,Å	R_{Bragg}	χ^2
5.669391	4.02	7.992

Table 7: Lattice parameters, R_{Bragg} and χ^2 for synthesised $ZnSe$, sample $ZnSe\ III$

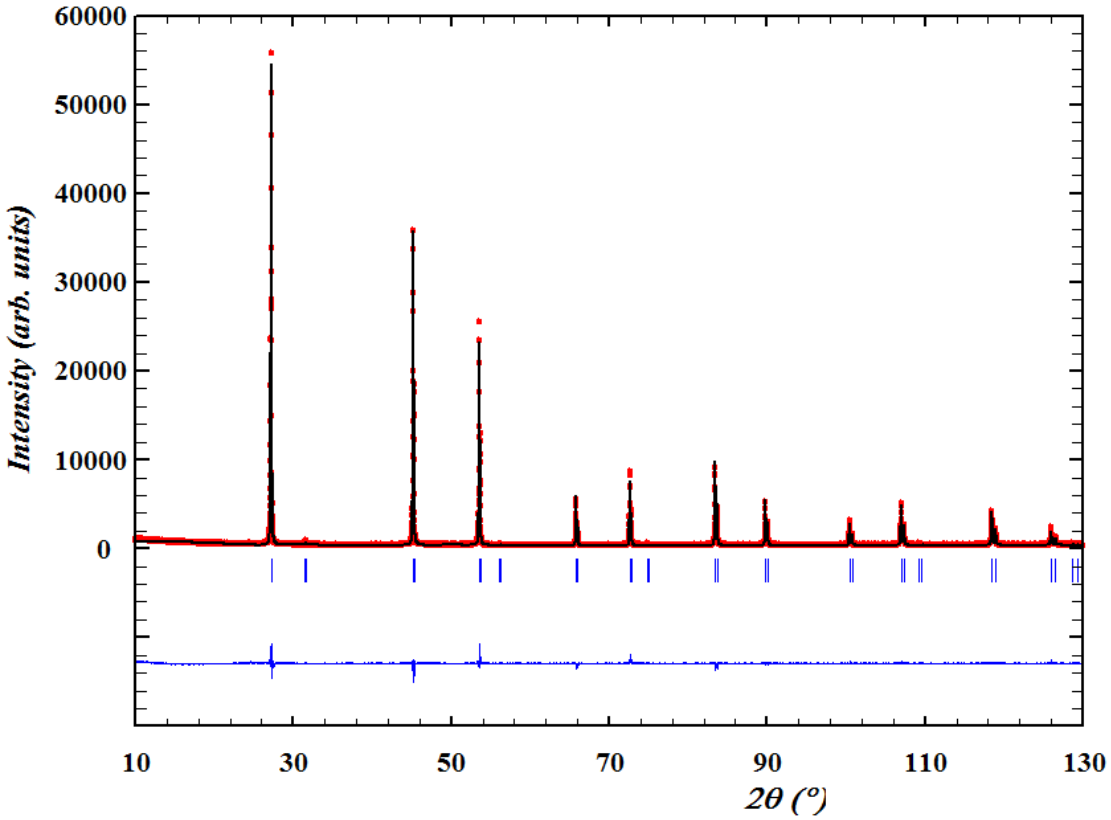

Figure 7: Diffractrogram for synthesised $ZnSe$, sample $ZnSe\ III$

R_{Bragg} for $ZnSe$	R_{Bragg} for CZTSe	χ^2
5.53	8.11	5.265

Table 8: R_{Bragg} and χ^2 for the 20% mixture of $ZnSe$. Scale technique.

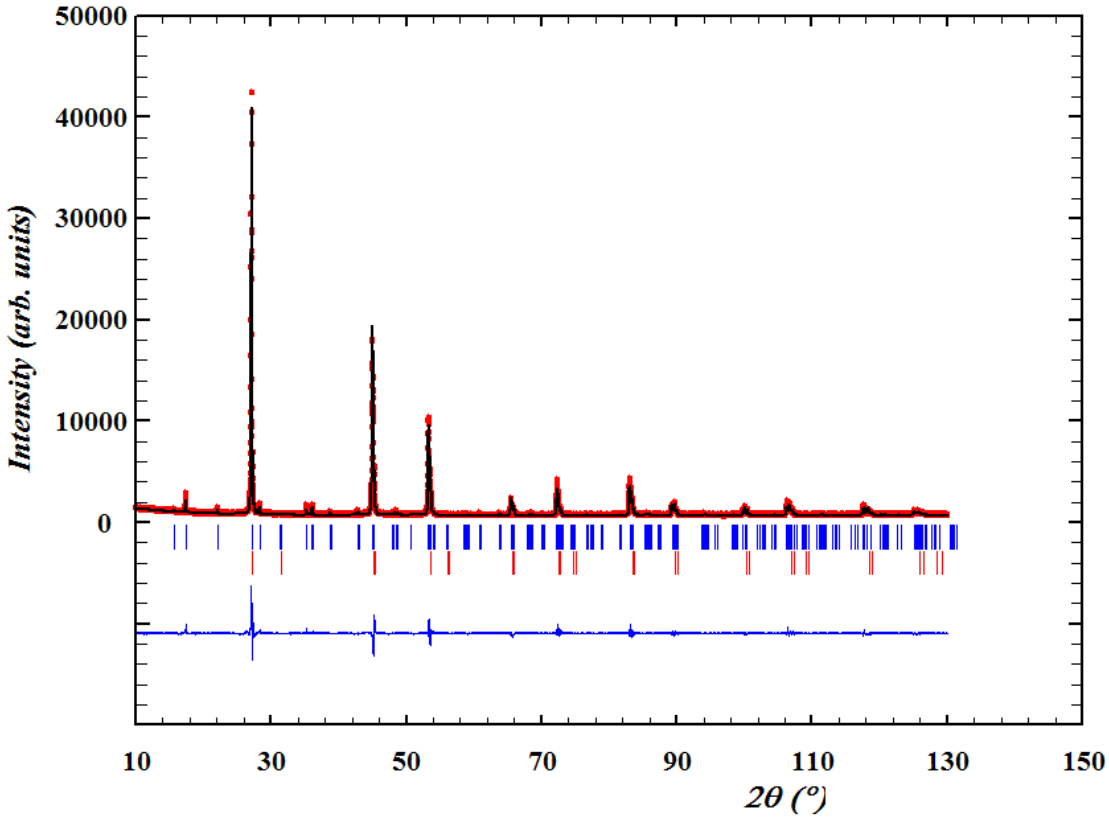

Figure 8: Diffractrogram for the 20% mixture of $ZnSe$. Scale technique

R_{Bragg} for $ZnSe$	R_{Bragg} for CZTSe	χ^2
4.80	6.52	3.794

Table 9: R_{Bragg} and χ^2 for the 20% mixture of $ZnSe$. Asymmetry technique.

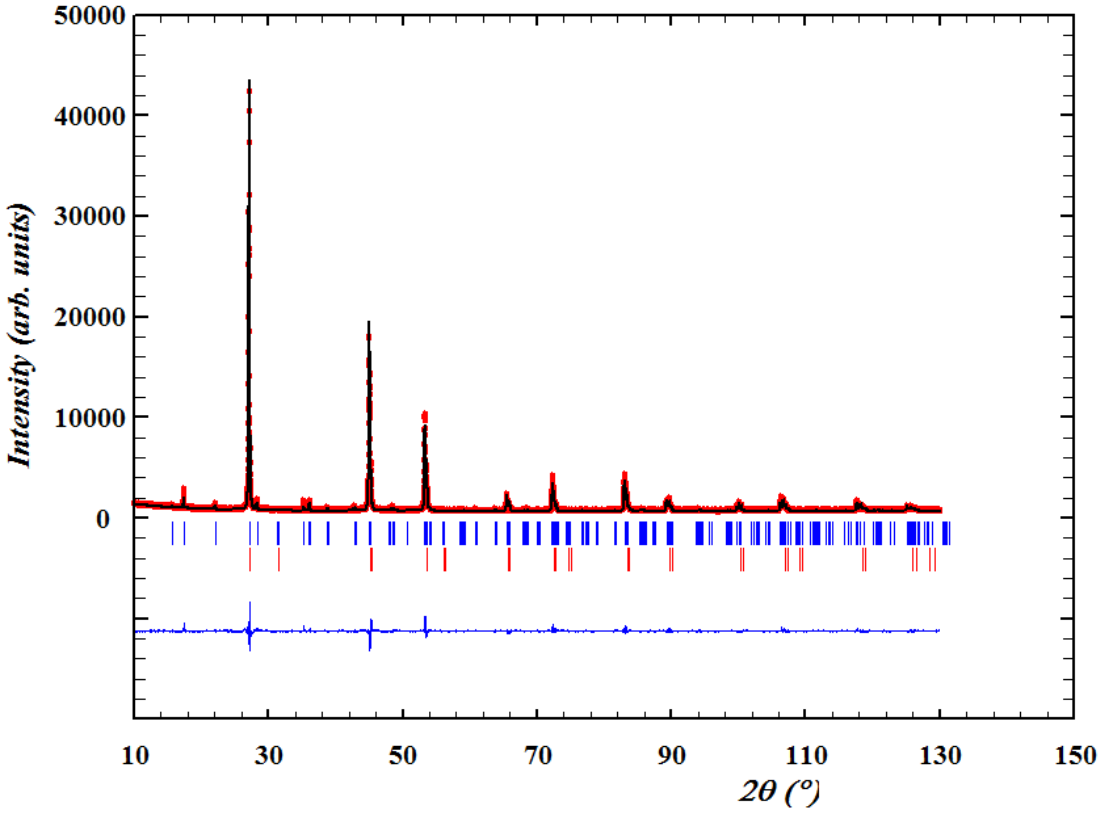

Figure 9: Diffractrogram for the 20% mixture of $ZnSe$. Asymmetry technique.

R_{Bragg} for $ZnSe$	R_{Bragg} for CZTSe	χ^2
5.66	8.11	5.326

Table 10: R_{Bragg} and χ^2 for the 20% mixture of $ZnSe$. Scale technique, hkl method.

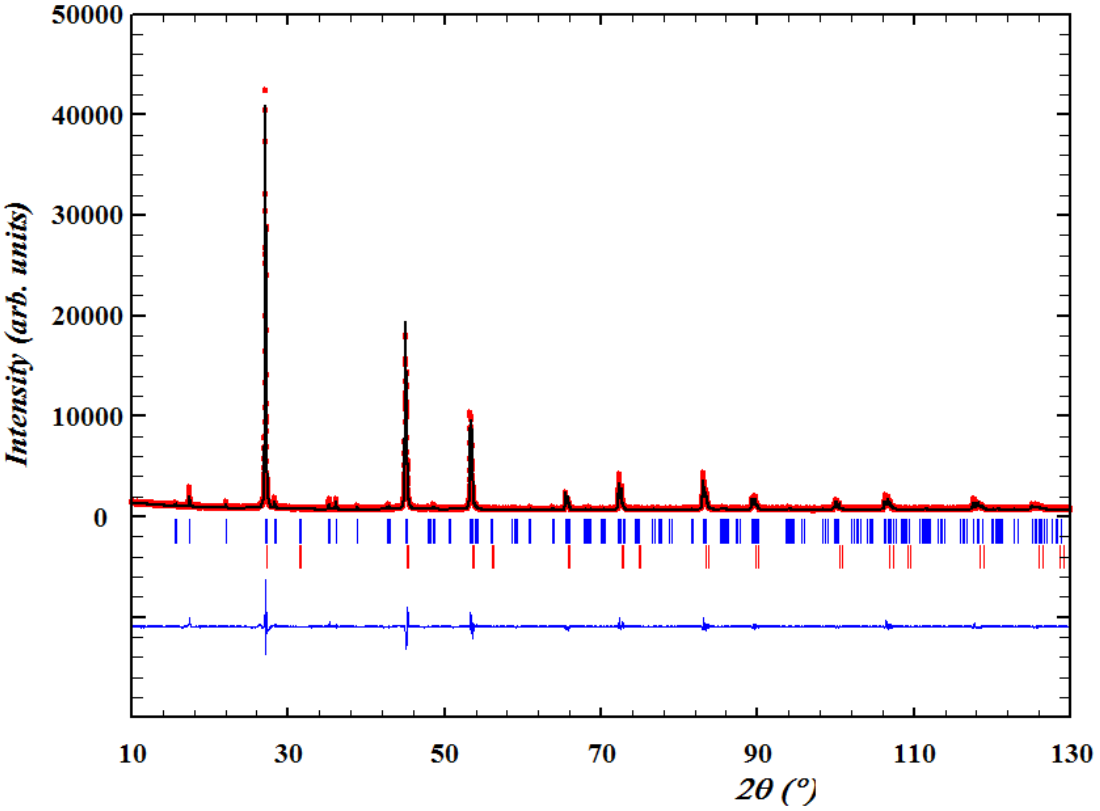

Figure 10: Diffractrogram for the 20% mixture of $ZnSe$. Scale technique, hkl method.

R_{Bragg} for $ZnSe$	R_{Bragg} for CZTSe	χ^2
4.34	6.87	3.897

Table 11: R_{Bragg} and χ^2 for the 20% mixture of $ZnSe$. Asymmetry technique, hkl method.

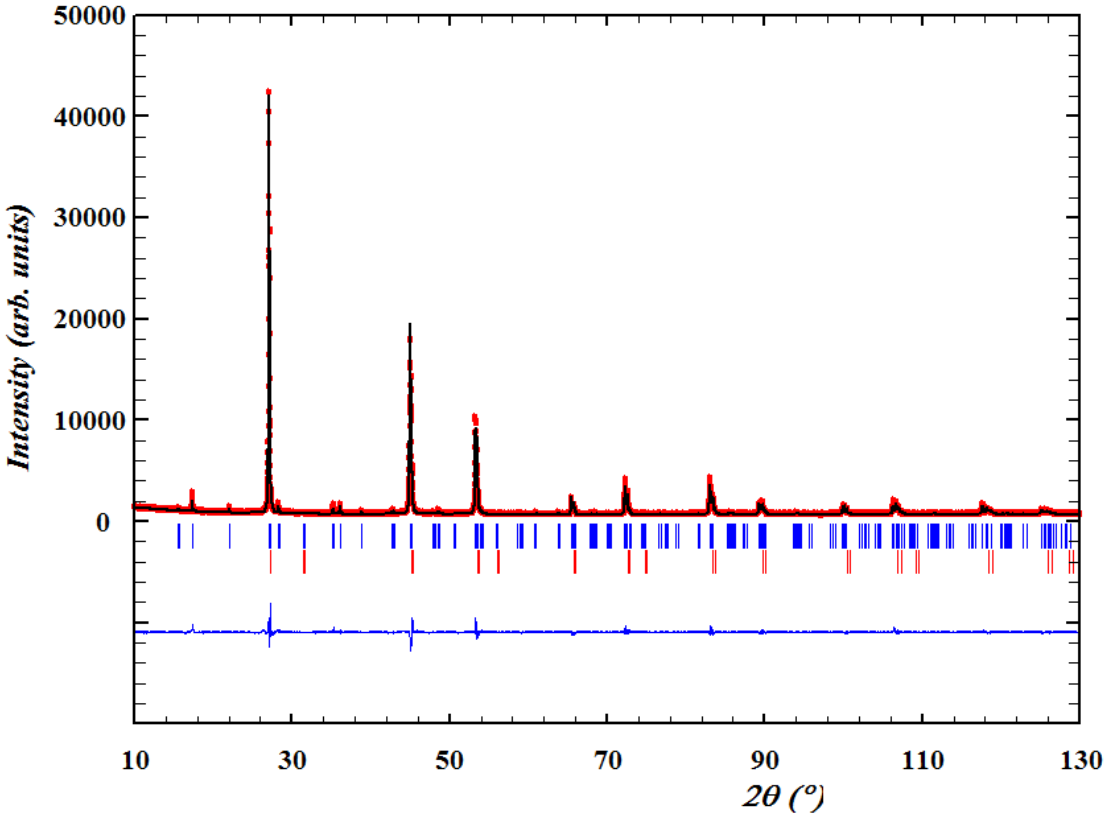

Figure 11: Diffractrogram for the 20% mixture of $ZnSe$. Asymmetry technique, hkl method.

R_{Bragg} for $ZnSe$	R_{Bragg} for CZTSe	χ^2
6.30	7.68	5.768

Table 12: R_{Bragg} and χ^2 for the 10% mixture of $ZnSe$. Scale technique.

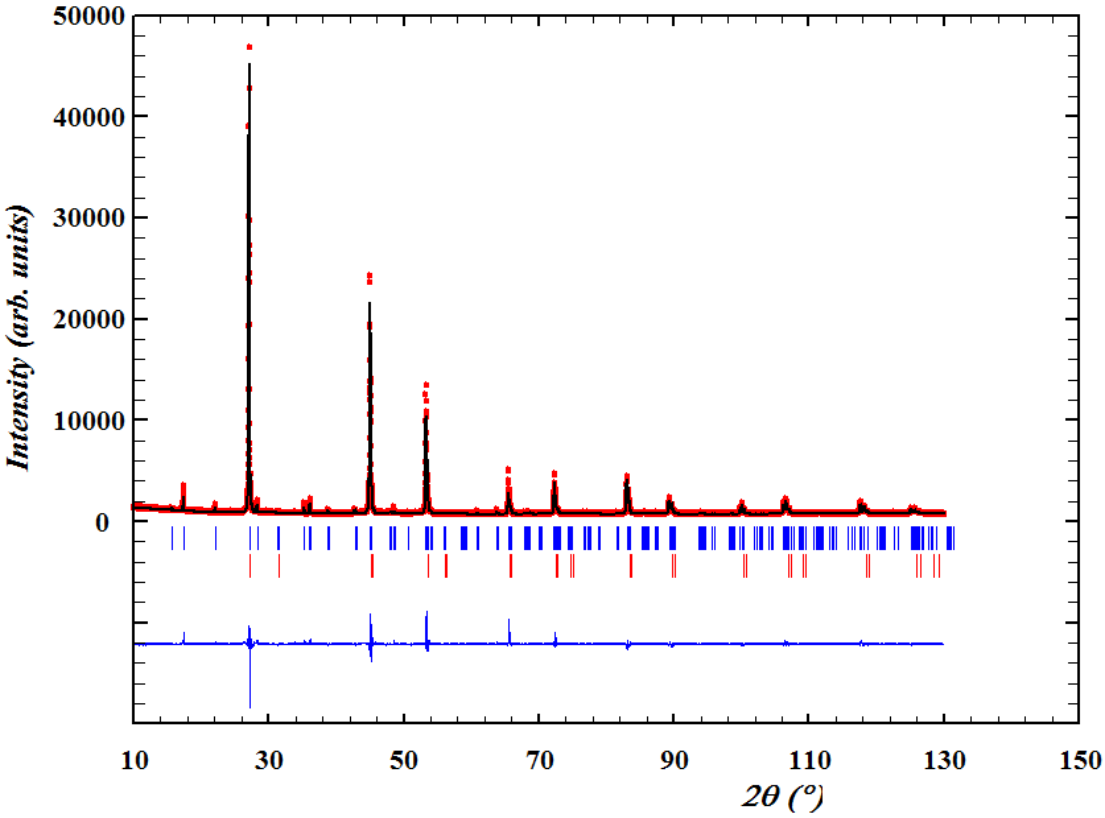

Figure 12: Diffractrogram for the 10% mixture of $ZnSe$. Scale technique

R_{Bragg} for $ZnSe$	R_{Bragg} for CZTSe	χ^2
5.98	7.43	5.558

Table 13: R_{Bragg} and χ^2 for the 10% mixture of $ZnSe$. Asymmetry technique.

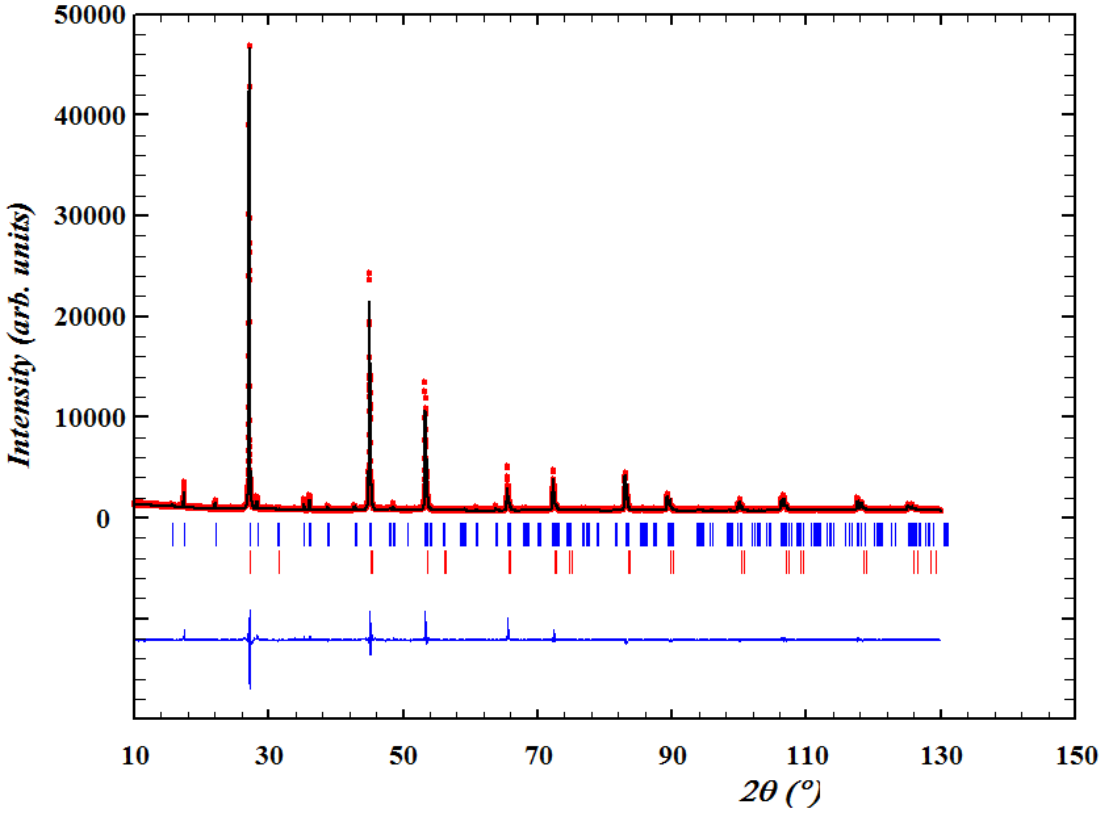

Figure 13: Diffractrogram for the 10% mixture of $ZnSe$. Asymmetry technique.

R_{Bragg} for $ZnSe$	R_{Bragg} for CZTSe	χ^2
5.93	7.70	5.834

Table 14: R_{Bragg} and χ^2 for the 10% mixture of $ZnSe$. Scale technique, hkl method.

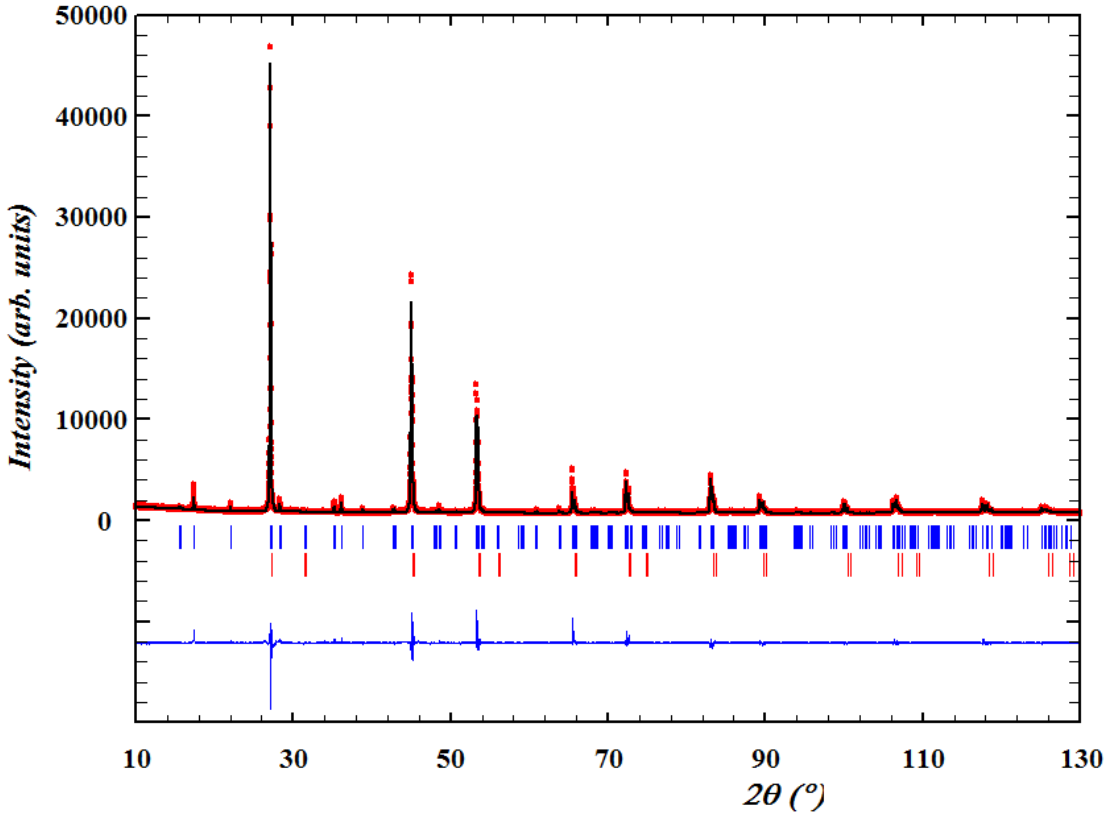

Figure 14: Diffractrogram for the 10% mixture of $ZnSe$. Scale technique, hkl method.

R_{Bragg} for $ZnSe$	R_{Bragg} for CZTSe	χ^2
6.10	7.42	5.773

Table 15: R_{Bragg} and χ^2 for the 10% mixture of $ZnSe$. Asymmetry technique, hkl method.

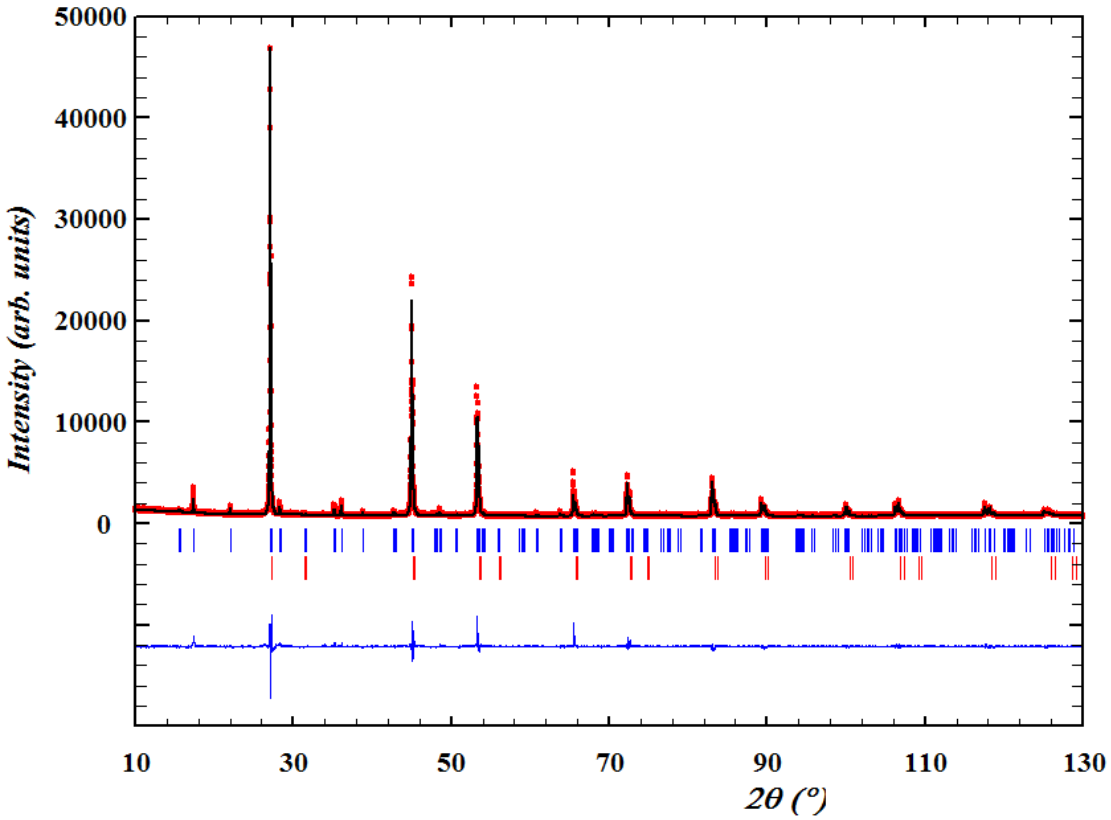

Figure 15: Diffractrogram for the 10% mixture of $ZnSe$. Asymmetry technique, hkl method.

R_{Bragg} for $ZnSe$	R_{Bragg} for CZTSe	χ^2
10.33	6.37	3.848

Table 16: R_{Bragg} and χ^2 for the 5% mixture of $ZnSe$. Scale technique.

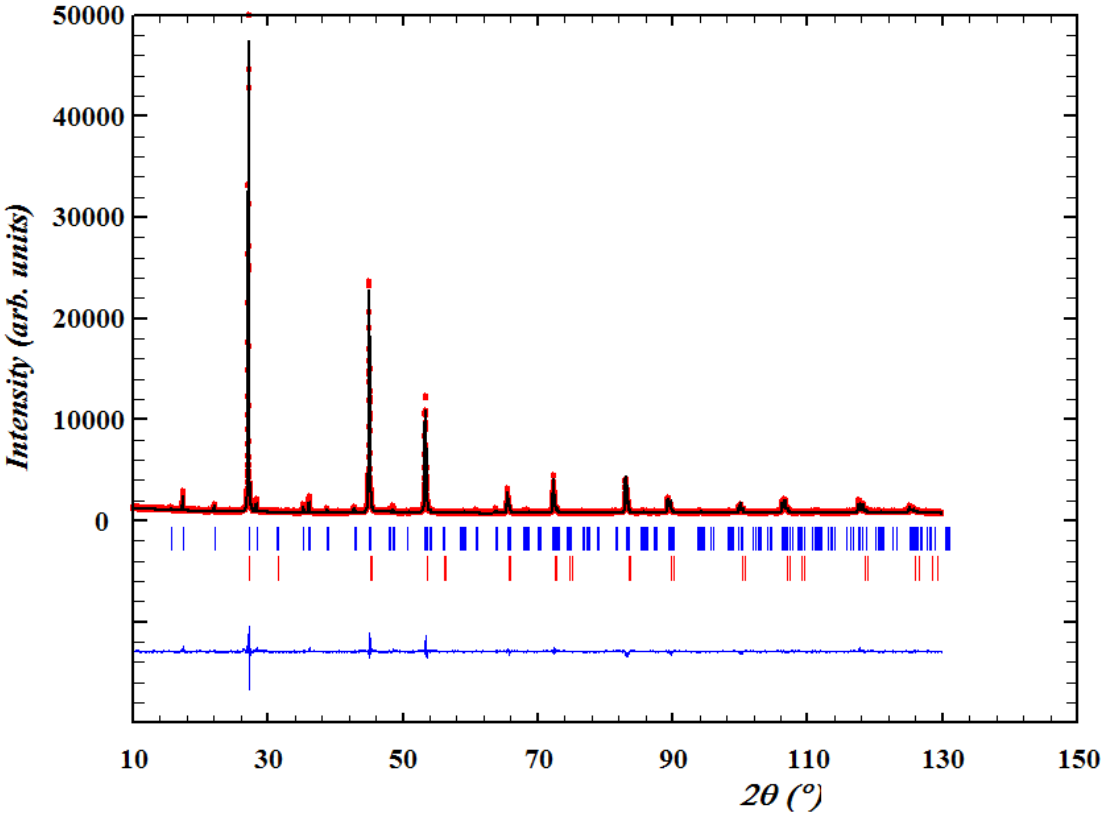

Figure 16: Diffractrogram for the 5% mixture of $ZnSe$. Scale technique

R_{Bragg} for $ZnSe$	R_{Bragg} for CZTSe	χ^2
10.07	6.21	3.666

Table 17: R_{Bragg} and χ^2 for the 5% mixture of $ZnSe$. Asymmetry technique.

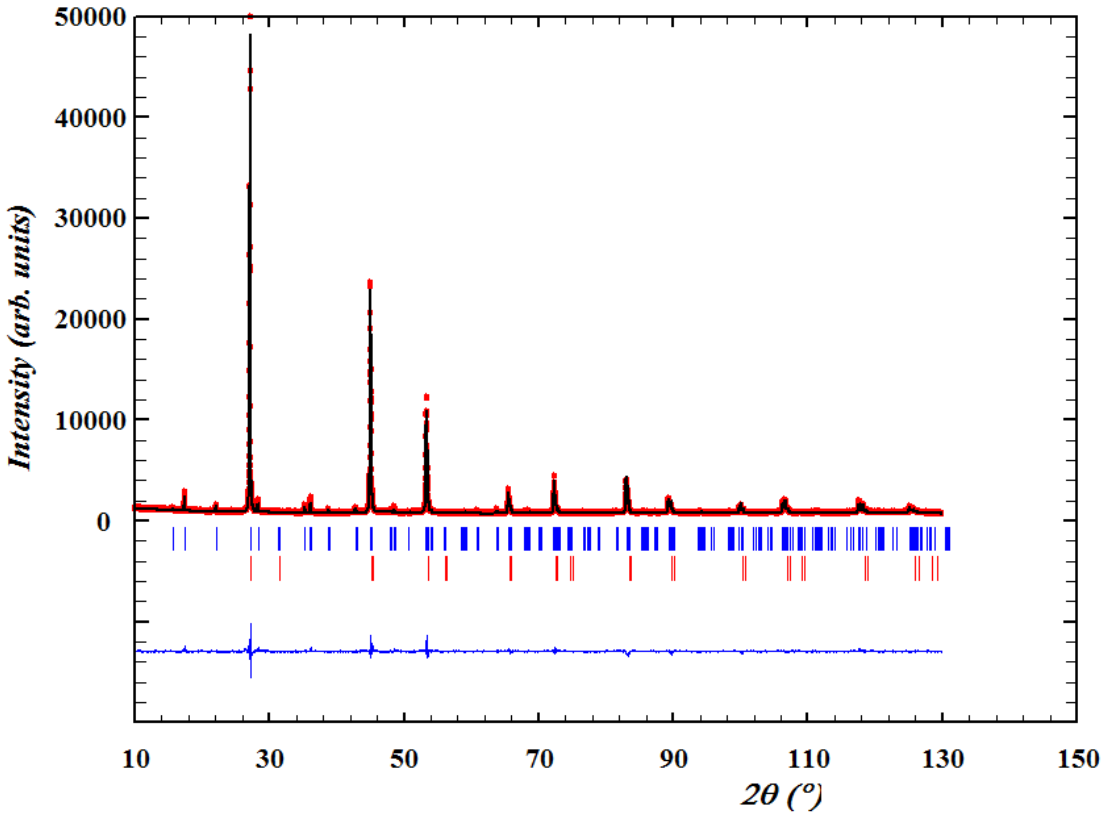

Figure 17: Diffractrogram for the 5% mixture of $ZnSe$. Asymmetry technique.

R_{Bragg} for $ZnSe$	R_{Bragg} for CZTSe	χ^2
10.19	6.40	3.869

Table 18: R_{Bragg} and χ^2 for the 5% mixture of $ZnSe$. Scale technique, hkl method.

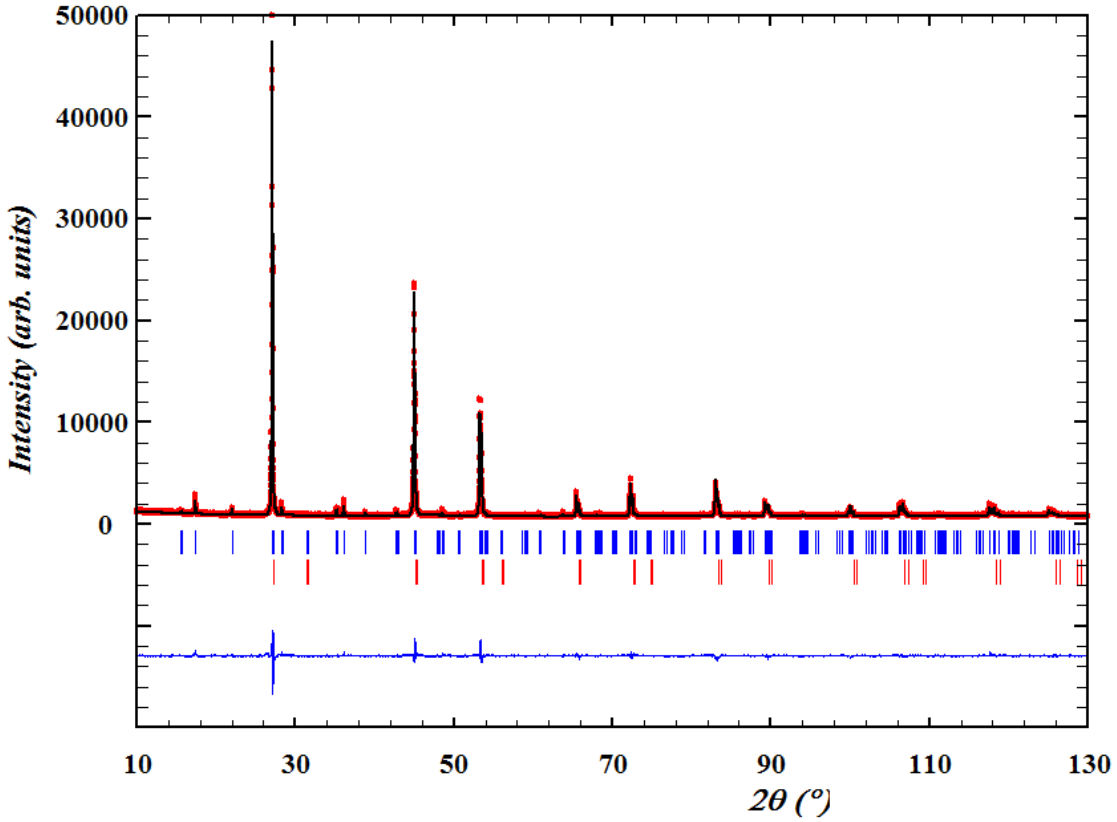

Figure 18: Diffractrogram for the 5% mixture of $ZnSe$. Scale technique, hkl method.

R_{Bragg} for $ZnSe$	R_{Bragg} for CZTSe	χ^2
9.54	6.25	3.802

Table 19: R_{Bragg} and χ^2 for the 5% mixture of $ZnSe$. Asymmetry technique, hkl method.

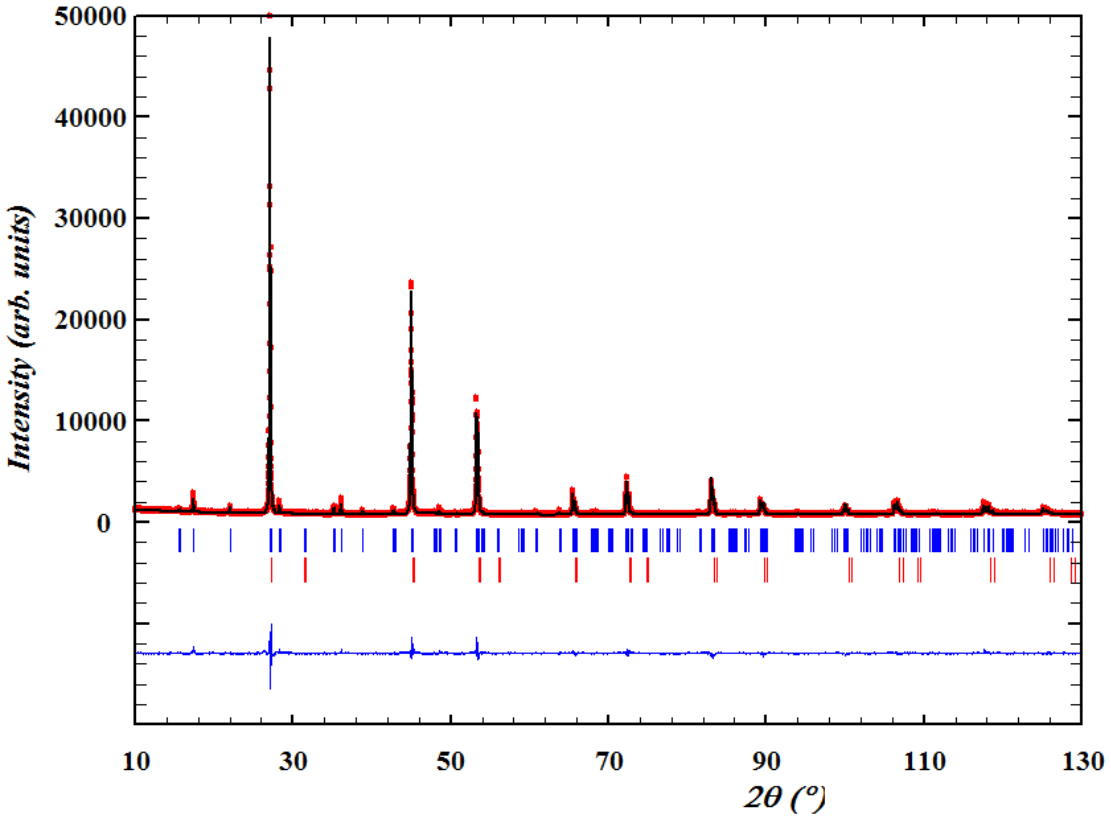

Figure 19: Diffractrogram for the 5% mixture of $ZnSe$. Asymmetry technique, hkl method.

R_{Bragg} for $ZnSe$	R_{Bragg} for CZTSe	χ^2
21.70	6.37	3.848

Table 20: R_{Bragg} and χ^2 for the 3% mixture of $ZnSe$. Scale technique.

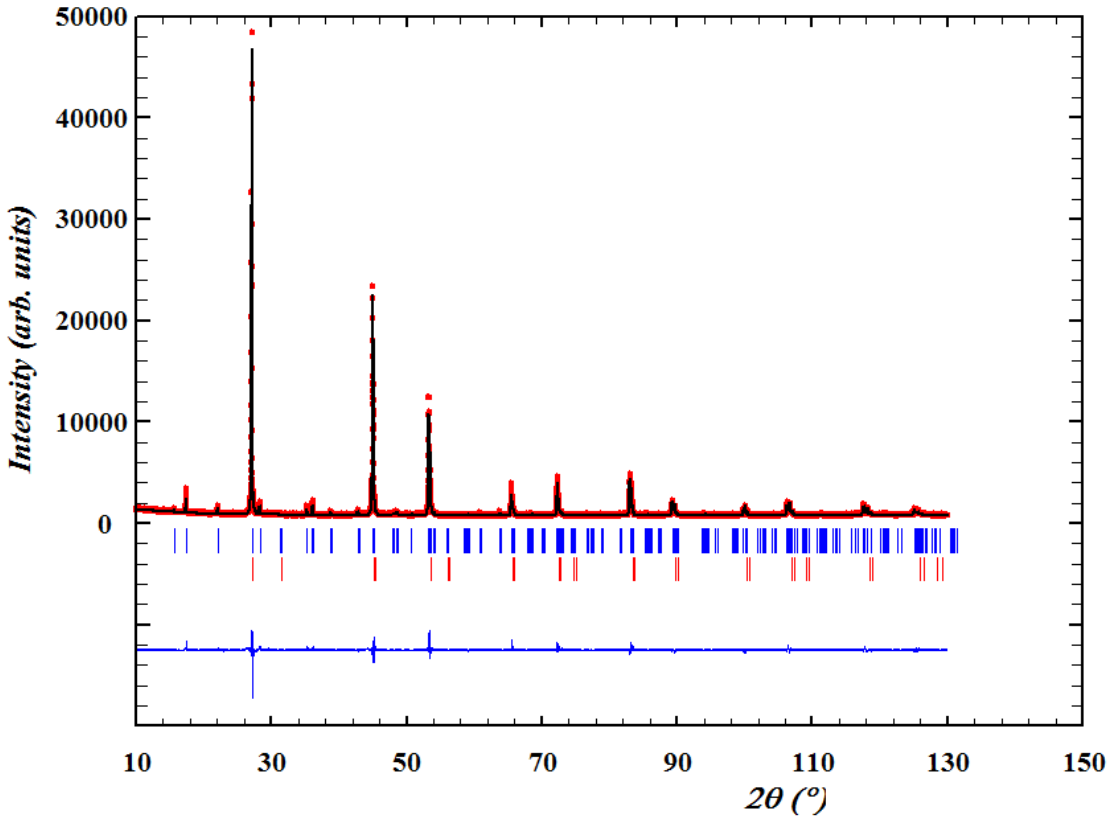

Figure 20: Diffractrogram for the 3% mixture of $ZnSe$. Scale technique

R_{Bragg} for $ZnSe$	R_{Bragg} for CZTSe	χ^2
22.29	6.72	4.175

Table 21: R_{Bragg} and χ^2 for the 3% mixture of $ZnSe$. Asymmetry technique.

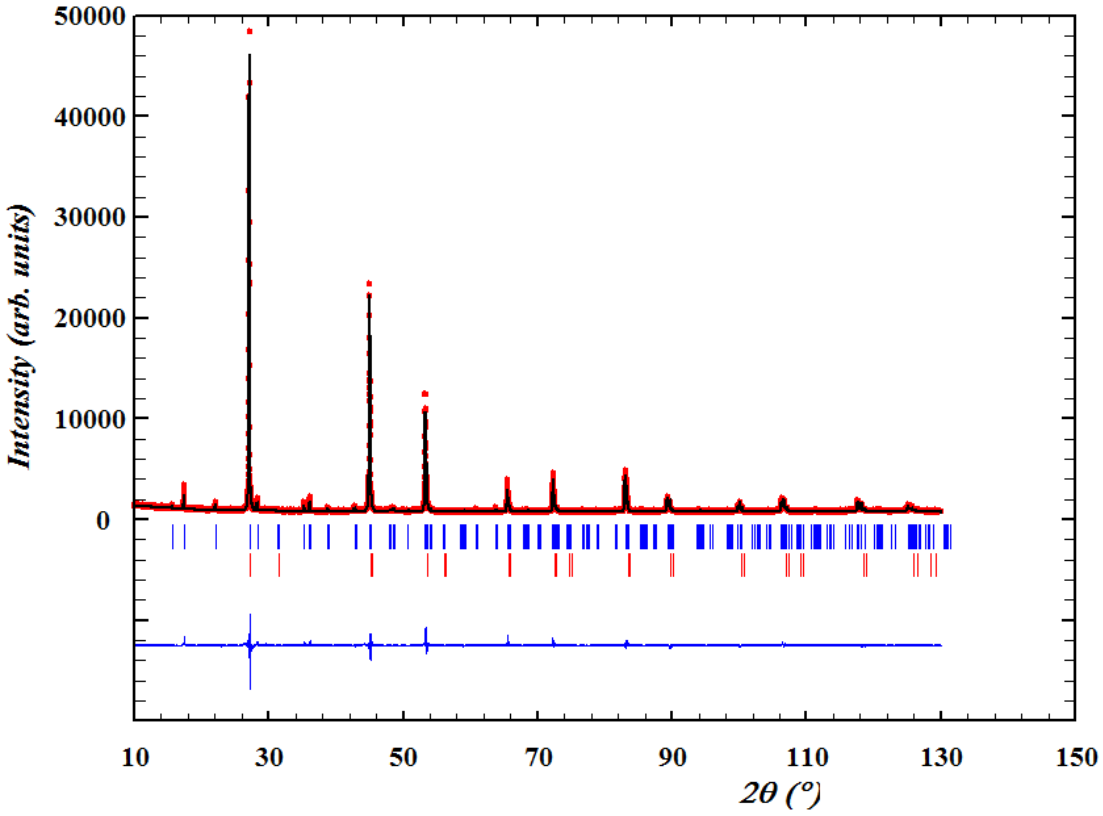

Figure 21: Diffractrogram for the 3% mixture of $ZnSe$. Asymmetry technique.

R_{Bragg} for $ZnSe$	R_{Bragg} for CZTSe	χ^2
19.34	6.85	4.488

Table 22: R_{Bragg} and χ^2 for the 3% mixture of $ZnSe$. Scale technique, hkl method.

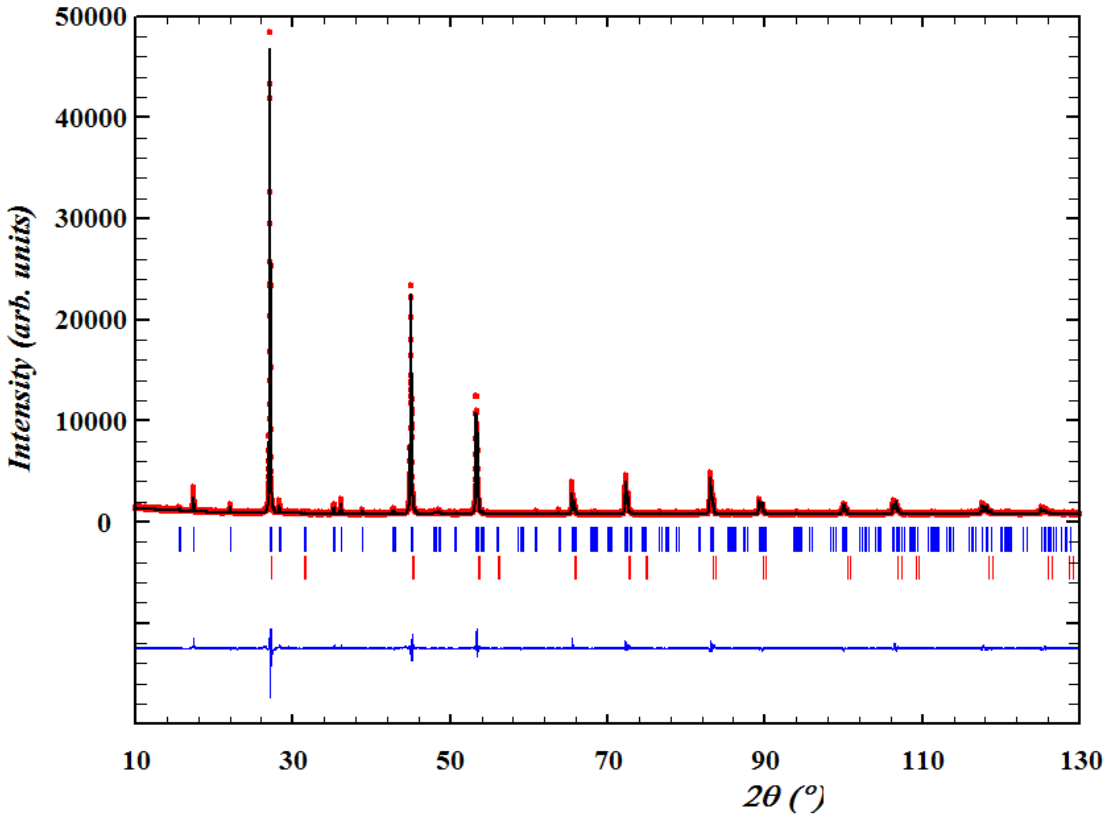

Figure 22: Diffractrogram for the 3% mixture of $ZnSe$. Scale technique, hkl method.

R_{Bragg} for $ZnSe$	R_{Bragg} for CZTSe	χ^2
18.17	6.75	4.473

Table 23: R_{Bragg} and χ^2 for the 3% mixture of $ZnSe$. Asymmetry technique, hkl method.

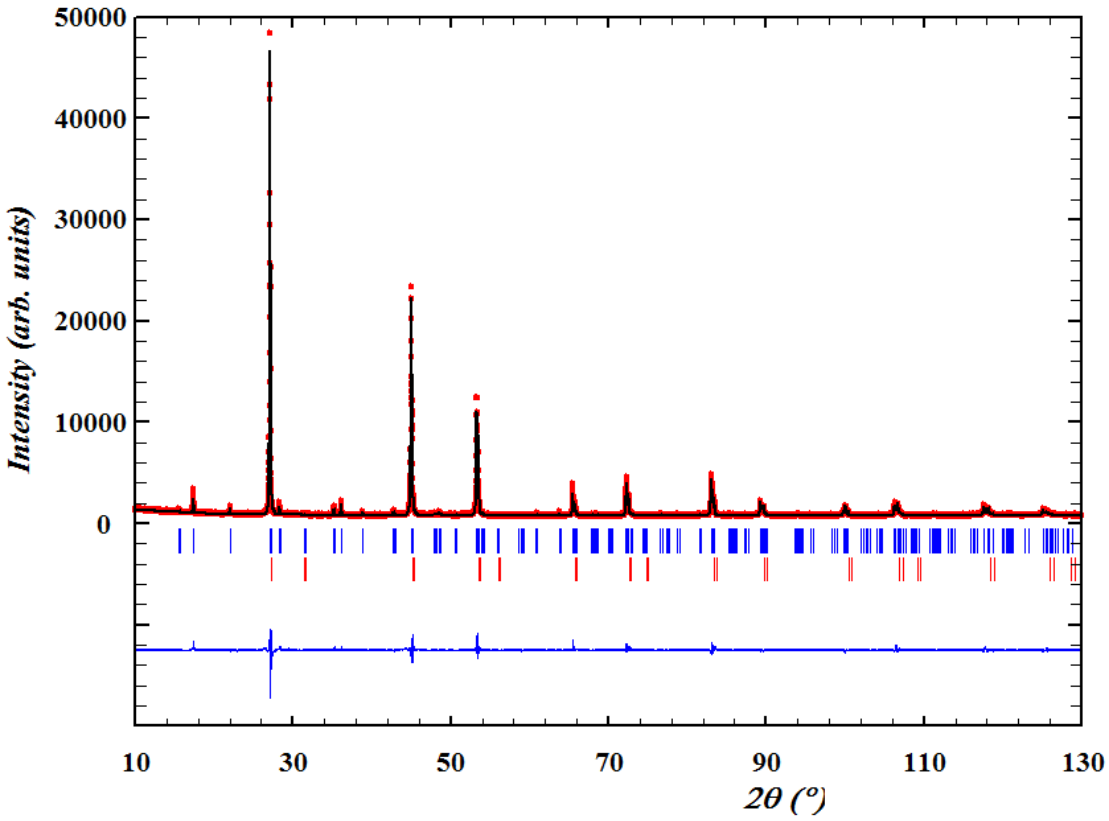

Figure 23: Diffractrogram for the 3% mixture of $ZnSe$. Asymmetry technique, hkl method.

R_{Bragg} for $ZnSe$	R_{Bragg} for CZTSe	χ^2
20.40	7.45	5.040

Table 24: R_{Bragg} and χ^2 for the 2% mixture of $ZnSe$. Scale technique.

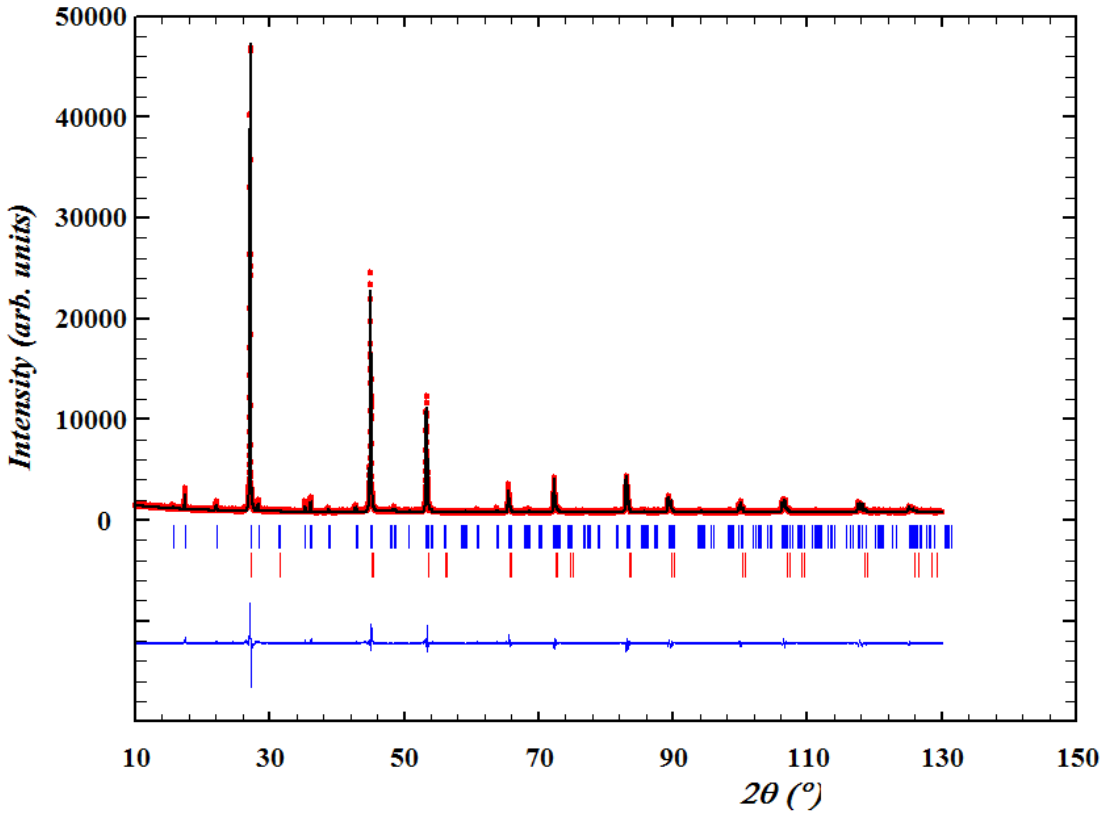

Figure 24: Diffractrogram for the 2% mixture of $ZnSe$. Scale technique

R_{Bragg} for $ZnSe$	R_{Bragg} for CZTSe	χ^2
13.42	6.70	4.784

Table 25: R_{Bragg} and χ^2 for the 2% mixture of $ZnSe$. Asymmetry technique.

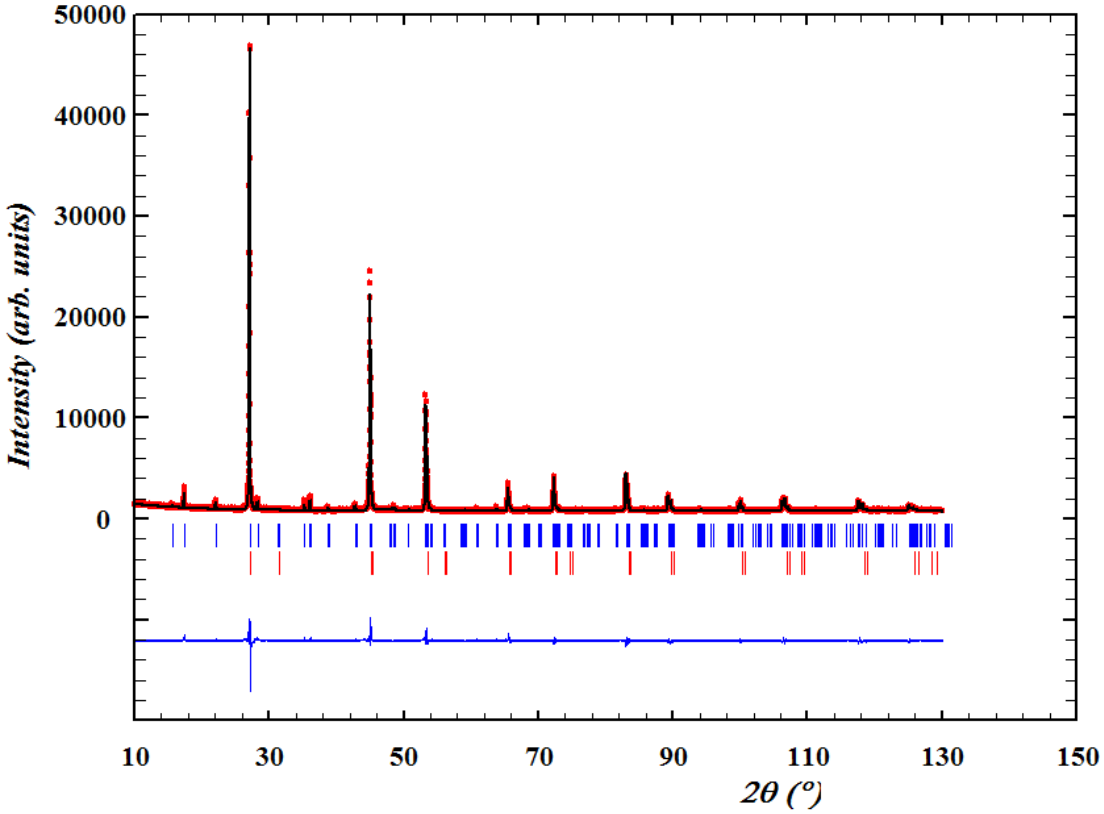

Figure 25: Diffractrogram for the 2% mixture of $ZnSe$. Asymmetry technique.

R_{Bragg} for $ZnSe$	R_{Bragg} for CZTSe	χ^2
18.68	7.43	5.084

Table 26: R_{Bragg} and χ^2 for the 2% mixture of $ZnSe$. Scale technique, hkl method.

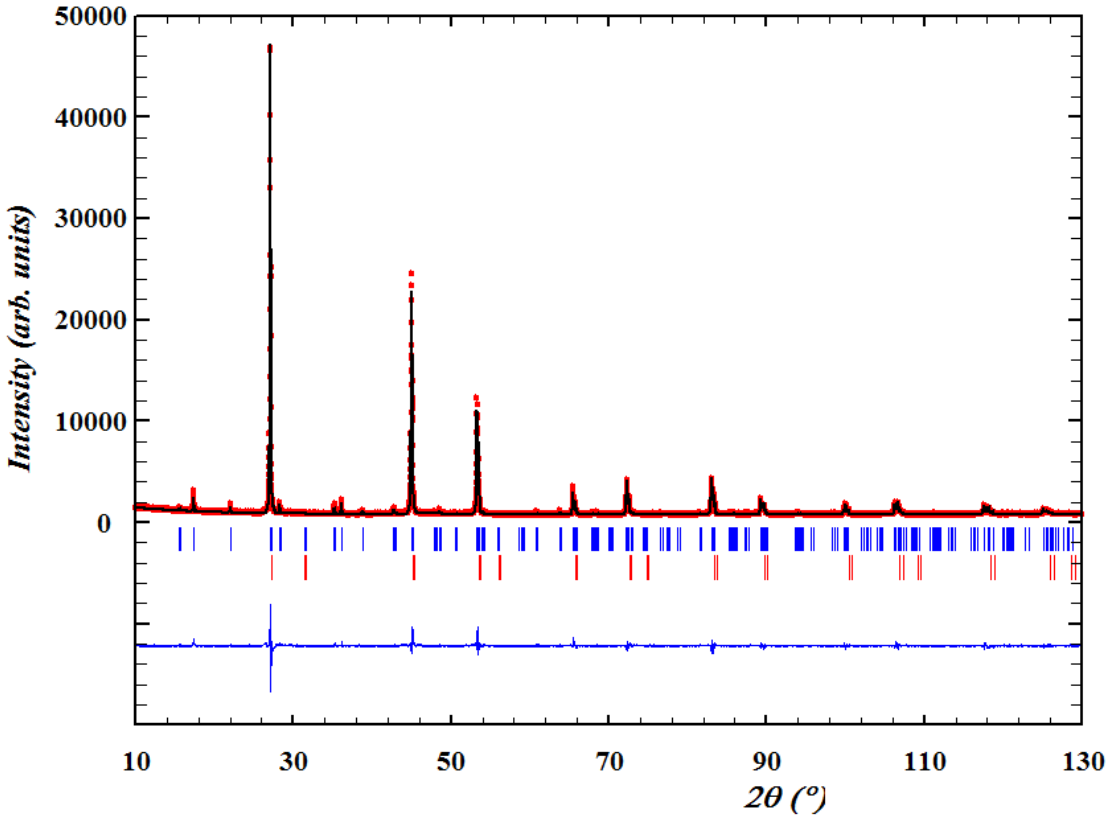

Figure 26: Diffractrogram for the 2% mixture of $ZnSe$. Scale technique, hkl method.

R_{Bragg} for $ZnSe$	R_{Bragg} for CZTSe	χ^2
18.09	7.33	5.062

Table 27: R_{Bragg} and χ^2 for the 2% mixture of $ZnSe$. Asymmetry technique, hkl method.

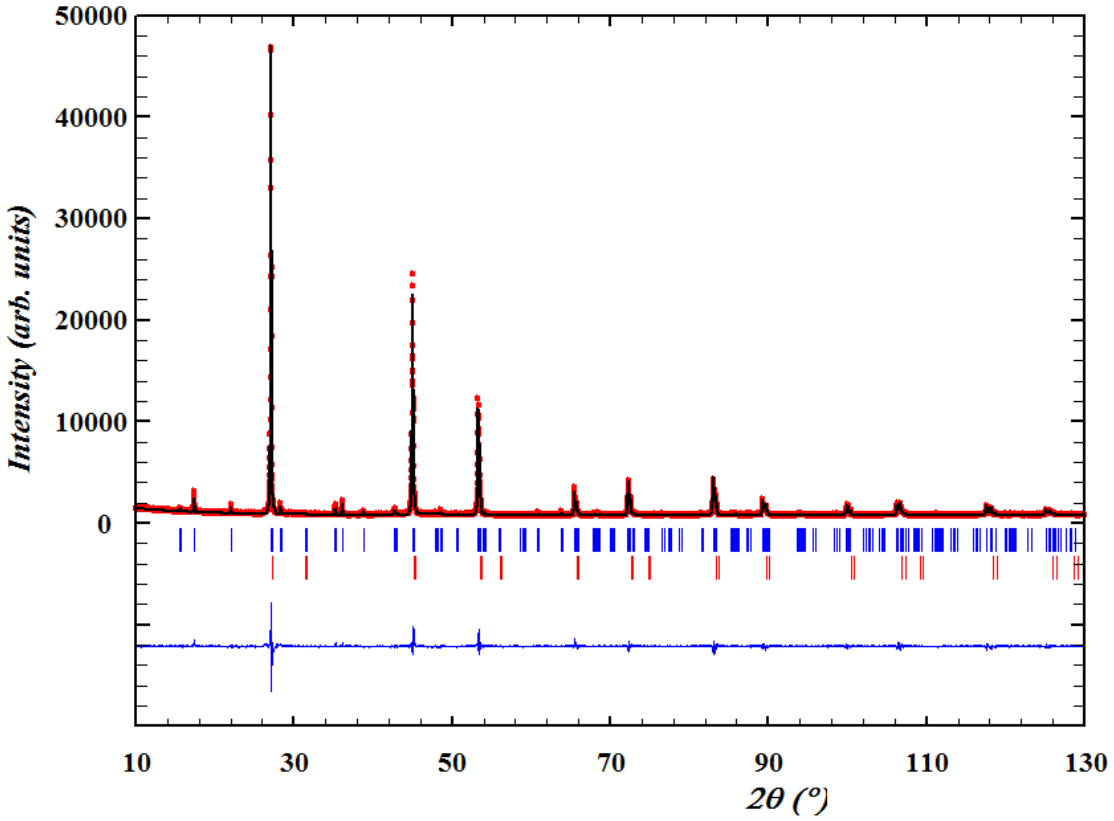

Figure 27: Diffractrogram for the 2% mixture of $ZnSe$. Asymmetry technique, hkl method.

R_{Bragg} for $ZnSe$	R_{Bragg} for CZTSe	χ^2
6.15	9.93	5.113

Table 28: R_{Bragg} and χ^2 for the 1% mixture of $ZnSe$. Scale technique.

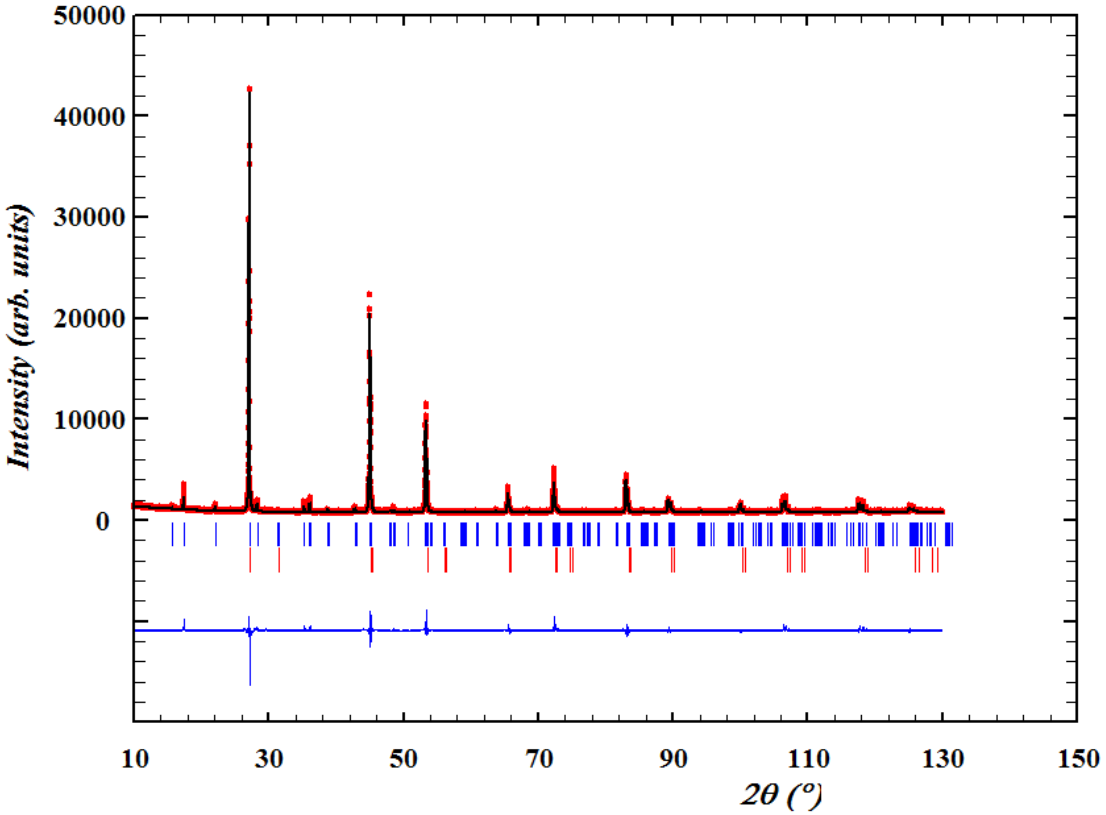

Figure 28: Diffractrogram for the 1% mixture of $ZnSe$. Scale technique

R_{Bragg} for $ZnSe$	R_{Bragg} for CZTSe	χ^2
1.18	9.60	5.075

Table 29: R_{Bragg} and χ^2 for the 1% mixture of $ZnSe$. Asymmetry technique.

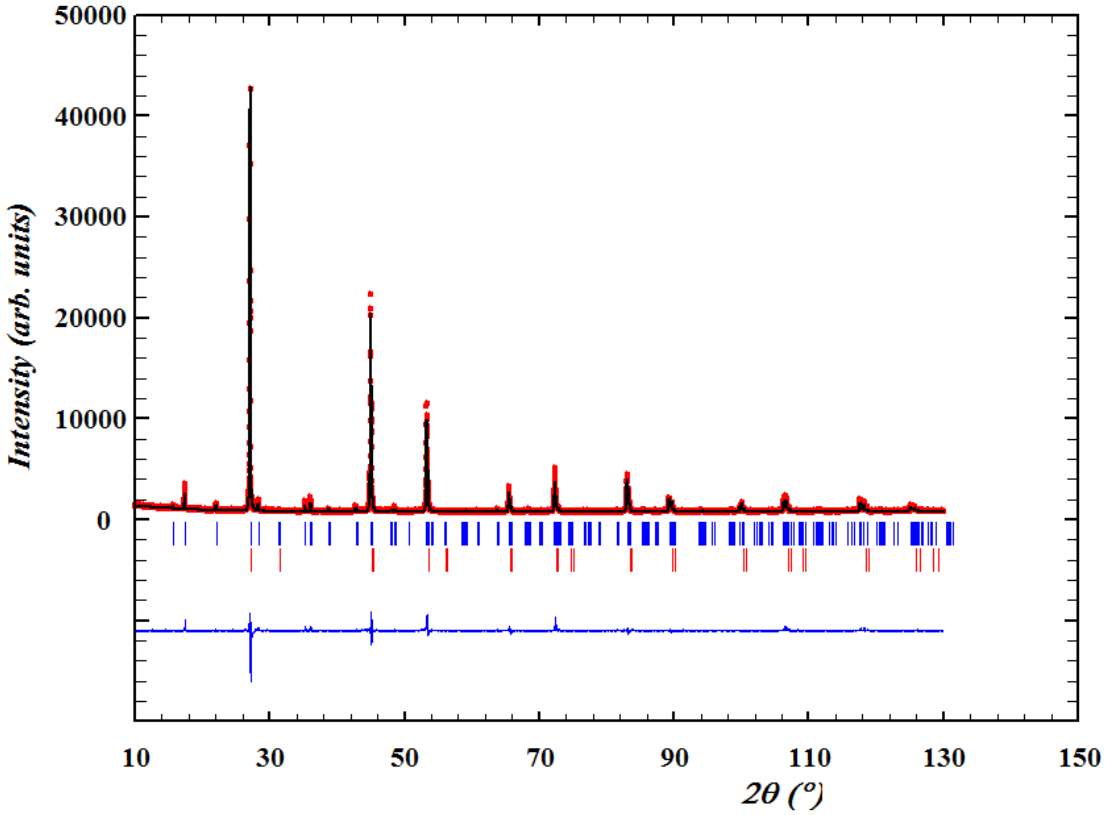

Figure 29: Diffractrogram for the 1% mixture of $ZnSe$. Asymmetry technique.

R_{Bragg} for $ZnSe$	R_{Bragg} for CZTSe	χ^2
5.28	9.94	5.168

Table 30: R_{Bragg} and χ^2 for the 1% mixture of $ZnSe$. Scale technique, hkl method.

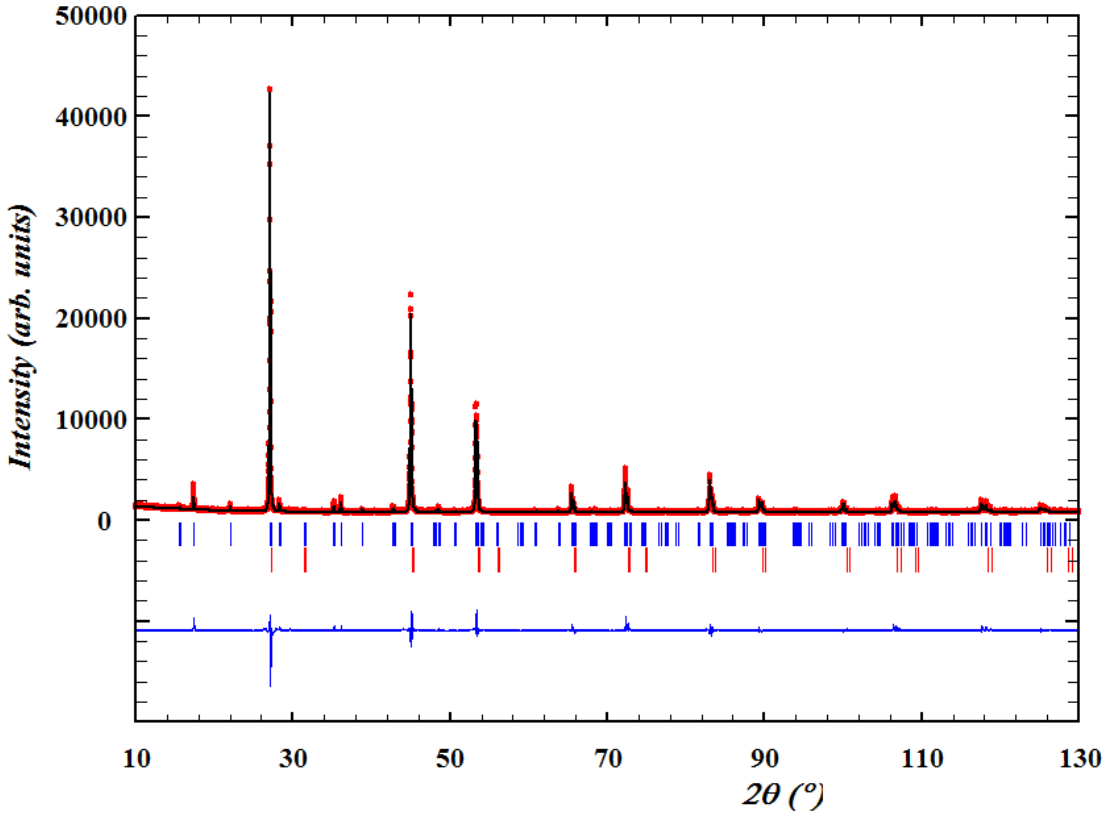

Figure 30: Diffractrogram for the 1% mixture of $ZnSe$. Scale technique, hkl method.

R_{Bragg} for $ZnSe$	R_{Bragg} for CZTSe	χ^2
2.65	9.57	5.356

Table 31: R_{Bragg} and χ^2 for the 1% mixture of $ZnSe$. Asymmetry technique, hkl method.

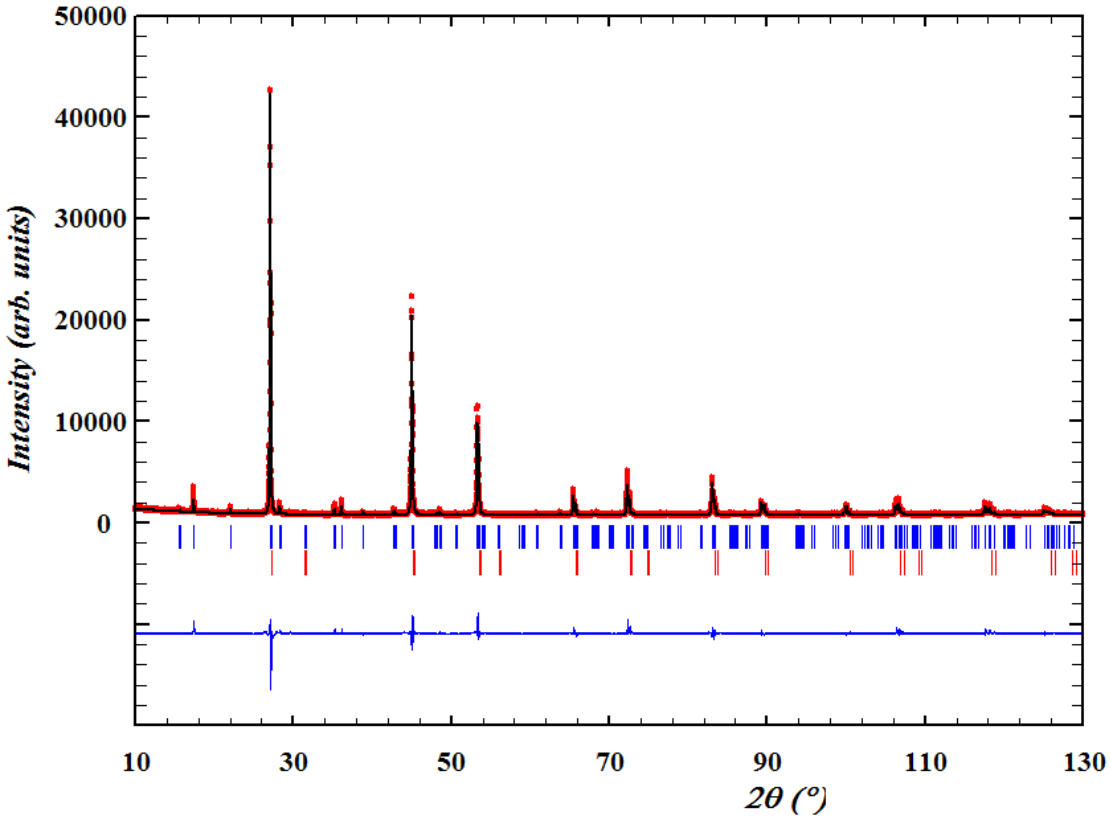

Figure 31: Diffractrogram for the 1% mixture of $ZnSe$. Asymmetry technique, hkl method.

R_{Bragg} for $ZnSe$	R_{Bragg} for CZTSe	χ^2
5.74	7.85	5.831

Table 32: R_{Bragg} and χ^2 for an extra 20% mixture of $ZnSe$. Scale technique.

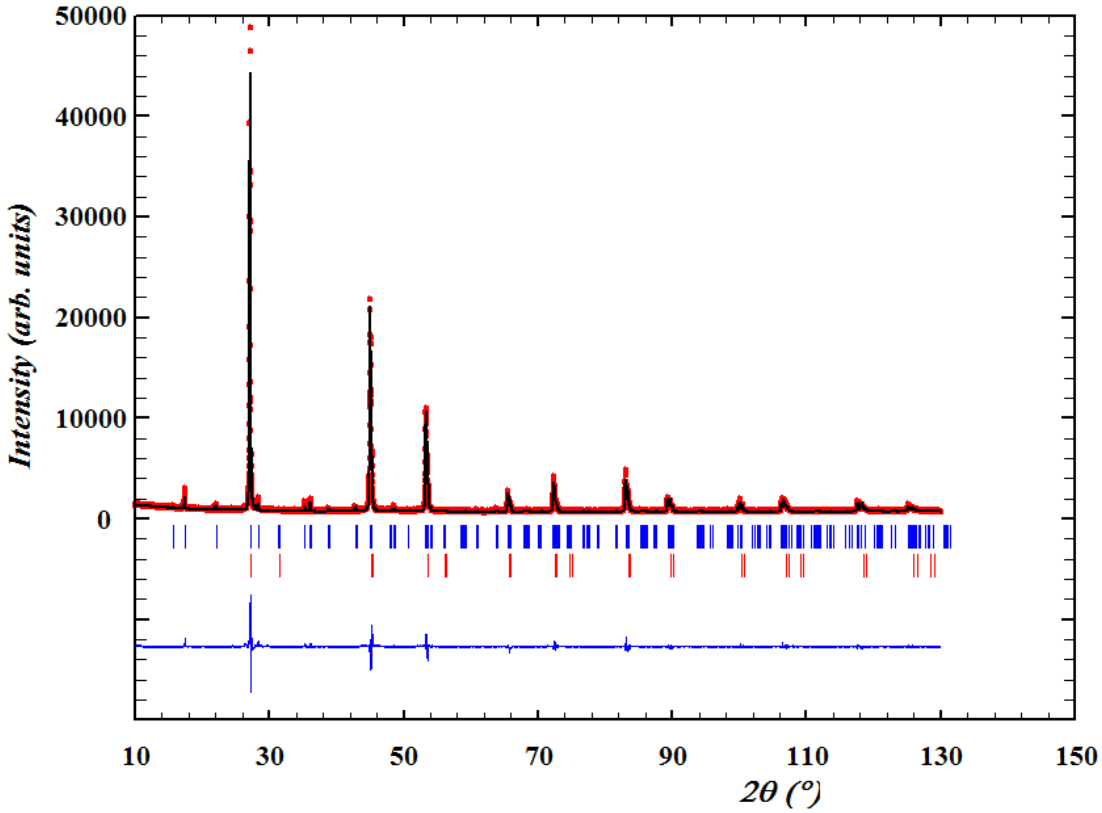

Figure 32: Diffractrogram for an extra the 20% mixture of $ZnSe$. Scale technique

R_{Bragg} for $ZnSe$	R_{Bragg} for CZTSe	χ^2
11.35	9.54	5.834

Table 33: R_{Bragg} and χ^2 for the 20% mixture of synthesised $ZnSe$. Scale technique.

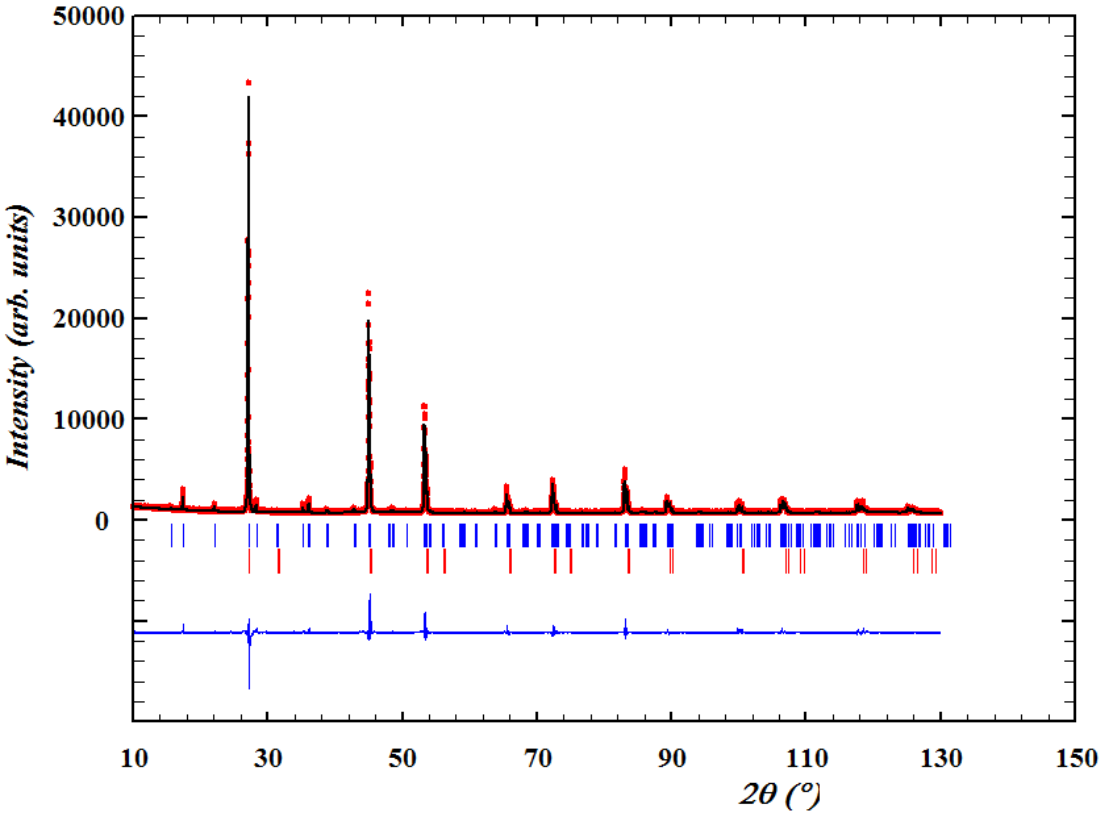

Figure 33: Diffractrogram for a 20% mixture of synthesised $ZnSe$. Scale technique.

R_{Bragg} for CTSe	R_{Bragg} for CZTSe	χ^2
9.79	7.63	3.423

Table 34: R_{Bragg} and χ^2 for the 20% mixture of CTSe. Scale technique.

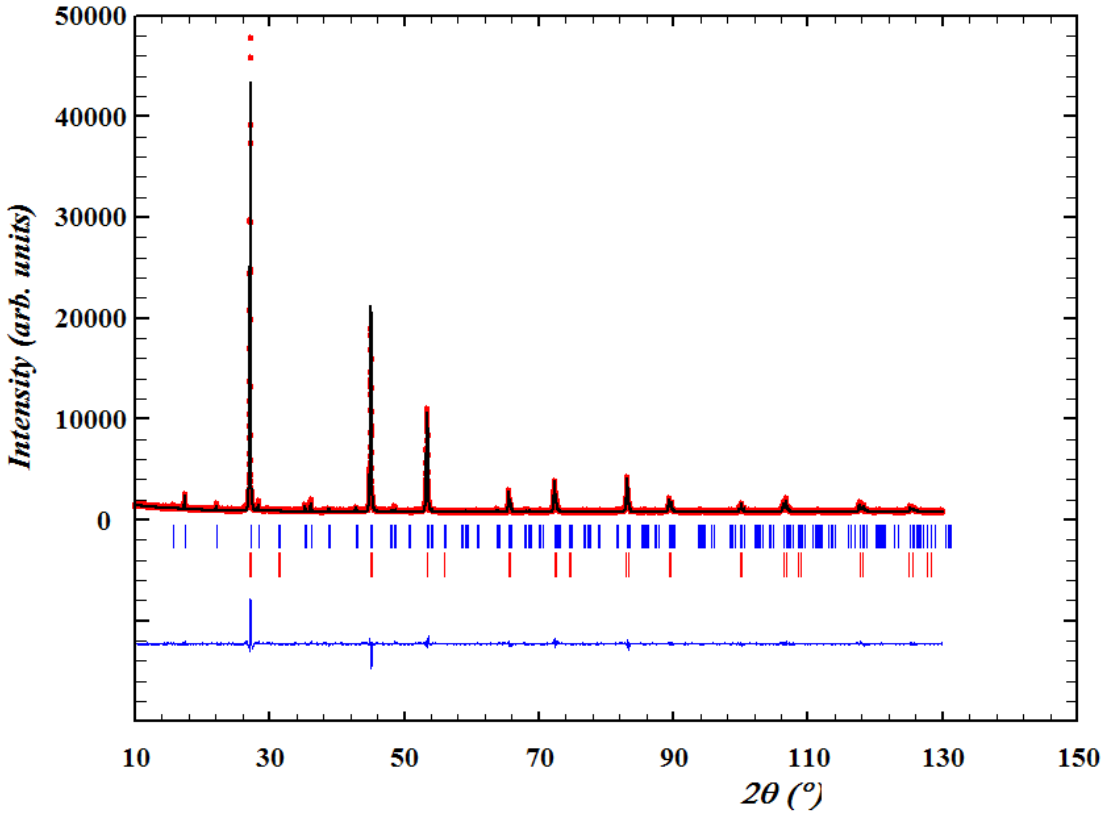

Figure 34: Diffractrogram for the 20% mixture of CTSe. Scale technique.

R_{Bragg} for CTSe	R_{Bragg} for CZTSe	χ^2
7.42	6.39	3.425

Table 35: R_{Bragg} and χ^2 for the 20% mixture of CTSe. Asymmetry technique.

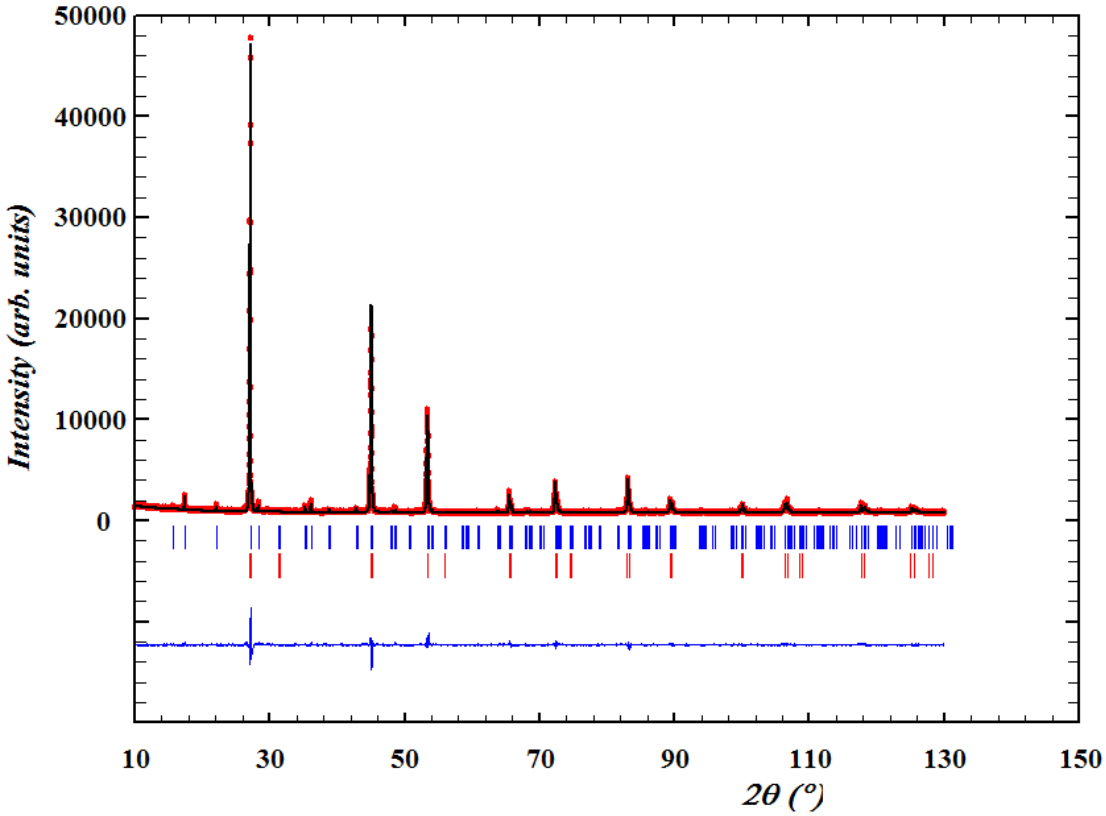

Figure 35: Diffractrogram for the 20% mixture of CTSe. Asymmetry technique.

R_{Bragg} for CTSe	R_{Bragg} for CZTSe	χ^2
9.78	7.61	3.431

Table 36: R_{Bragg} and χ^2 for the 20% mixture of CTSe. Scale technique, hkl method.

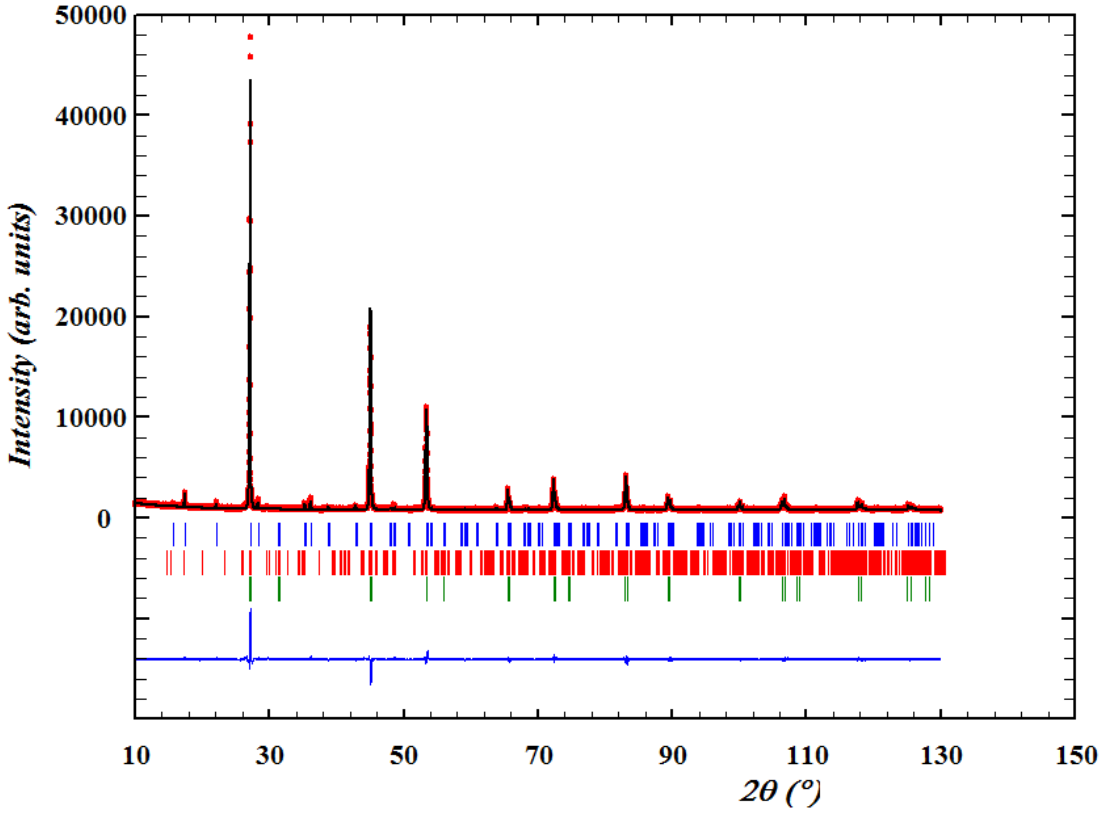

Figure 36: Diffractrogram for the 20% mixture of CTSe. Scale technique, hkl method.

R_{Bragg} for CTSe	R_{Bragg} for CZTSe	χ^2
9.53	6.33	3.010

Table 37: R_{Bragg} and χ^2 for the 20% mixture of CTSe. Asymmetry technique, hkl method.

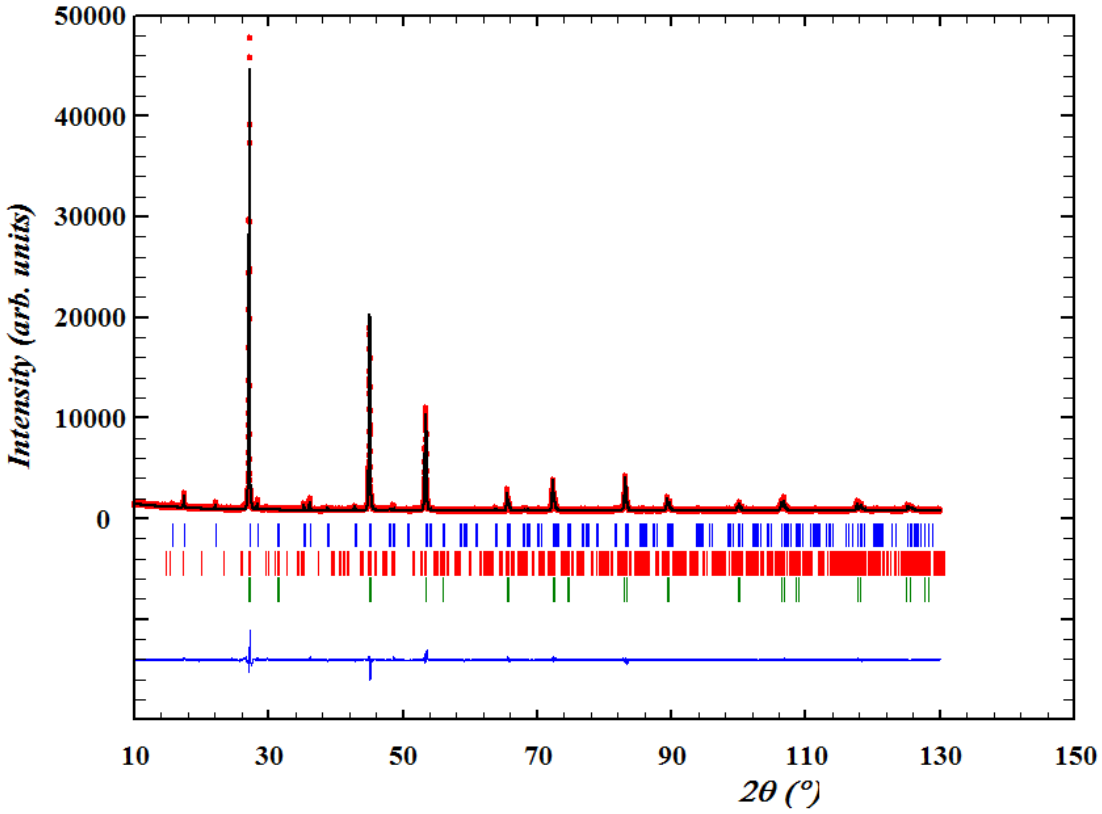

Figure 37: Diffractrogram for the 20% mixture of CTSe. Asymmetry technique, hkl method.

R_{Bragg} for CTSe	R_{Bragg} for CZTSe	χ^2
10.58	9.32	3.960

Table 38: R_{Bragg} and χ^2 for the 10% mixture of CTSe. Scale technique.

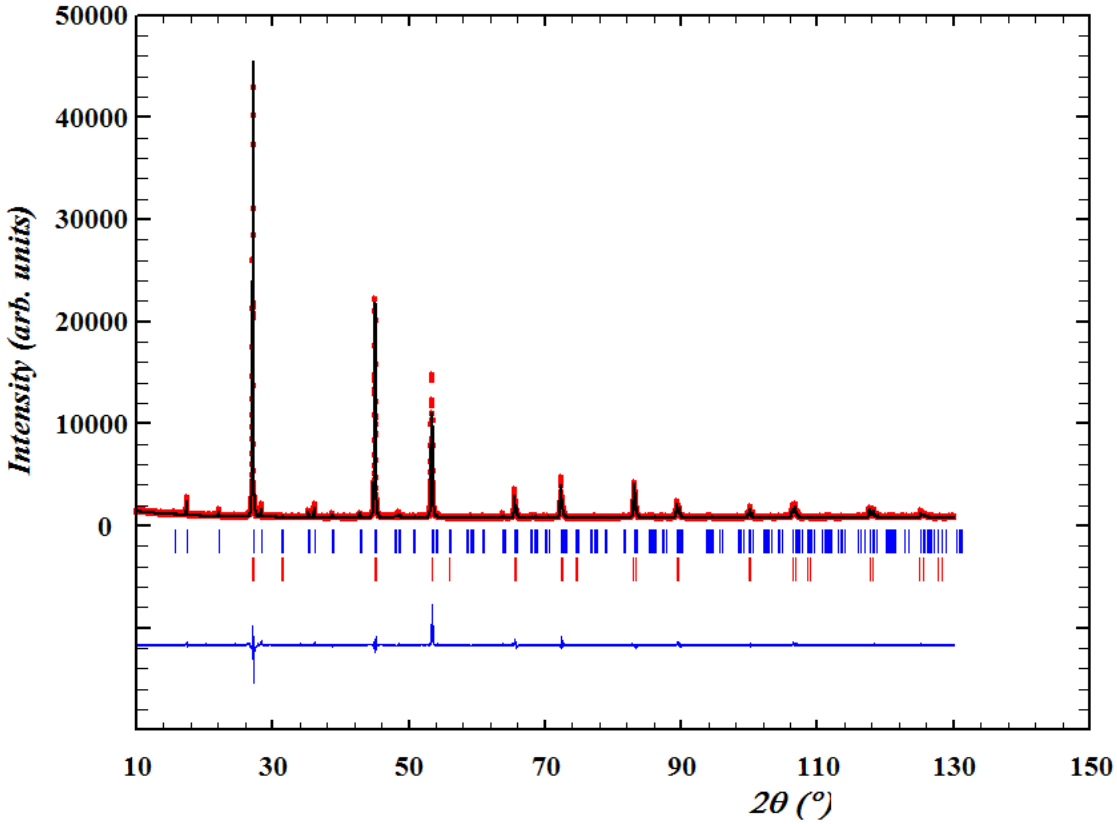

Figure 38: Diffractrogram for the 10% mixture of CTSe. Scale technique.

R_{Bragg} for CTSe	R_{Bragg} for CZTSe	χ^2
6.53	7.64	3.570

Table 39: R_{Bragg} and χ^2 for the 10% mixture of CTSe. Asymmetry technique.

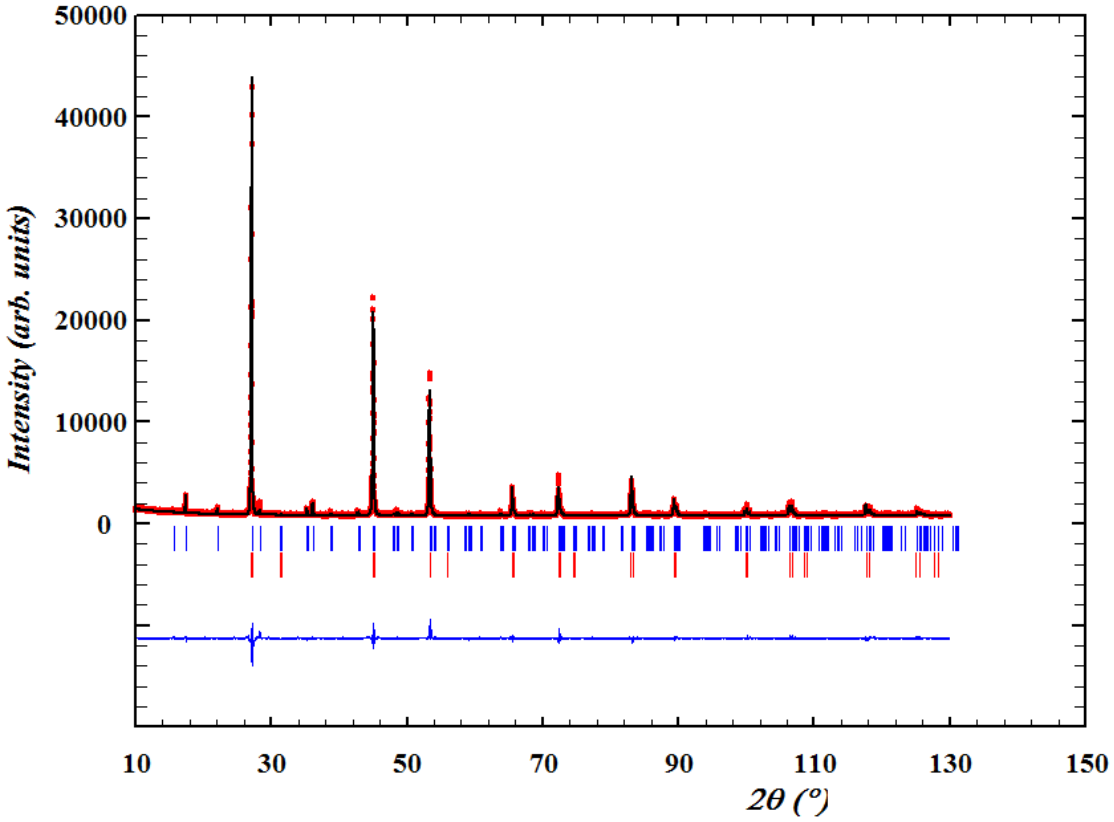

Figure 39: Diffractrogram for the 10% mixture of CTSe. Asymmetry technique.

R_{Bragg} for CTSe	R_{Bragg} for CZTSe	χ^2
10.58	9.32	3.965

Table 40: R_{Bragg} and χ^2 for the 10% mixture of CTSe. Scale technique, hkl method.

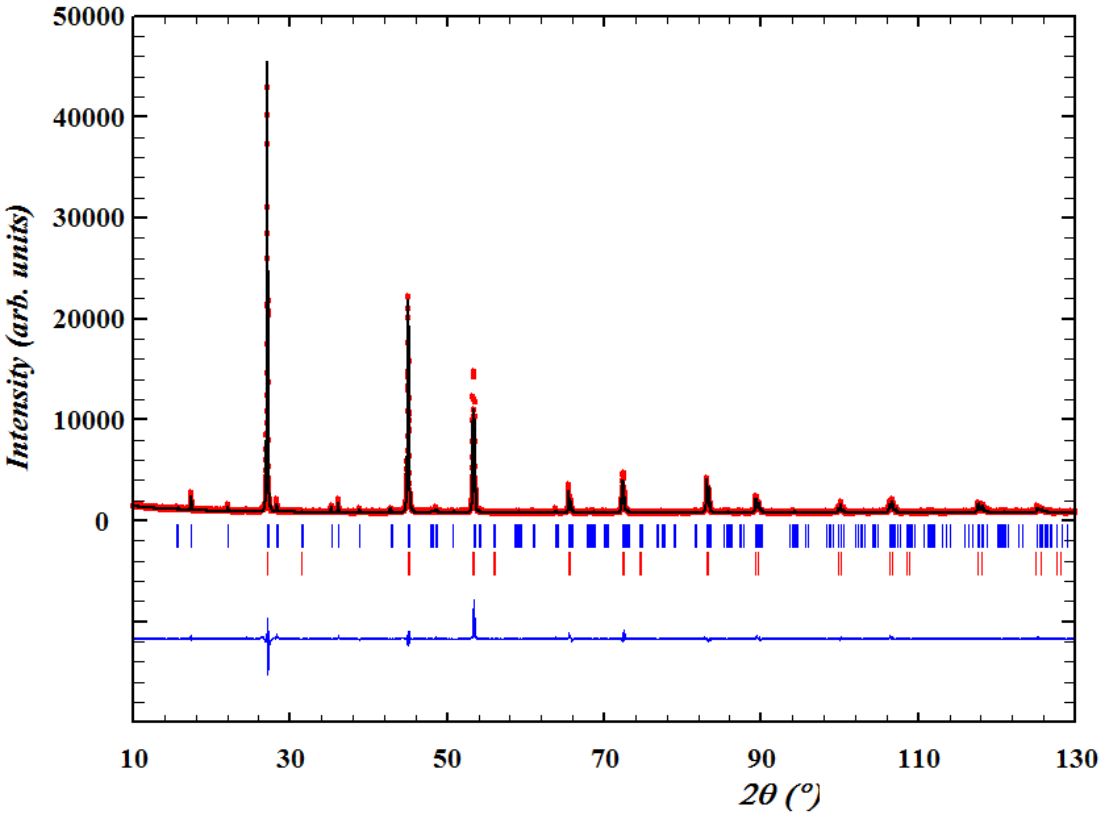

Figure 40: Diffractrogram for the 10% mixture of CTSe. Scale technique, hkl method.

R_{Bragg} for CTSe	R_{Bragg} for CZTSe	χ^2
6.97	8.00	3.621

Table 41: R_{Bragg} and χ^2 for the 10% mixture of CTSe. Asymmetry technique, hkl method.

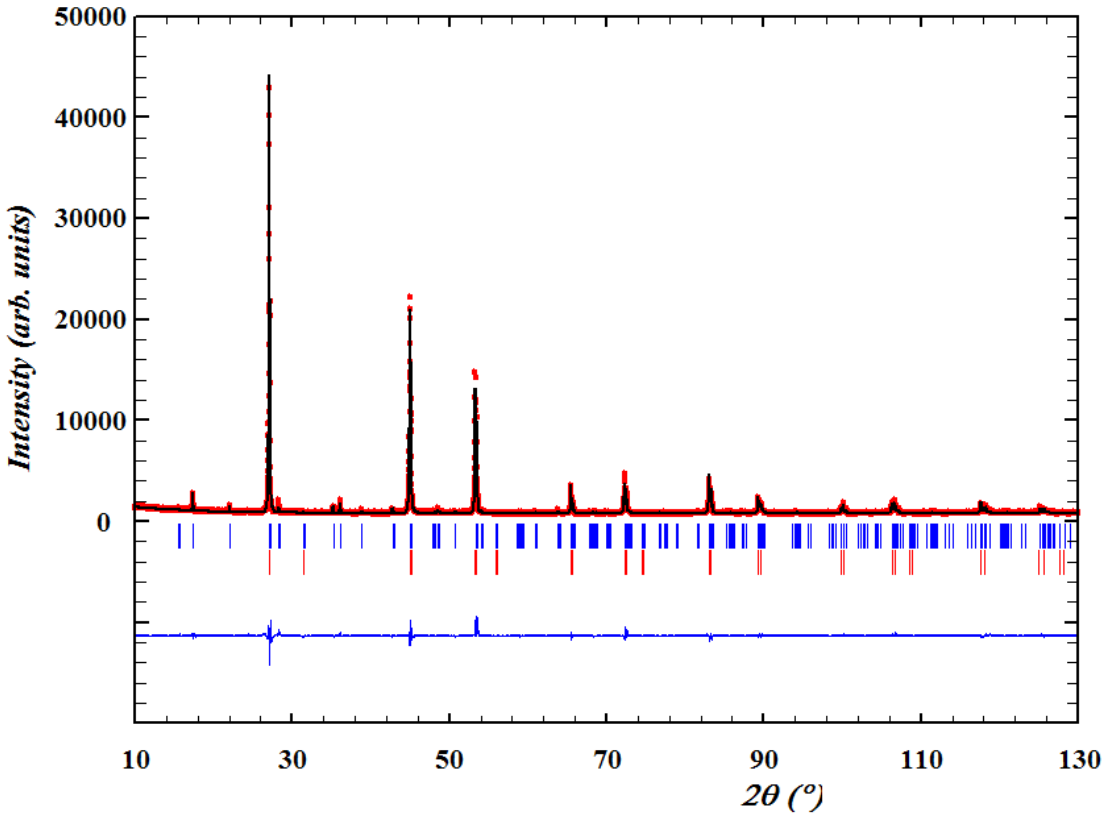

Figure 41: Diffractrogram for the 10% mixture of CTSe. Asymmetry technique, hkl method.

R_{Bragg} for CTSe	R_{Bragg} for CZTSe	χ^2
18.05	8.25	3.941

Table 42: R_{Bragg} and χ^2 for the 5% mixture of CTSe. Scale technique.

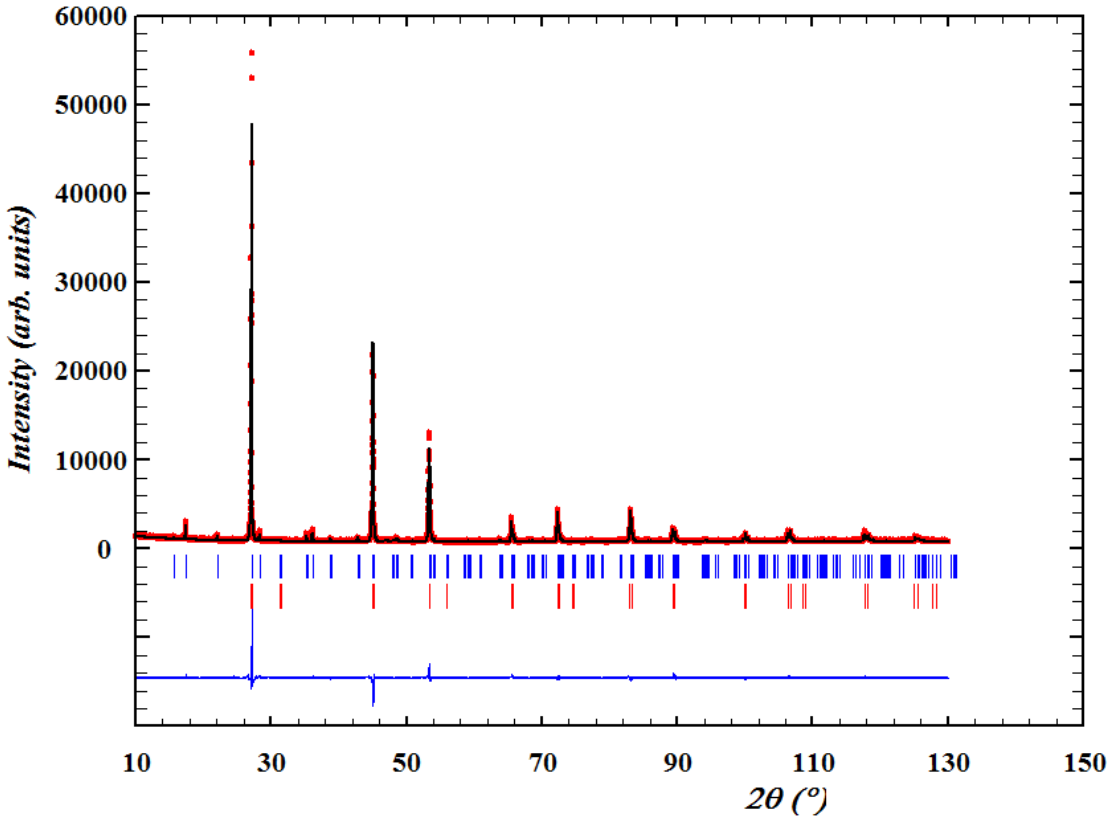

Figure 42: Diffractrogram for the 5% mixture of CTSe. Scale technique.

R_{Bragg} for CTSe	R_{Bragg} for CZTSe	χ^2
15.69	7.36	3.817

Table 43: R_{Bragg} and χ^2 for the 5% mixture of CTSe. Asymmetry technique.

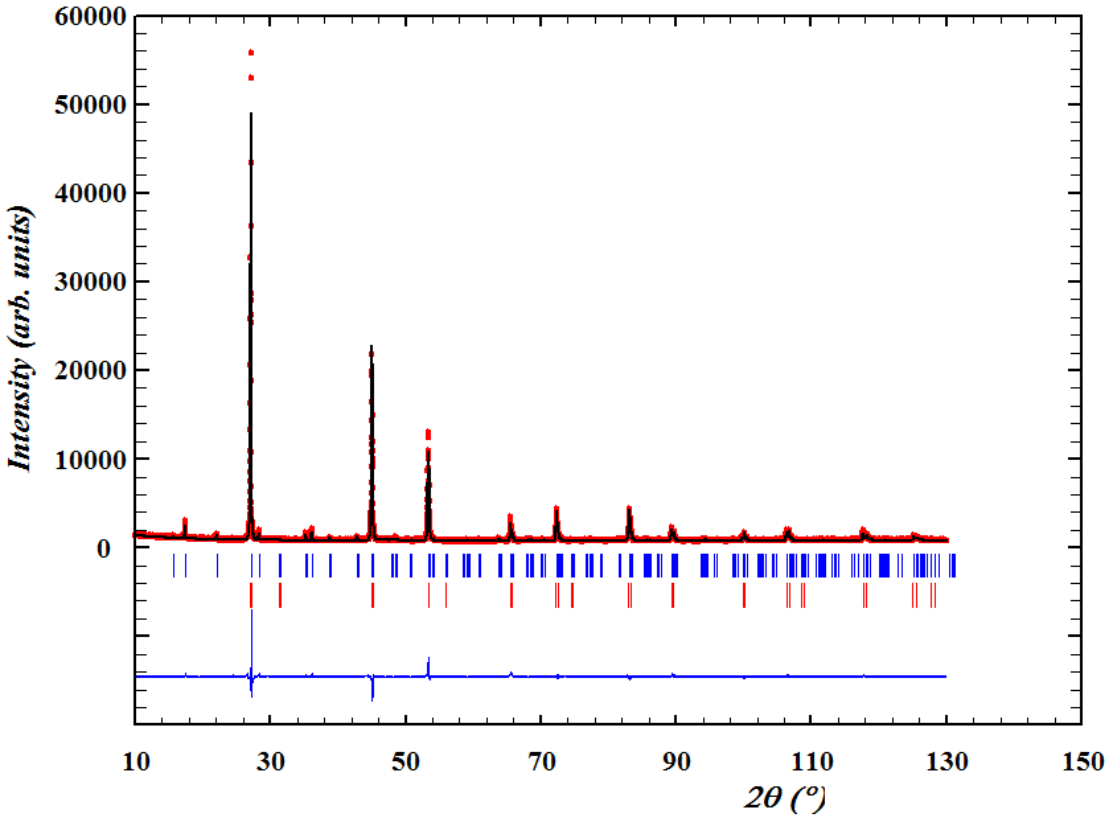

Figure 43: Diffractrogram for the 5% mixture of CTSe. Asymmetry technique.

R_{Bragg} for CTSe	R_{Bragg} for CZTSe	χ^2
16.85	8.24	3.951

Table 44: R_{Bragg} and χ^2 for the 5% mixture of CTSe. Scale technique, hkl method.

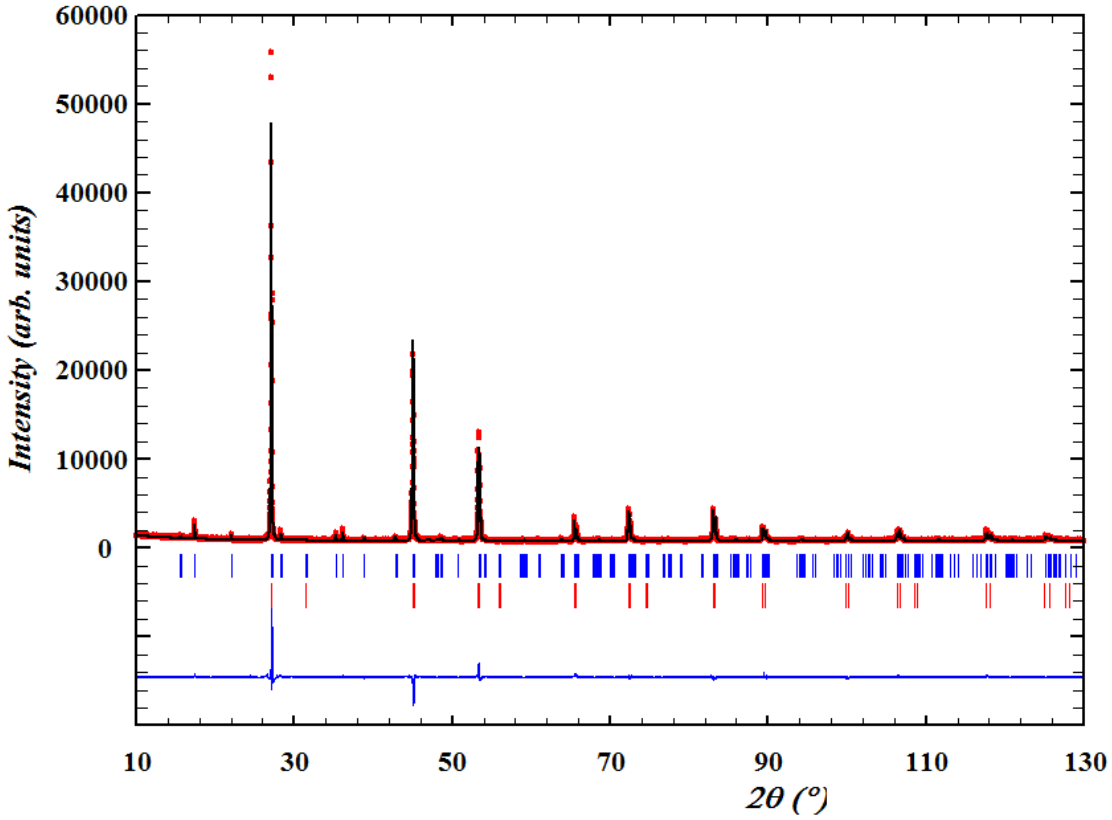

Figure 44: Diffractrogram for the 5% mixture of CTSe. Scale technique, hkl method.

R_{Bragg} for CTSe	R_{Bragg} for CZTSe	χ^2
15.42	7.37	3.819

Table 45: R_{Bragg} and χ^2 for the 5% mixture of CTSe. Asymmetry technique, hkl method.

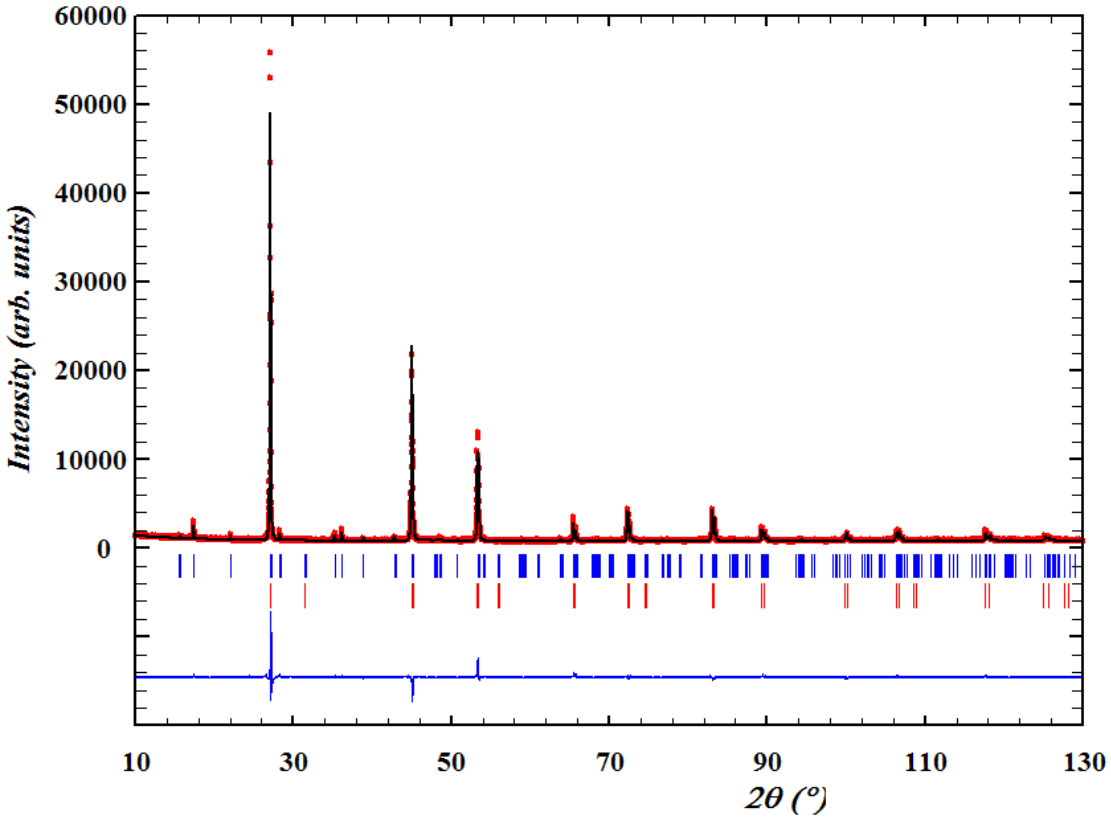

Figure 45: Diffractrogram for the 5% mixture of CTSe. Asymmetry technique, hkl method.

R_{Bragg} for CTSe	R_{Bragg} for CZTSe	χ^2
34.34	7.99	3.933

Table 46: R_{Bragg} and χ^2 for the 3% mixture of CTSe. Scale technique.

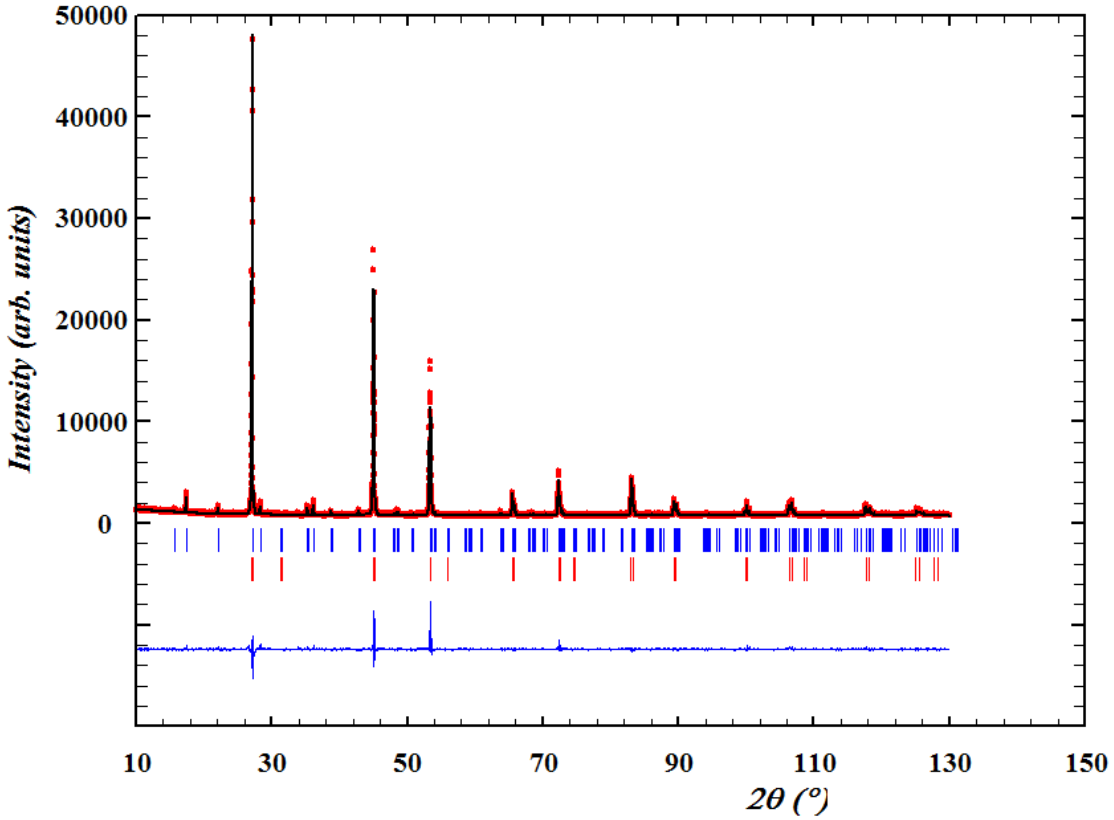

Figure 46: Diffractrogram for the 3% mixture of CTSe. Scale technique.

R_{Bragg} for CTSe	R_{Bragg} for CZTSe	χ^2
26.12	7.93	4.040

Table 47: R_{Bragg} and χ^2 for the 3% mixture of CTSe. Asymmetry technique.

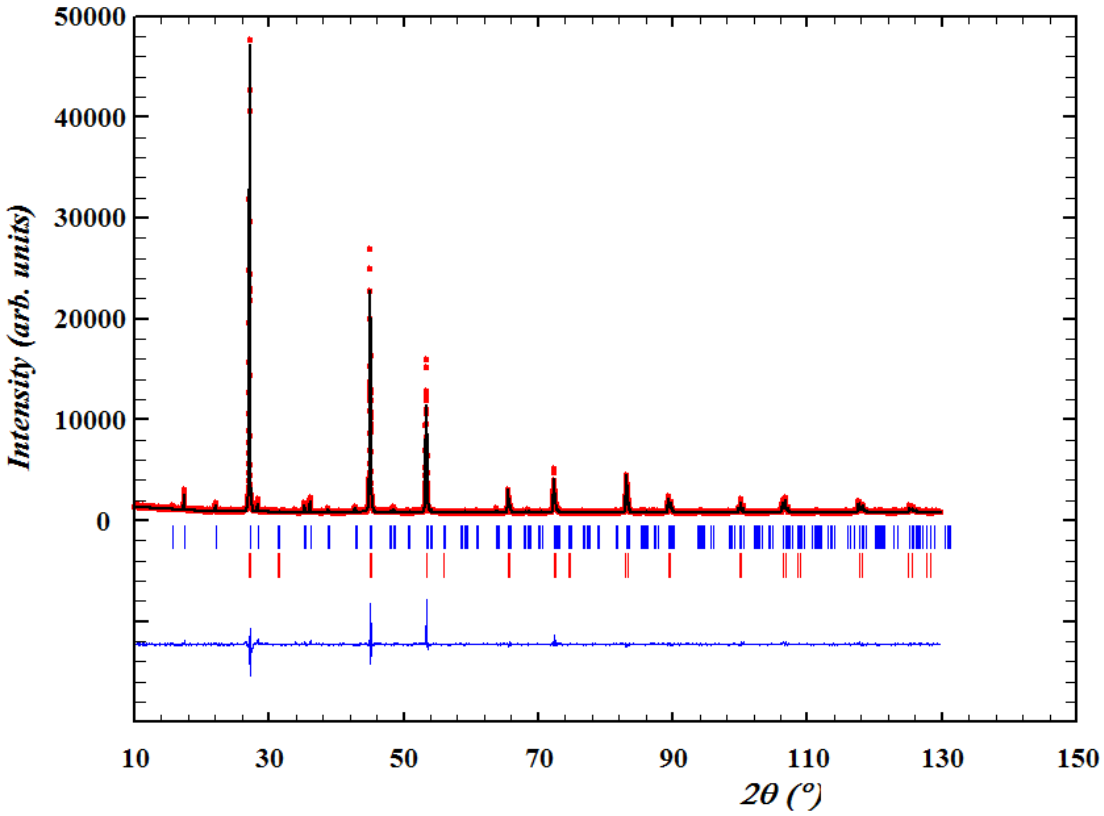

Figure 47: Diffractrogram for the 3% mixture of CTSe. Asymmetry technique.

R_{Bragg} for CTSe	R_{Bragg} for CZTSe	χ^2
35.27	7.96	3.928

Table 48: R_{Bragg} and χ^2 for the 3% mixture of CTSe. Scale technique, hkl method.

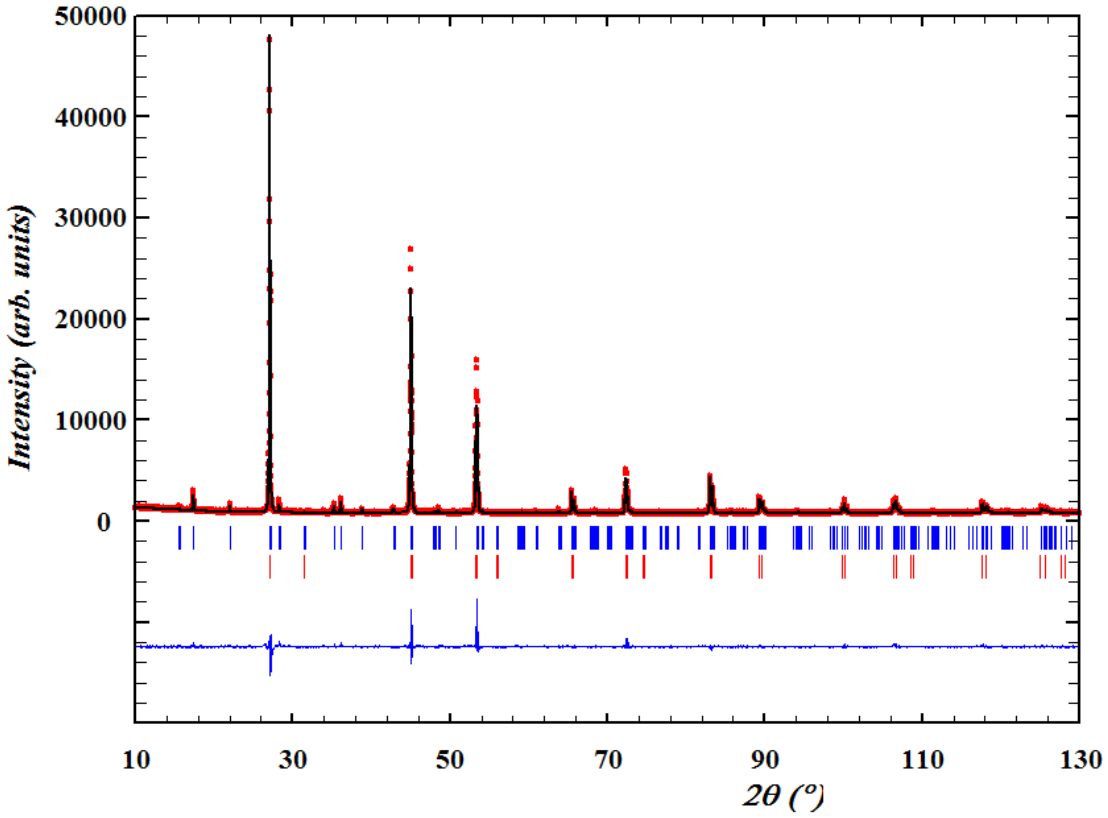

Figure 48: Diffractrogram for the 3% mixture of CTSe. Scale technique, hkl method.

R_{Bragg} for CTSe	R_{Bragg} for CZTSe	χ^2
26.40	7.97	4.050

Table 49: R_{Bragg} and χ^2 for the 3% mixture of CTSe. Asymmetry technique, hkl method.

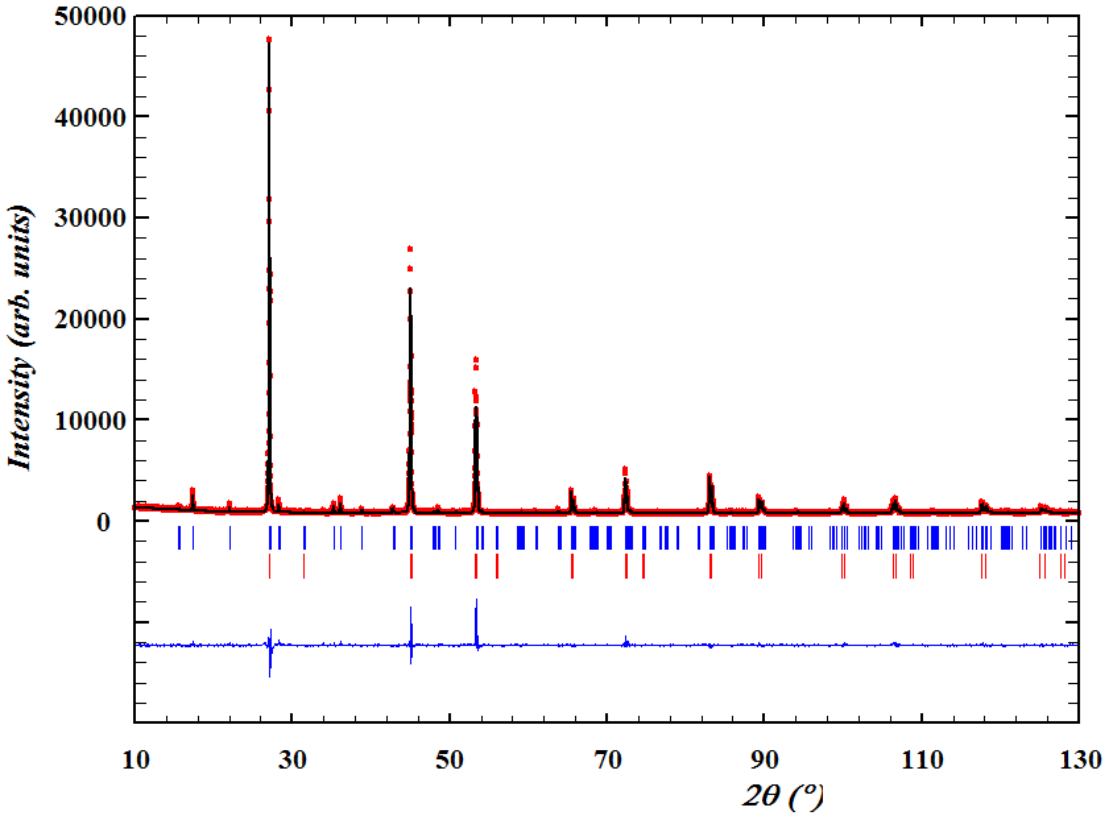

Figure 49: Diffractrogram for the 3% mixture of CTSe. Asymmetry technique, hkl method.

R_{Bragg} for CTSe	R_{Bragg} for CZTSe	χ^2
34.45	7.90	3.717

Table 50: R_{Bragg} and χ^2 for the 2% mixture of CTSe. Scale technique.

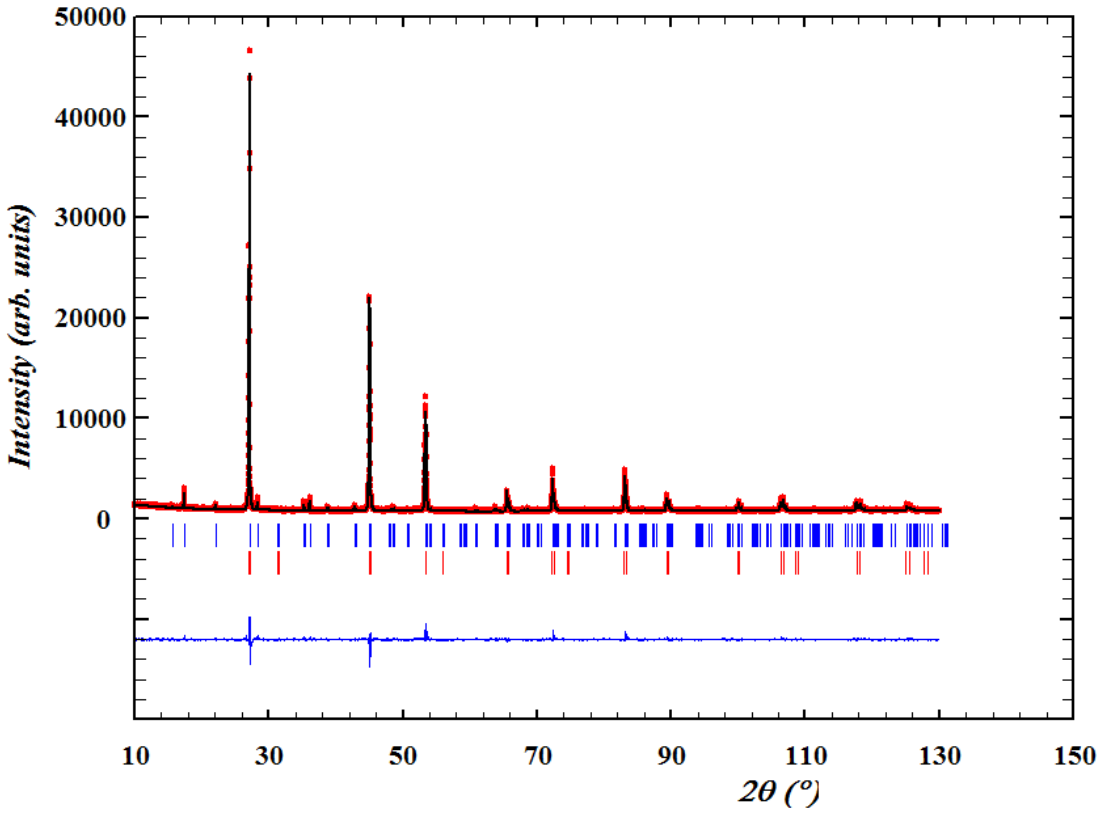

Figure 50: Diffractrogram for the 2% mixture of CTSe. Scale technique.

R_{Bragg} for CTSe	R_{Bragg} for CZTSe	χ^2
21.41	8.04	3.504

Table 51: R_{Bragg} and χ^2 for the 2% mixture of CTSe. Asymmetry technique.

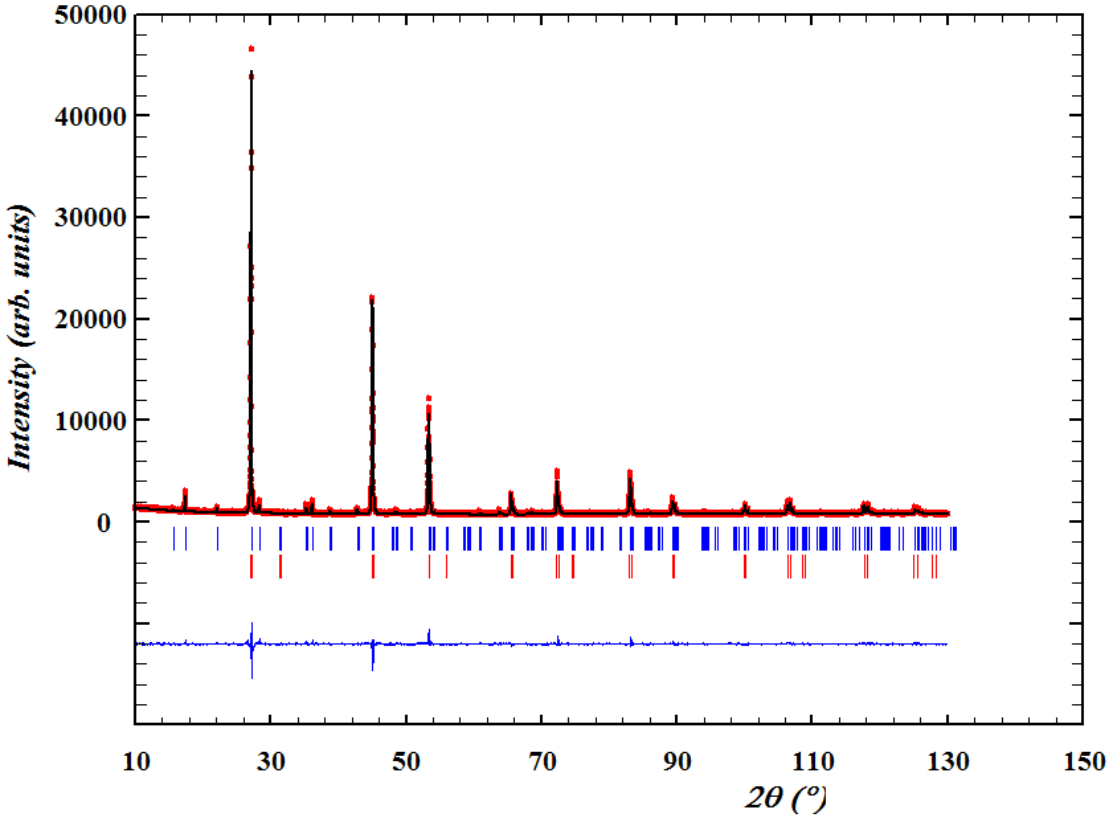

Figure 51: Diffractrogram for the 2% mixture of CTSe. Asymmetry technique.

R_{Bragg} for CTSe	R_{Bragg} for CZTSe	χ^2
28.57	7.18	3.501

Table 52: R_{Bragg} and χ^2 for the 2% mixture of CTSe. Scale technique, hkl method.

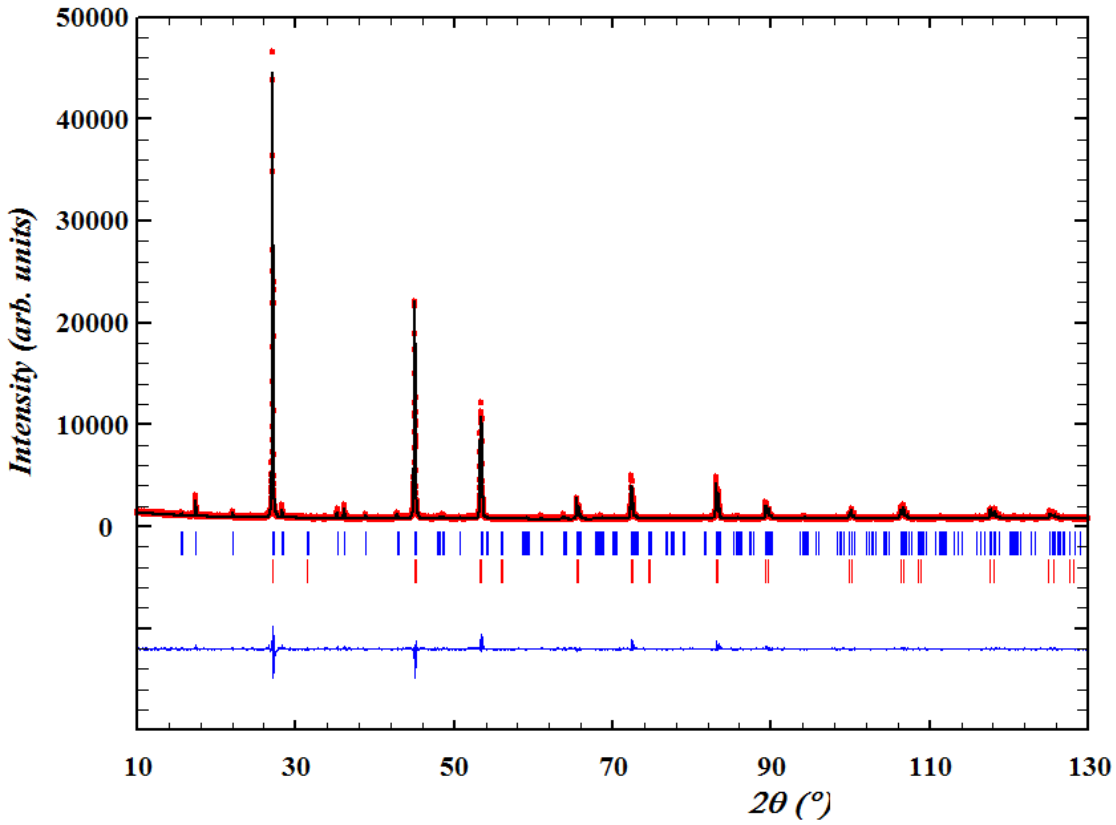

Figure 52: Diffractrogram for the 2% mixture of CTSe. Scale technique, hkl method.

R_{Bragg} for CTSe	R_{Bragg} for CZTSe	χ^2
20.38	7.26	3.442

Table 53: R_{Bragg} and χ^2 for the 2% mixture of CTSe. Asymmetry technique, hkl method.

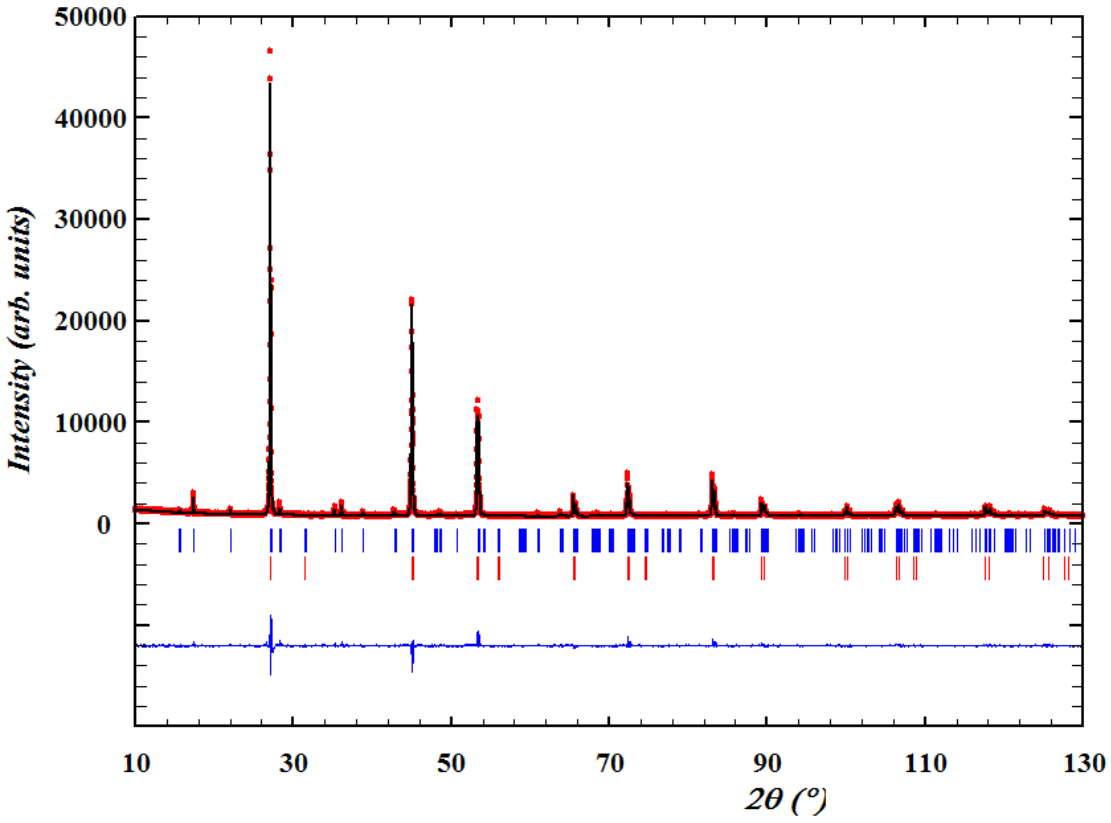

Figure 53: Diffractrogram for the 2% mixture of CTSe. Asymmetry technique, hkl method.

R_{Bragg} for CTSe	R_{Bragg} for CZTSe	χ^2
53.67	11.22	4.151

Table 54: R_{Bragg} and χ^2 for the 1% mixture of CTSe. Scale technique.

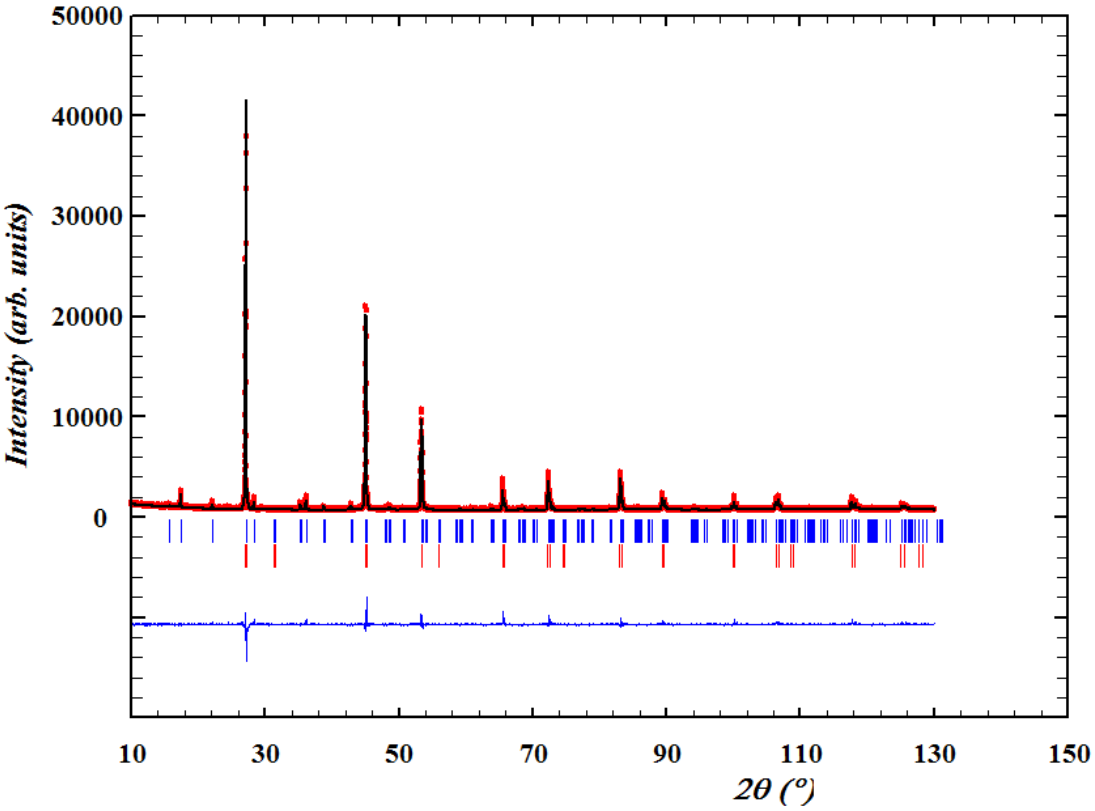

Figure 54: Diffractrogram for the 1% mixture of CTSe. Scale technique.

R_{Bragg} for CTSe	R_{Bragg} for CZTSe	χ^2
17.06	11.33	4.212

Table 55: R_{Bragg} and χ^2 for the 1% mixture of CTSe. Asymmetry technique.

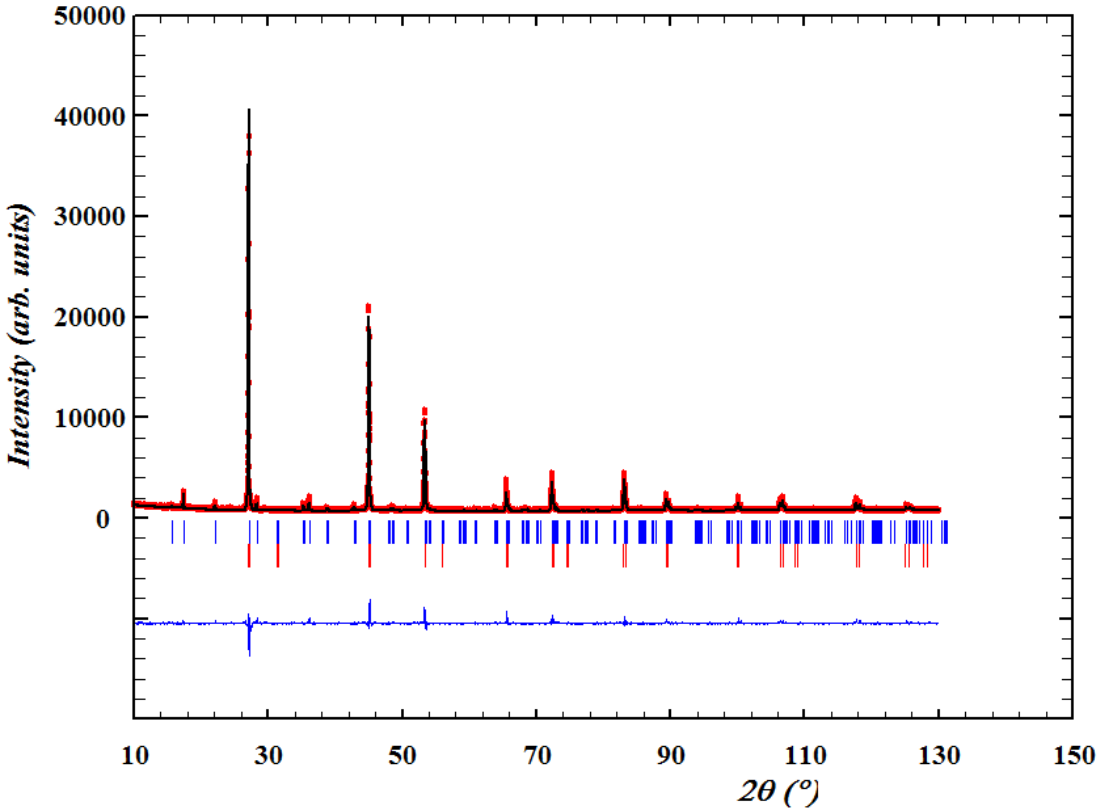

Figure 55: Diffractrogram for the 1% mixture of CTSe. Asymmetry technique.

R_{Bragg} for CTSe	R_{Bragg} for CZTSe	χ^2
93.23	11.31	4.172

Table 56: R_{Bragg} and χ^2 for the 1% mixture of CTSe. Scale technique, hkl method.

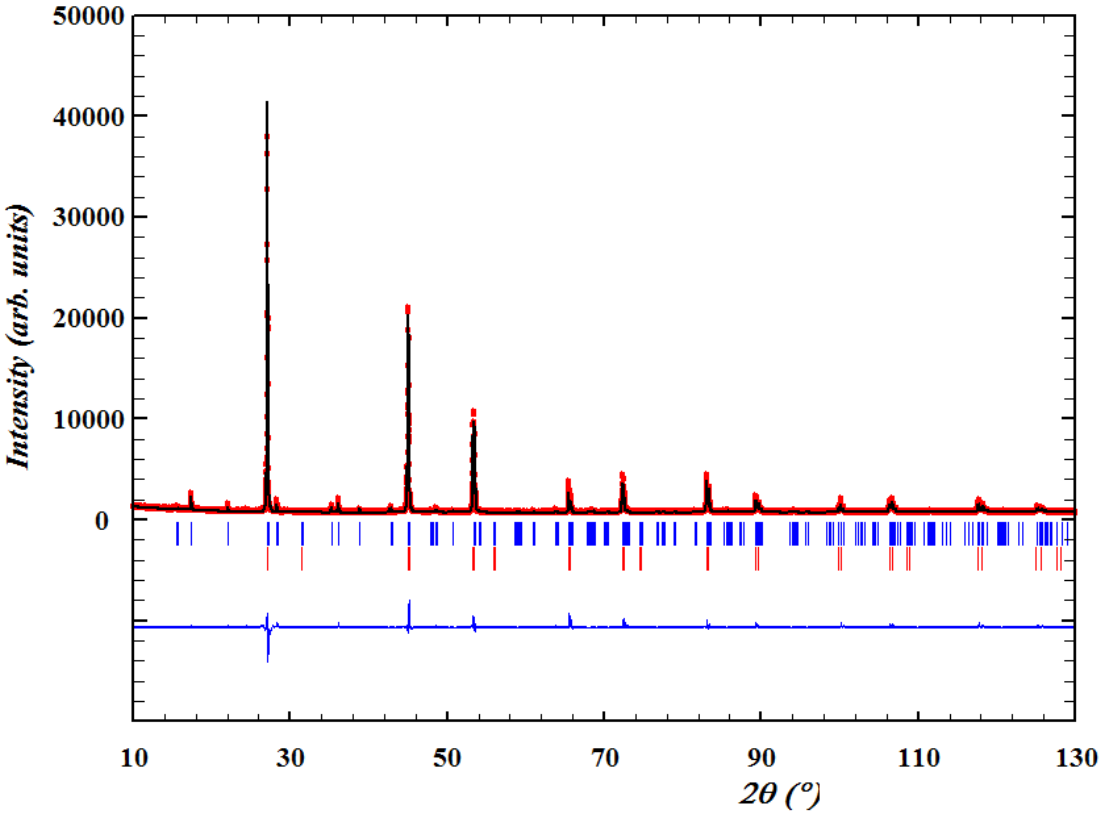

Figure 56: Diffractrogram for the 1% mixture of CTSe. Scale technique, hkl method.

R_{Bragg} for CTSe	R_{Bragg} for CZTSe	χ^2
55.26	12.03	4.501

Table 57: R_{Bragg} and χ^2 for the 1% mixture of CTSe. Asymmetry technique, hkl method.

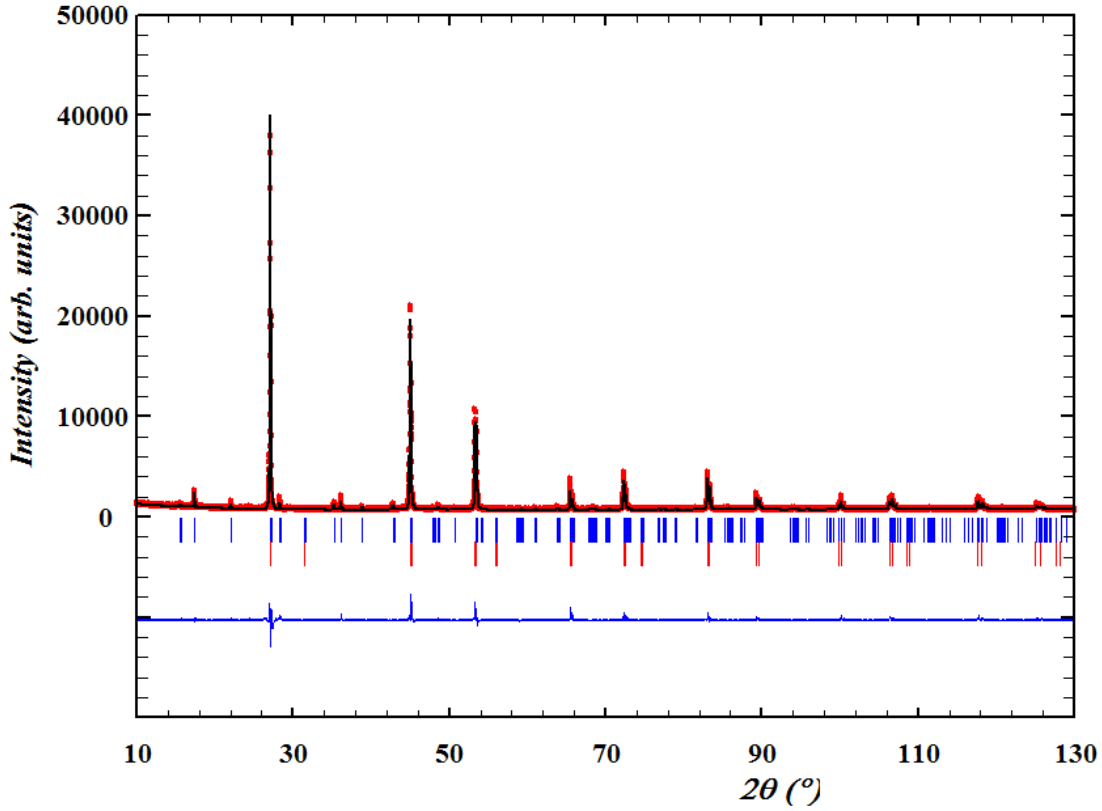

Figure 57: Diffractrogram for the 1% mixture of CTSe. Asymmetry technique, hkl method.

References

[1] Current world population, *http://www.geohive.com/earth/population_now.aspx*, (2016)

[2] Germany nearly reached 100 percent renewable power on Sunday, *http://energytransition.de/2016/05/germany-nearly-reached-100-percent-renewable-power-on-sunday/*, (2016)

[3] Portugal runs for four days straight on renewable energy alone, *http://www.theguardian.com/environment/2016/may/18/portugal-runs-for-four-days-straight-on-renewable-energy-alone*, (2016)

[4] Neil W. Ashcroft and N. David Mermin, *Solid state physics*, (1976)

[5] Christopher Hammond, *The basics of crystallography and diffraction*, Oxford Science publications, (2001)

[6] Alexander J. Brake, William Clegg et al, *Crystal Structure Analysis Principles and Practice*, Oxford Science publications, (2001)

[7] T. Tanaka, T. Nagatomo, D. Kawasaki, M. Nishio, Q. Guo, A. Wakahara, A. Yoshida, and H. Ogawa *Electrical and Optical Properties of Stannite-Type Quaternary Semiconductor Thin Films*, J. Phys. Chem. Sol. 66, (1988)

[8] W. Wang, M.T. Winkler, O. Gunawan, T. Gokmen, T.K. Todorov, Y. Zhu, D.B. Mitzi, *Device characteristics of CZTSSe thin-film solar cells with 12.6% efficiency*, Adv. Energy Mater. 4 , (2014)

[9] Dominik M.Berg, Monika Arasimowicz, Rabie Djemour, Levent Gütay, Susanne Siebentritt, Susan Schorr, Xavier Fontané, Victor Izquierdo-Roca, Alejandro Pérez-Rodriguez, Phillip J. Dale *Discrimination and detection limits of secondary phases in Cu_2ZnSnS_4 using X-ray diffraction and Raman spectroscopy*, Thin Solid State Films 569, 113-123, (2014)

[10] J. Zhang, L. X. Shao, Y. J. Fu, and E. Q. Xie *Cu_2ZnSnS_4 thin films prepared by sulfurization of ion beam sputtered precursor and their electrical and optical properties*, Rare Metals 25:315, (2006)

[11] Juan Rodriguez-Carvajal and Thierry Roisnel *https://www.psi.ch/sinq/dmc/ManualsEN/fullprof.pdf*, Fullprof userguide, (2014)

[12] L'analyse quantitative dans FullProf, *http://www.cdifx.univ-rennes1.fr/fps/FullProf_quantitative_analysis.pdf*, (2016)

[13] FullProf manual, *http://www.ccp14.ac.uk/tutorial/fullprof/doc/fp_text.htm*, (2016)

[14] Laura Elisa Valle Rios, Kai Neldner, Galina Gurieva, Susan Schorr *Existence of off-stoichiometric single phase kesterite*, Journal of Alloys and Compounds 408-413, (2016)

[15] A. Lafond, L. Choubrac, C. Guillot-Deudon, P. Deniard, S. Jobic *Crystal structures of photovoltaic chalcogenides, an intricate puzzle to solve: the cases of CIGSe and CZTS materials*, Z. für Anorg. Allg. Chem. 638 (2012)

[16] Finger, Cox and Jephcoat *A Correction for Powder Diffraction Peak Asymmetry due to Axial Divergence*, J. Appl. Cryst. 27, 892-900 , (1994)

[17] Kern Balance, *http://www.kern-sohn.com/cgi-bin/cosmoshop/lshop.cgi?wkid=13739647661660 6&ls=en&action=suche&fresh=1&suchbegriff=ABT+100-5M+&suchbegriff_nulltext=Your+search+term&setAjaxSb=1*, (2016)

[18] PanAnalytical diffractometer, *http://www.panalytical.com/Xray-diffractometers.htm*, (2016)

[19] Hugo Rietveld, *https://en.wikipedia.org/wiki/Hugo_Rietveld*, (2016)

[20] Fullprof, *https://www.ill.eu/sites/fullprof/php/reference.html*, (2016)

[21] Vacuum System, *https://www.pfeiffer-vacuum.com/productPdfs/PMP03993.en.pdf*, (2016)

[22] Furnace, *http://www.carbolite-gero.de/de/*, (2016)

[23] OriginLab, *http://www.originlab.com/*, (2016)

[24] MATLAB, *http://de.mathworks.com/products/matlab/*, (2016)